

April 2009

Fundamental Blocks for a 0.18 μ m Cyclic Analog-to-Digital Converter

Alvaro Soares

Worcester Polytechnic Institute

Shant Orchanian

Worcester Polytechnic Institute

Follow this and additional works at: <https://digitalcommons.wpi.edu/mqp-all>

Repository Citation

Soares, A., & Orchanian, S. (2009). *Fundamental Blocks for a 0.18 μ m Cyclic Analog-to-Digital Converter*. Retrieved from <https://digitalcommons.wpi.edu/mqp-all/2261>

This Unrestricted is brought to you for free and open access by the Major Qualifying Projects at Digital WPI. It has been accepted for inclusion in Major Qualifying Projects (All Years) by an authorized administrator of Digital WPI. For more information, please contact digitalwpi@wpi.edu.



Fundamental Blocks for a Cyclic Analog-to-Digital Converter

The design of vital blocks for a 0.18 μ m process converter that is self-calibrating, fully differential, and performs 1 million samples per second.

A Major Qualifying Project

in partial fulfillment of the requirements for the

Degree of Bachelor of Science

in

Electrical Engineering

by

Shant Orchanian

Gentian Rudho

Alvaro Soares Jr.

March 2009

Approved by:

Dr. John McNeill, Advisor

CONTENTS

1	Introduction	5
1.1	Goals and Specifications.....	5
1.2	Project Motivation	6
1.2.1	Non-Linearity.....	6
1.2.2	Digital Calibration.....	6
1.2.3	Simplicity and Innovation	6
2	Background	8
2.1	Analog-to-Digital Converters	8
2.2	ADC Performance Metrics.....	8
2.3	Oversampling Converters.....	12
2.4	Nyquist Converters	13
2.4.1	Pipelined ADCs	13
2.4.2	Successive Approximation ADCs	14
2.4.3	The Cyclic ADC.....	18
2.5	The Role of Capacitors	20
2.5.1	Thermal Noise.....	20
2.6	Options for Output Driving.....	21
2.6.1	Understanding LVDS.....	21
2.6.2	The Concepts behind LVDS	21
2.6.3	Different Types of LVDS	22
2.6.4	Contrasting LVDS Types and Configurations	23
2.6.5	A Typical LVDS Circuit	24
2.6.6	Applications	25
2.6.7	Assessing LVDS in the ADC Design Process.....	25
2.7	The Split-ADC Concept.....	26
2.8	The Current Mirror.....	27
2.9	The Differential Pair	29
2.9.1	Bartlett's Bisection Theorem	30
3	High-Level Design.....	33
3.1	Block Diagram	33
4	The Input Block.....	34

4.1	Transistor Size Optimization	35
4.1.1	Dealing with the Presence of Distortion	35
4.1.2	Performing a Parametric Analysis	35
4.1.3	Choosing Total Width	39
4.2	Reducing the Noise Floor	40
4.2.1	Resistor Tolerance	42
4.2.2	Implementation of Input Block	43
5	The Switched Capacitor Network	45
5.1	Defining the Correct Number of Capacitors for the Network	46
5.1.1	Using One Capacitor	46
5.1.2	Using Two Capacitors	47
5.1.3	Testing the Two Capacitor System	48
5.2	The Final Switch Capacitor Design: Four Capacitors	49
5.3	Determining Voltage Reference Values for Switched Capacitors	54
6	Differential Amplifier	55
6.1	Fundamental Components of the Differential Amplifier	55
6.2	Differential Amplifier Voltage Levels	56
6.2.1	KT/C Capacitor Sizing	59
6.2.2	Derivations of Resistive Load Values and Bias Current	60
6.3	Replica Bias Analysis	61
6.3.1	Advantages and Purpose of Using Replica Bias	61
6.3.2	Designing Replica Bias	61
6.3.3	Simulation of the Replica Bias Circuit	62
6.3.4	Differential Pair Symbol Representation	62
7	The Logic Block	63
7.1	driving transistor gates through optimization	63
7.1.1	Tapered Buffer	63
7.1.2	Advantages of Using Tapered Buffers	64
7.2	sample and hold circuit simulations	65
7.3	Driving Transistor Gates at Capacitor Array	72
7.3.1	Implementing Residue Amplifier Decisions	73
7.3.2	Example of a Decision Implementation	74
7.3.3	Final Step in Designing the Gate Digital Driver	75

7.4	Driving Transistor Gates of Input-Output Capacitors of Residue Amplifier	76
7.4.1	Realizing the digital Block	77
7.5	Designing “genericDemux”	78
7.5.1	“genericDemux” Symbol Representation	78
8	The Comparators	80
8.1	The Pre-Amplifiers	80
8.1.1	The ± 1 Preamp	80
8.1.2	The 0 Preamp	85
8.2	Analog Latch	87
8.3	Digital latch	89
8.4	Putting it all together	91
9	The Output Block	94
9.1	Creating LVDS Drivers	94
9.2	Making the Choice between LVDS and LVCMOS	97
9.3	Output Process	97
10	Conclusion	98
10.1	Future Work	98
10.2	Recommendations for Future Projects	98
10.3	Recapitulation	99
10.4	Importance and Impact	100
	Table of Figures	101
	Index of Tables	103
	References	104

1 INTRODUCTION

The electronics world is faced with various challenges when attempting to integrate analog signals with digital and discrete systems. Therefore, the existence of a tool that enables this integration is vital to many electrical engineers in today's world. The Analog-to-Digital Converter (ADC) is not a new concept by any means, but is still a topic of interest when it comes to technology, due to its inevitable necessity in many systems being used today. Mixed Signal design engineers are always faced with important questions, such as: How can signals be converted faster, more accurately? How do we optimize our systems so that we can achieve simpler, yet smarter converters? Other issues, such as power consumption, complexity, interaction with other systems, price, and many other specifications have spawned several different types and designs of analog-to-digital converters. Yet, the market is still open to different options. Our project focuses on presenting a new option among the many present, with distinct features that are aimed to satisfy various applications for analog-to-digital converters.

1.1 GOALS AND SPECIFICATIONS

The goal of the project is to build vital components for the design of a Cyclic ADC, resulting in functional blocks that enable the simulation of a full conversion, complying with the following specifications:

Table 1 - Specifications

Specifications	
Circuit Type	Integrated Circuit
Maximum Size	1 mm ²
Process Type	0.18 μm
Resolution	12 Bits
Throughput	1 Msps
Test Time	Less than 1 sec
Other Specifications	Fully Differential

The project is sponsored by the New England Center for Analog and Mixed Signal Design (NECAMSID) located at WPI. The manufacturing of the integrated circuit will take place at Jazz Semiconductor and the simulation components used are from Jazz Semiconductor's library in ICFB.

1.2 PROJECT MOTIVATION

Our group's choice to develop a self-calibrating, fully differential, cyclic analog-to-digital converter as a Major Qualifying Project was suggested to us by Professor John McNeill, who had previously worked in a similar project. Upon being given the project, we analyzed the academic and practical contributions that would be consequential to our research. The project shows itself to be unique due to a combination of characteristics.

1.2.1 *NON-LINEARITY*

Possibly one of the most interesting aspects of our design is that a linear relationship between the input and output within the chip's differential amplifier is not necessary. This concept is very appealing to integrated circuit designers because it removes a requirement that is often tough to comply without complicated circuitry [1].

1.2.2 *DIGITAL CALIBRATION*

Another attractive feature of the circuit is that its calibration is expected to be done entirely in the digital domain. In other words, the correction for non-linearity in the circuit is done by an algorithm. This is considered a favorable feature because it allows for the chip to be smaller or enhanced, due to area not being consumed by a calibration portion of the circuit, which may include laser trimmed resistors, fuses to burn or other calibration tools. Also, it may save analog designers from adding components to calibrate and test the chip before using it. An example of when this feature is useful is an application where several ADCs are needed and can be connected to one digital module.

The digital calibration will be done by a field-programmable gate array (FPGA) via an algorithm created specifically for this ADC. However, the scope of this document includes the analog integrated circuit design of this cyclic ADC. The digital algorithm was created simultaneously by Hattie Spetla, a graduate research student at New England Center for Analog and Mixed Signal Design (NECAMSID) at Worcester Polytechnic Institute. Hattie's thesis¹ includes details of the algorithm's functionality.

1.2.3 *SIMPLICITY AND INNOVATION*

Cyclic ADCs have a few advantages when compared to other types of converters – the first being that it generally involves less complex circuitry as a consequence of the digital calibration algorithm and the lack of a strictly linear differential amplifier. More importantly, in the realm of analog-to-

¹ Citation not included, since thesis is being compiled in parallel with this paper and is not currently published.

digital converters, cyclic ADCs have not been used as often as others, leaving more room for innovation and significant contributions to the field.

As noted above, the potential of this project is enormous. Therefore, we decided to tackle the challenge. The purpose of this document is to provide detailed understanding of our design of the Cyclic ADC and its components.

2 BACKGROUND

The purpose of this section is to provide the reader enough background information to make design choices and configurations easier to understand. The materials and fields of study from which we obtain our design principles and theories shall all be introduced in this section.

2.1 ANALOG-TO-DIGITAL CONVERTERS

Analog-to-digital converters are devices used to transfer a continuous real-world signal into the discrete digital domain. The use of these converters is advantageous to society because they allow signals present in nature to be represented digitally. Since the ultimate goal of this project is to create an analog-to-digital converter (ADC), we must define the existent types present in today's market. A common way to categorize these ADCs relates to the sampling frequency of the converter. The two most commonly used ADC types are Oversampling converters and Nyquist converters.

2.2 ADC PERFORMANCE METRICS

Before we can discuss some other characteristics and features of integrated circuits and ADCs, we must first define key terminology and performance metrics used to develop specifications for such circuits. This section will define and briefly explain some important metrics and terms used in ADC design (definitions provided by [2], [3], [4], [5], and [6]).

Acquisition time (t_{acq})

Acquisition time is the time during the sample stage in a sample-and-hold circuit output to experience a full-scale transition and settle within a specified percentage of its final value.

Dynamic Range

Dynamic Range is the ratio of the maximum allowable input swing to the minimum input level that can be sampled with a specified level of accuracy.

Spurious-Free Dynamic Range (SFDR)

Sometimes referred to as a measurement of fidelity for circuits, the SFDR is the ratio of the rms value of the peak signal amplitude to the rms value of the amplitude of the peak spurious spectral component, over the specified bandwidth.

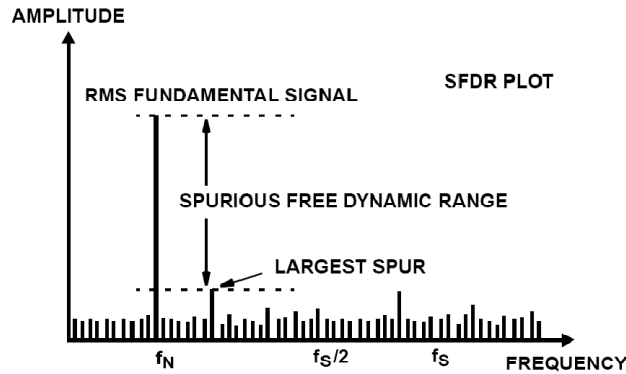


Figure 1 - Spurious-Free Dynamic Range Illustration[7]

Effective Number of Bits (ENOB)

It is a measure of the true dynamic performance level of a data converter. ENOB is calculated from the measured SNR based on the equation[2]:

$$ENOB = \frac{(SNR+Distortion)-1.76+20\log\left[\frac{Full\ Scale\ Amplitude}{Actual\ Input\ Amplitude}\right]}{6.02} \quad \text{Eq. 1}$$

Signal-to-Noise Ratio (SNR)

The ratio of the signal power to the noise power at the output is known as SNR. Mathematically it can be described simply as

$$SNR = \frac{rms\ Signal}{rms\ Noise} \quad \text{Eq. 2}$$

However, SNR has also a relationship with the effective number of bits, shown below:

$$SNR(dB) = 6.02(ENOB) + 1.76 \quad \text{Eq. 3}$$

Differential Non-Linearity (DNL)

The difference between the actual step and the ideal step length of the ADC's output is known as differential non-linearity[4]. For an ADC, DNL is the measure of variation in the digital output code, normalized to full scale, associated with a 1 least significant bit (LSB) change in the input code [2].

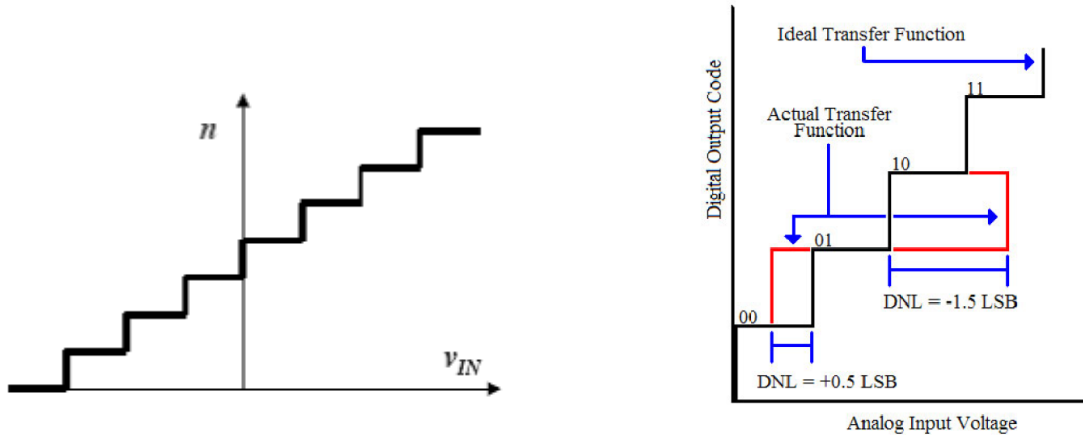


Figure 2 - Ideal (left) and Non-Ideal (right) Examples of ADC Transfer Function [4]

A change resulting in an error greater than 1 LSB results in lost bits.

Integral Non-Linearity (INL)

Differently from DNL, the integral non-linearity relates to the maximum difference between the converter's output from its ideal value. The ideal value can be described as a theoretical straight line drawn from minus full scale to positive full scale [2]. The figure below shows a graphical representation of this concept:

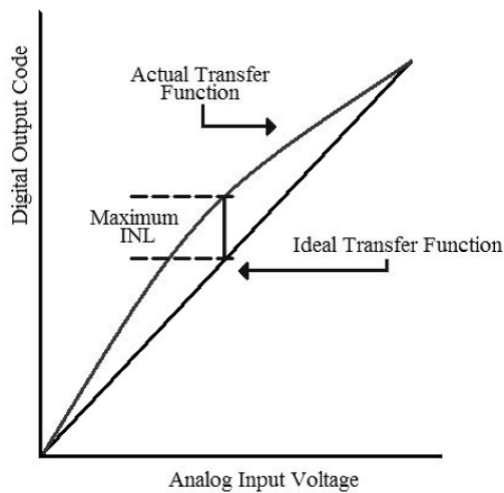


Figure 3 - Integral Non-Linearity Example [4]

Quantization Error

When a conversion is made, the number is quantized to a finite number of discrete values. The error associated with this process is known as quantization error.

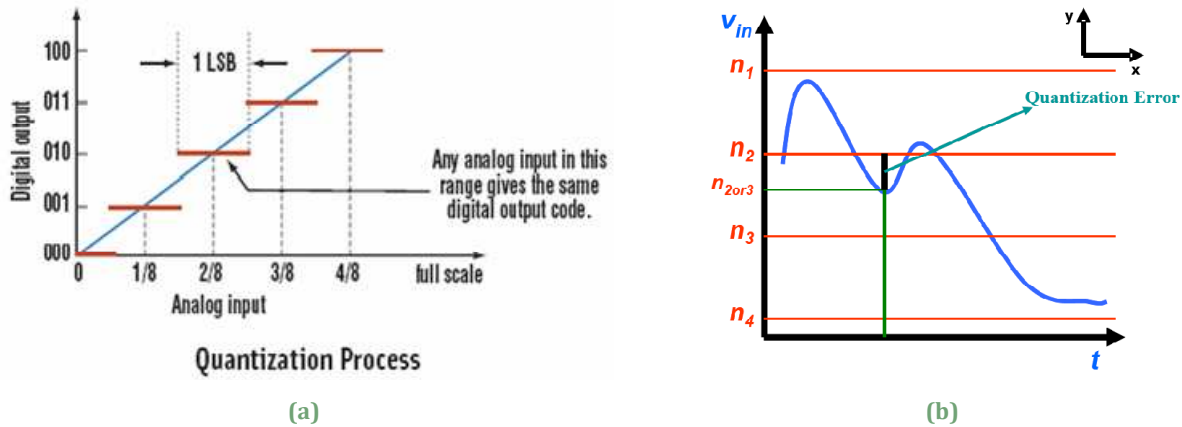


Figure 4 - (a) Quantization Process [8] and (b) Quantization Error Illustrations (right) [4]

As Figure 4 shows, an analog input is quantized to a digital value. However, as Figure 4 indicates, there is always a margin where the input value falls between two quantization levels, giving the ADC its quantization error. Improving this margin correlates to increasing the ADCs resolution.

Total Harmonic Distortion

The concept of total harmonic distortion (THD) applies mostly to nonlinear systems where the power is present in the fundamental frequency as well as its harmonics. This presence of power in other frequencies contributes to THD. In general, total harmonic distortion is defined as the ratio of all harmonics generated to the original signal frequency [5]. Mathematically it is mainly expressed in units of dB by the following relationship [9],

$$THD = 10 \log \left(\frac{V_{h2}^2 + V_{h3}^2 + V_{h4}^2 + \dots}{V_f^2} \right) \quad \text{Eq. 4}$$

where V_{hn} is the voltage corresponding to the n-th harmonic of the signal and V_f is the fundamental's voltage.

THD can also be represented as a percentage,

$$THD = \frac{\sqrt{V_{h2}^2 + V_{h3}^2 + V_{h4}^2 + \dots}}{V_f} \times 100 \quad \text{Eq. 5}$$

Total harmonic distortion is especially important in ADCs when building the input and sampling blocks, as this report will further detail in its design section.

2.3 OVERSAMPLING CONVERTERS

As mentioned in Section 2.1, one of the major types of converters is the oversampling ADC, which exists in many variations. Oversampling ADCs are characterized as such due to having their sampling frequency being much greater than twice the bandwidth of the signal, i.e. $f_n > 2 \cdot (Bandwidth_{signal})$. These types of circuits are implemented when attempting to obtain very high accuracy. This is possible because complex and precise analog circuitry is substituted by the oversampling ADC's use of digital signal processing techniques. The sacrifice that is made in this case is the throughput that can be achieved [3].

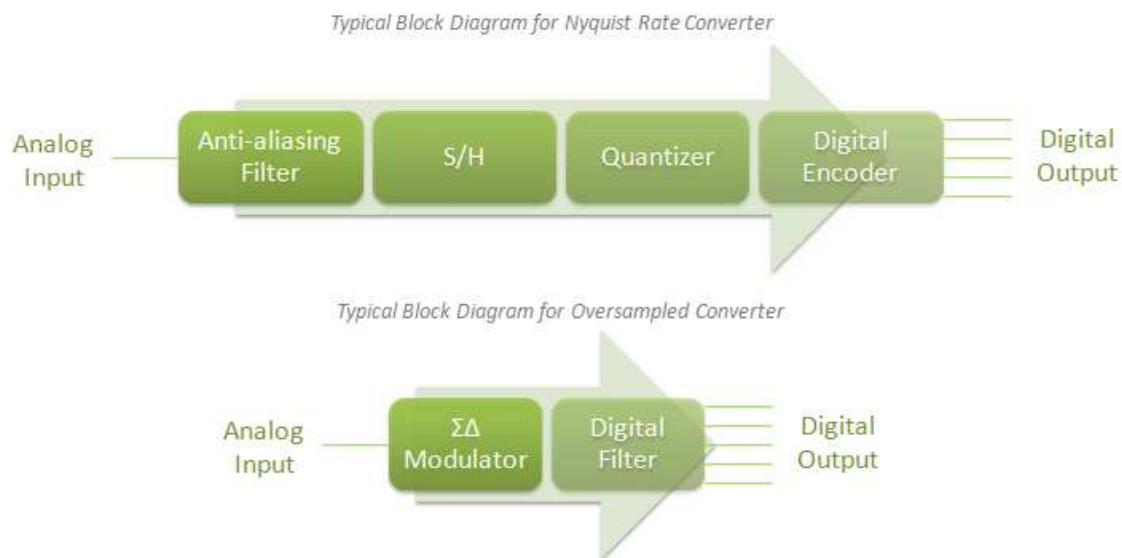


Figure 5 - Block Diagrams for Nyquist and Oversampled ADCs

One of the advantages of oversampled ADCs is that aliasing is much less of a concern, in comparison with Nyquist ADCs [3]. That is because the signal's frequency spectrum has frequencies much more widely spaced, since the sampling rate is much greater than the signal's bandwidth. A disadvantage of oversampling converters is that a large amount of samples are required to perform a conversion to a desired accuracy, versus the Nyquist ADCs, in which every conversion yields an individual result.

Oversampled ADCs are a good option for converters where the signal is band limited, like music systems, etc. Since this project does not deal with an oversampling converter, we will not delve into more detail concerning oversampling converters.

2.4 NYQUIST CONVERTERS

A Nyquist ADC is a type of ADC that can resolve frequencies up to $\frac{1}{2}$ the sampling frequency. This is the sampling rate adequate for recovering the original signal according to the Nyquist theorem, i.e. $f_n = 2 \cdot (Bandwidth_{ADC})$, where f_n is the sampling frequency of the converter. There are several types of Nyquist ADCs in the analog design world. Johns and Martin [9] compares the present ADC types with their common uses in terms of speed and accuracy, shown below:

Table 2 - Speed and Accuracy Correlation with ADCs

Low-to-Medium Speed, High Accuracy	Medium Speed, Medium Accuracy	High Speed, Low-to-Medium Accuracy
Integrating	Successive Approximation	Flash
		Two-Step
		Interpolating
		Folding
Oversampling	Cyclic	Pipelined
		Time-Interleaved

In the background portion of this paper, we will overview three types of converters that have been recently used in the NECAMSID Lab: Pipelined, Successive Approximation, and Cyclic.

2.4.1 PIPELINED ADCs

A common ADC structure, the pipeline converter receives its name from its multistage nature.

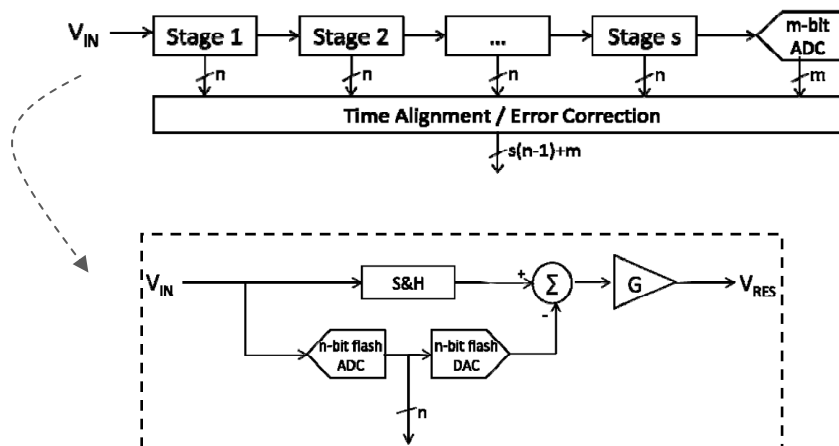


Figure 6 - Block Diagram of a 16-bit Pipelined ADC [8]

As Figure 8 shows, the analog input voltage V_{IN} is sampled and enters the ADC. Each stage of the converter is responsible for the quantization of a range of bits. Once a stage is completed, its output residue voltage becomes the next block's input. A final block, containing an n-bit ADC resolves the less significant bits of the converter. Finally a digital block receives each block's output and corrects for time and errors. The final decision is then composed.

2.4.2 SUCCESSIVE APPROXIMATION ADCs

Successive-approximation ADCs are one of the most popular techniques for analog-to-digital conversion since they are fairly quick in terms of conversion time, while having moderate circuit complexity. There are several configurations that would qualify as successive-approximation converters. For brevity of this report, we will elaborate on main successive-approximation concept and a few variations. For more complete descriptions of different types of successive-approximation ADCs refer to [9].

Some authors recommend that the reader compare the functionality of a basic successive-approximation converter as a "binary search" algorithm[9]. An interesting way to think about this algorithm is to imagine a book with 256 pages, in which you have to guess the page number containing a specific event in the novel. However, you are only allowed to ask "yes/no" questions. Therefore, using the binary search algorithm, one would try to approximate the number by first asking the owner of the book if the event occurs on a page number greater than 128. If the answer is no, then the next question would then address if the event occurs on a page number greater than 64. If so, then the remaining page range would then be divided by two and the same process would be repeated. A flow chart presented by [10] is shown below:

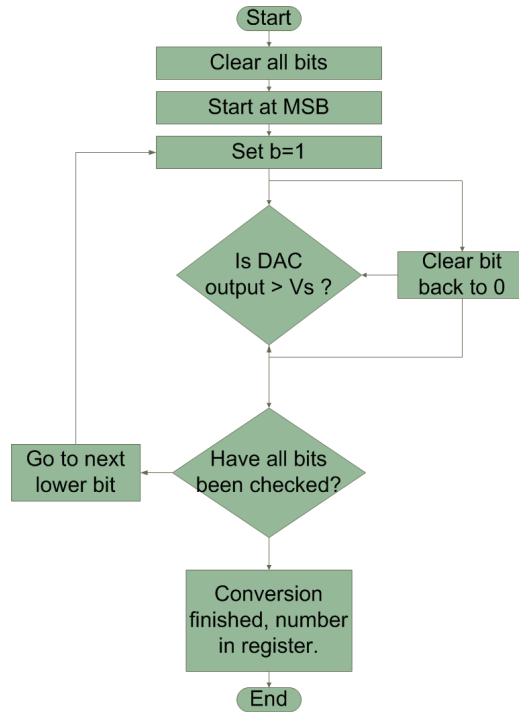


Figure 7 - Flow Chart of Successive-Approximation Approach

The successive-approximation approach is similar to the anecdote above. The ADC works by successively determining the bits of the output starting from the most significant bit (MSB) and then checking the next bits. However, this method is very primitive for the world class types of ADCs found today. Therefore, many improvements to that concept have been added, such as a digital-to-analog converter (DAC) based approximation, using a block known as the Successive-Approximation Register (SAR). A simple diagram of this functionality is shown below:

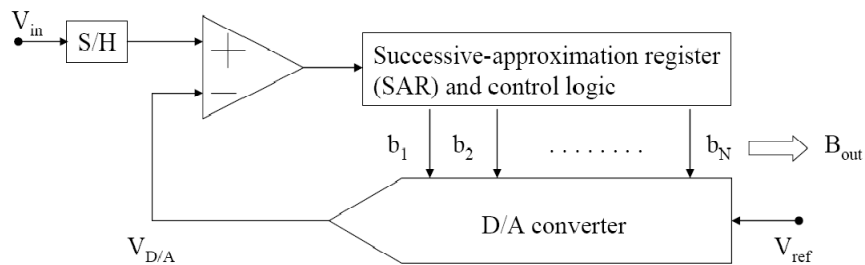


Figure 8 - DAC-based Successive-Approximation Converter [9]

In this case, a sample-and-hold block is usually needed so that the value being converted remains constant through the conversion. The SAR is entirely digital and the DAC's specifications will mostly determine the speed and accuracy of the converter.

2.4.2.1 Charge Redistribution ADC

Shown in figure Figure 9 is an example of a charge-redistribution ADC [9]. In this case, an array of capacitors is used. Its advantage is that the sample and hold, DAC, and comparator blocks are all combined into one block. The following chart explains the operation of Figure 9:

Table 3 - Charge-Redistribution (Figure 9) ADC Explanation

Operation Mode	Description
Sample	<ul style="list-style-type: none">– All but the largest capacitor are charged to input voltage V_{in} while comparator is being reset.– The largest capacitor is set to $V_{ref}/2$
Hold	<ul style="list-style-type: none">– Comparator is taken off reset mode.– Capacitors are switched to ground, with the exception of largest capacitor, causing voltage on negative terminal of comparator V_x to become $-V_{in}/2$.
Bit Cycling	<ul style="list-style-type: none">– If V_{in} is negative, the largest capacitor is switched to ground.– If V_{in} is positive, the largest capacitor is remains at $V_{ref}/2$.

Johns and Martin [9] catalogue other more complex types of SAR ADCs, which include calibration and error correction blocks.

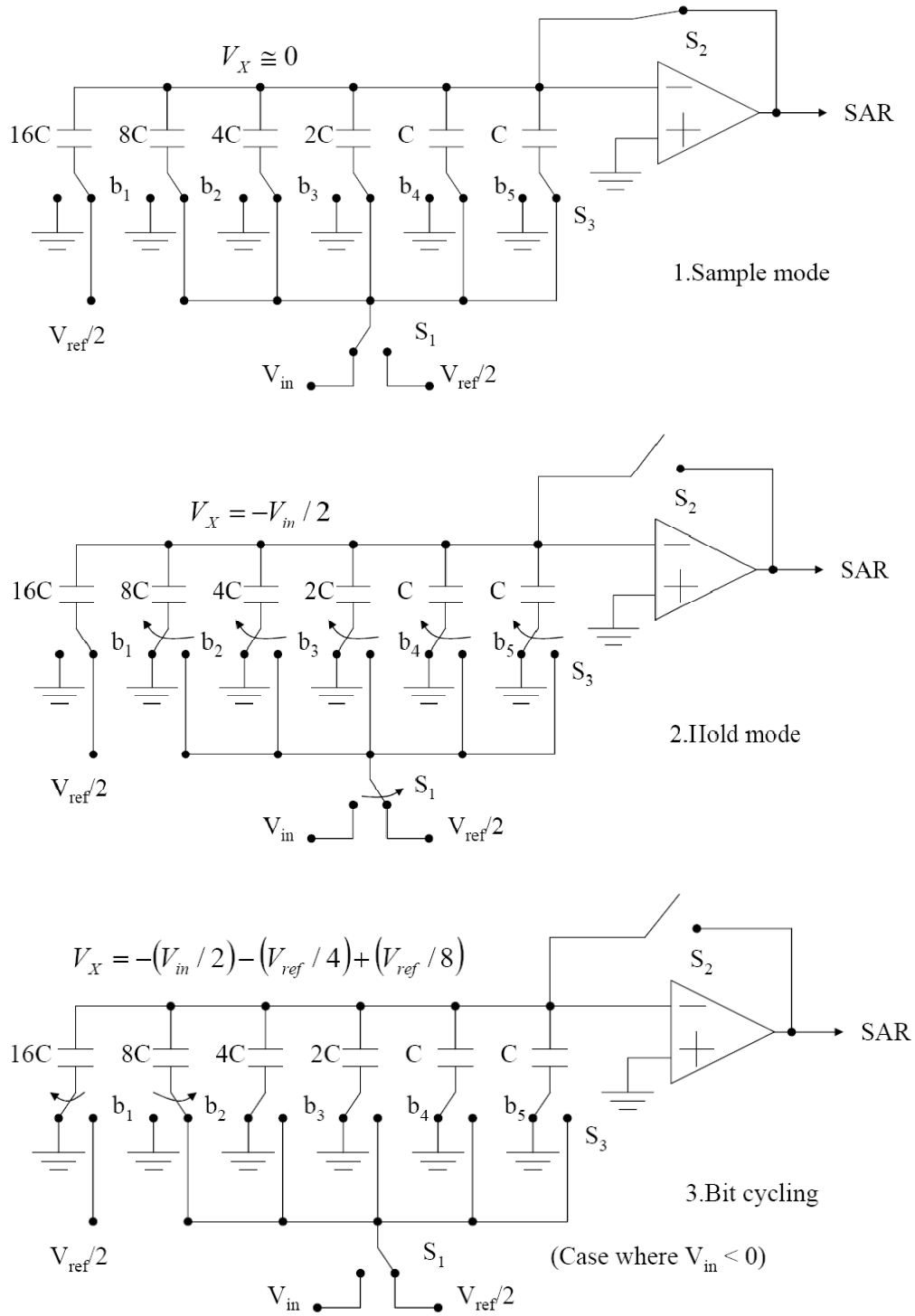


Figure 9 - 5-bit Charge-Redistribution ADC [9]

2.4.3 THE CYCLIC ADC

A Cyclic converter, also known as an Algorithmic converter, is similar in operation to the successive approximation converter. However, in the case of the Cyclic ADC, the reference voltage is not altered. Instead, the error (or residue) of the amplifier is doubled [9].

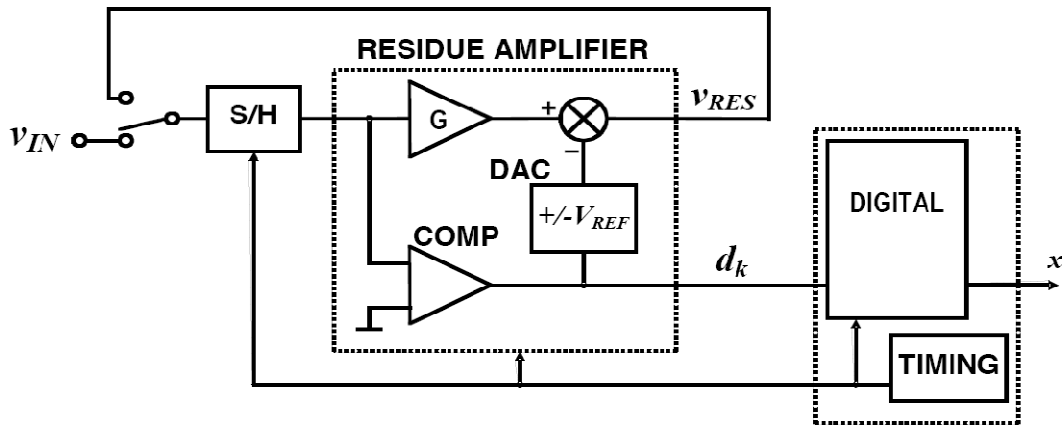


Figure 10 – High Level Block Diagram of a Cyclic Converter [11]

As the block diagram above outlines, the operation of the cyclic converter functions in the following manner: First, the input voltage is sampled by the sample-and-hold block. That value is then compared to a threshold voltage, upon which a digital decision is made, determining a bit value in the final sequence of the number sampled. A reference voltage is generated by a 1-bit digital-to-analog converter which is dictated by the digital decision previously made. At the same time, the input value is amplified by a factor two (ideally). The amplified value is then summed to a reference voltage $\pm V_{REF}$, leaving a residue voltage. The residue voltage then becomes the input of the residue amplifier. This cycle is repeated enough times required to achieve the desired resolution, earning the device its name. The sequence of decisions corresponds to the output value of the ADC.

2.4.3.1 Understanding the Residue Amplifier

A major part of the cyclic ADC is the residue amplifier. Therefore, in order to better comprehend the operation of the ADC, we can take a mathematical approach to explain this concept[11]. The equation below shows the relationship between the residue amplifier's input and output:

$$v_{res_{out}} = G \cdot v_{res_{in}} - d \cdot V_{ref} \quad \text{Eq. 6}$$

where G is the gain of the amplifier and d is the digital decision.

Assuming ideal conditions, after performing N cycles, the amplifier exhibits the following negative feedback loop relationship:

$$v_{res_{out}(N)} = [G^N \cdot v_{res_{in}}] - [G^{N-1}d_1 + G^{N-2}d_2 + \dots + G^0d_N] \cdot V_{ref} \quad \text{Eq. 7}$$

We can also predict the output code of the ADC by rearranging Eq. 7 into the following form[11]:

$$\frac{v_{res_{in}}}{V_{ref}} = \left[\frac{1}{G}d_1 + \frac{1}{G^{N-1}}d_2 + \dots + \frac{1}{G^N}d_N \right] - \left[\frac{1}{G^N} \frac{v_{res_{out}(N)}}{V_{ref}} \right] \quad \text{Eq. 8}$$

We can define the $\left[\frac{1}{G^N} \frac{v_{res_{out}(N)}}{V_{ref}} \right]$ term of the equation as the quantization error, and the first term as the output code x:

$$x = \left(\frac{1}{G}\right) d_1 + \left(\frac{1}{G}\right)^2 d_2 + \dots + \left(\frac{1}{G}\right)^N d_N \quad \text{Eq. 9}$$

A plot relating the residue amplifier's input and output can be created, as shown below:

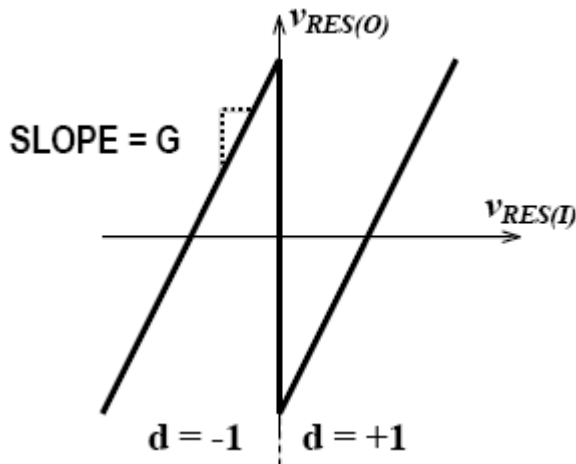


Figure 11 - Residue Plot at G=2 [11]

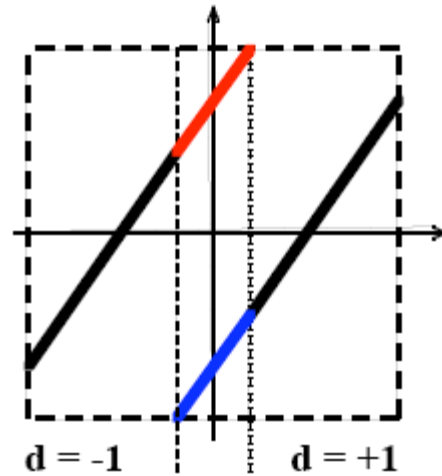


Figure 12 - Residue Plot with G < 2[11]

However, maintaining a constant gain of 2 may be challenging. Therefore, when $G < 2$, the residue plot would look like Figure 12. This event makes it possible for two possible decisions for the same input value, adding redundancy to the ADC. However, at the same time, it adds a level of complexity to the calibration of the converter, which will be discussed in a further section of the document.

2.5 THE ROLE OF CAPACITORS

As the previous section has outlined, the used of capacitors for ADCs is very common. In our, as the design sections of this paper will indicate, relies heavily on the use of multiple capacitors that will be switched constantly to perform the cyclic function of our ADC. Therefore, we must understand how they will affect our circuit and what constraints we are faced with when choosing the correct capacitors for our circuit.

2.5.1 THERMAL NOISE

Thermal noise is inherent to all electronic circuits and it is caused by a random motion of electrons in a conductor. It is a function of temperature and is constant over all frequencies. When designing an analog to digital converter, this noise must be accounted for in the design of the sampling capacitors. That way, the sample-and-hold amplifier (SHA) will achieve desirable signal-to-noise ratios. Since the SNR is the integral of all the noise in a system, the lower the noise bandwidth, the less noise is sampled by the ADC. Figure 13 below shows a model of a sample and hold switch with a dc input and a thermal noise.

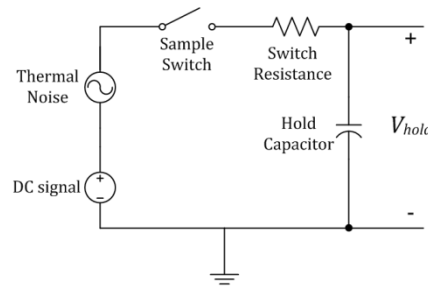


Figure 13- Diagram of Hold capacitor with Thermal Noise

When the sample switch is opened the voltage on the capacitor is the DC signal and the thermal noise at the instant the switch is opened. Since the characteristic of the sample and hold circuit is a low pass filter the noise above the cutoff frequency of the circuit is attenuated. In order to reduce the bandwidth of the noise the hold capacitor must be sized according to the SNR needed.

The equation below shows the relationship of capacitance and temperature to the RMS noise of a system, which is the ratio of capacitor size to the total thermal noise power of the RC circuit.

$$RMS\ noise = \sqrt{\frac{KT}{C}} \quad \text{Eq. 10}$$

2.6 OPTIONS FOR OUTPUT DRIVING

Every analog-to-digital converter has to interact with an off-chip digital domain, usually an FPGA or a computer. Although sometimes designers may choose additional output drivers in their circuit at the expense of simplicity, there are methods used to improve output performance. In this case, various methods were researched. One particular method, known as Low Voltage Differential Signaling (LVDS), showed itself to be a promising option for our circuit. Section 2.6 outlines the existing configurations and applications of LVDS.

2.6.1 UNDERSTANDING LVDS

Usually used for output blocks of ADCs, Low-Voltage Differential Signaling is a technology that was officially introduced in 1994 by National Semiconductor. It was born out of the necessity to create high performance solutions that consume little power and are susceptible to less noise than the common techniques of the time, while being cost-effective, such as RS-442 and RS-485 standards. A competing technology was Emitter Coupled Logic (ECL). However, it is incompatible with standard logic levels, uses negative power rails, and leads to high chip-power dissipation [12].

Table 4 - Comparison Table of Differential Standards

Parameter	RS-422	RS-485	ECL	LVDS	M-LVDS
Bus	Point-to-Point Multidrop	Point-to-Point Multidrop Multipoint	Point-to-Point Multidrop Multipoint	Point-to-Point Multidrop	Point-to-Point Multidrop Multipoint
Termination	100 Ω	50-60 Ω	depends	100 Ω	50 Ω
Signal Swing	2 V min	1.5 V min	0.8 – 1 V	250-450 mV	480-680 mV
Threshold	+/-200 mV	+/-200 mV	+/-200 mV	+/-100 mV	+/-50 mV
Common Mode Range	+/-7 V	-7 to +10 V	depends	+/-1 V	+/-2 V
Standard	TIA/EIA-422-B	TIA/EIA-485-A	none	TIA/EIA-644-A	TIA/EIA-899
Power	moderate	moderate	high	very low	low
Speed	< 10 Mbps	< 10 Mbps	< 2 Gbps	< 2 Gbps	< 500 Mbps

2.6.2 THE CONCEPTS BEHIND LVDS

LVDS, as the name suggests, is differential – meaning that it makes use of two signals to function. At the cost of using an extra trace, space, and power, noise is considerably reduced through common-mode rejection. As a consequence, many improvements can be made to the design, such as:

- Signal swing can be dropped to only a few hundred millivolts due to signal-to-noise rejection improvement
- Rise time is shorter, resulting in faster data rates
- Very low power consumption across a wide range of frequencies due to low swing and current-mode driver outputs
- Digital crosstalk onto analog circuitry is reduced

2.6.3 DIFFERENT TYPES OF LVDS

The table below shows the different variations of LVDS found in the market today:

Table 5 - Industry Standards for Various LVDS Technologies [13]

	Industry Standard	Maximum Data Rate	Output Swing (V_{OD})	Power Consumption
LVDS	TIA/EIA-644	3.125 Gbps	± 350 mV	Low
LVPECL	N/A	10+ Gbps	± 800 mV	Medium to High
CML	N/A	10+ Gbps	± 800 mV	Medium
M-LVDS	TIA/EIA-899	250 Mbps	± 550 mV	Low
B-LVDS	N/A	800 Mbps	± 550 mV	Low

While the concept of LVDS is the foundation of the standards found in the table above, there are various applications for each one. Power consumption, performance, and target application are among the differences listed above. For brevity, we will analyze the typical LVDS standard and how it applies to this project. If applicable, the other technologies may be explored.

Different Configurations of LVDS

There are three common Bus types of LVDS configurations. They are:

- Point-to-Point
- Multidrop
- Multipoint

2.6.3.1 Point-to-Point

Being the simplest configuration, Point-to-Point offers a direct path from the transmitter to the receiver. This is favorable for use in the highest data rates, due to the simple path. A variation of this configuration can be seen in Figure 15. All figures in this section are extracted from [12].

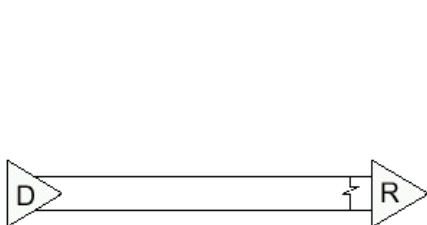


Figure 14 - Point-to-Point Configuration

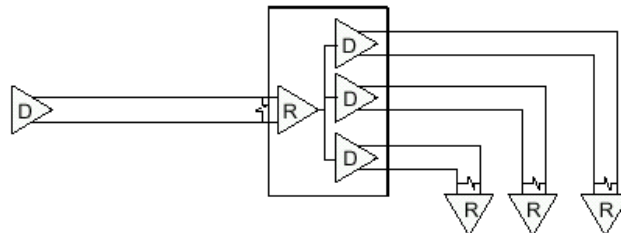


Figure 15 - Data Distribution Using Point-to-Point Configuration

2.6.3.2 Multidrop

Multidrop is most efficient when various parts of a circuit need to receive the same information. There is one driver and two or more receivers along the bus, as the figure below illustrates:

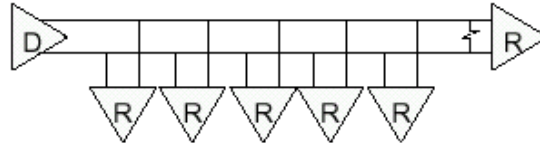


Figure 16 - Multidrop Configuration

2.6.3.3 Multipoint

A multipoint configuration uses various drivers and receivers. The advantage to this circuit is that it can send information from multiple areas of the circuit, if necessary. However, this configuration can get quite complex and speeds are generally lower than the other simpler configurations.

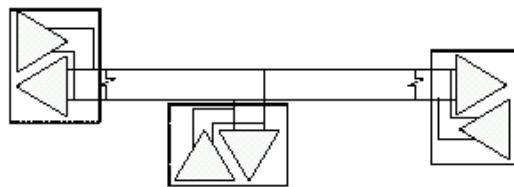


Figure 17 - Example of a Three-Node Multipoint Configuration

2.6.4 CONTRASTING LVDS TYPES AND CONFIGURATIONS

The article released by National Semiconductor entitled “The Many Flavors of LVDS” [12] summarizes the available technologies with the configurations used by them. This matrix is shown below:

Table 6 - Bus Configurations vs. Standards

Bus Configuration	LVDS	BLVDS	M-LVDS	GLVDS	LVDM
Point-to-Point	★	★	★	★	★
Multidrop	★	★	★		■
Multipoint		★	★		■
Multipoint (Backplane)		★	★		

★ = full support
 ■ = restrictions may apply

2.6.5 A TYPICAL LVDS CIRCUIT

The following picture illustrates a high-level configuration for a LVDS circuit. Notice the detail showing the reduction in interference due to the interaction in electric fields between the wires, which are usually placed as a twisted pair.

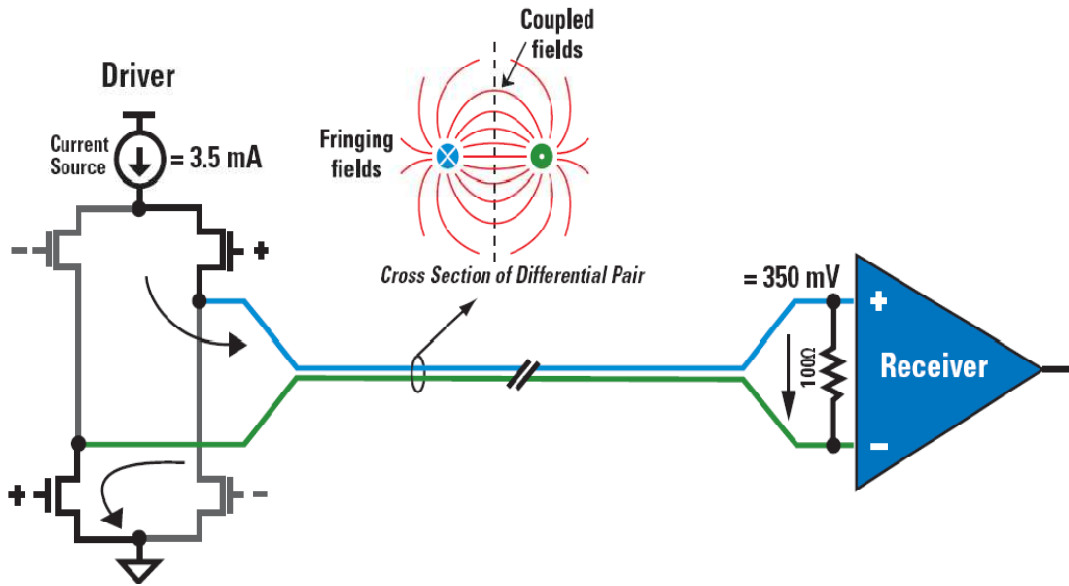


Figure 18 - LVDS Driver and Receiver [13]

In the driver-receiver configuration shown in Figure 18, a 3.5mA current source is found in the driver. Due to the high impedance “op-amp characteristic” of the receiver, all of the current flows through the 350mV resistor in place. When the driver makes a switch, the current changes direction of flow across the resistor and results in a logic state “one” or “zero.” Figure 19 illustrates this concept.



Figure 19 - Digital Signaling Model

2.6.6 APPLICATIONS

There are various applications for LVDS. As previously mentioned, the advantages presented by LVDS make it a popular technology. Listed below are three common applications of LVDS within integrated circuits.

- **Line drivers/receivers** – Commonly used to convert single-ended signals into formats for transmission over a cable or backplane.
- **SerDes** – Serializer/deserializer pairs are used to multiplex a number of low-speed CMOS lines and to transmit them as a single channel running at a higher data rate.
- **Switches** – Used instead of bus architectures for high data rates. Commonly used for clock distribution. LVDS is one of the most suitable signaling standards for clocks of any frequency because of reliable signal integrity.

2.6.7 ASSESSING LVDS IN THE ADC DESIGN PROCESS

There are various factors to consider when choosing a signaling standard, such as:

- Required bandwidth
- Ability to drive cables, backplanes, or long traces
- Power budget
- Network topology (point-to-point, multidrop, multipoint)
- Serialized or parallel data transport
- Clock or data distribution
- Compliance to industry standards
- Need or availability of signal conditioning

2.7 THE SPLIT-ADC CONCEPT

One of the key characteristics of our project is that it is meant to use a Split-ADC architecture. The figure below illustrates the basic principle of the split-ADC. Instead of using one converter, the chip will have two ADCs performing the same steps over the same input. The output then becomes the average of both results. The difference of each ADC's output is then sent to the error estimation block, which is located off chip, in the digital realm [14].

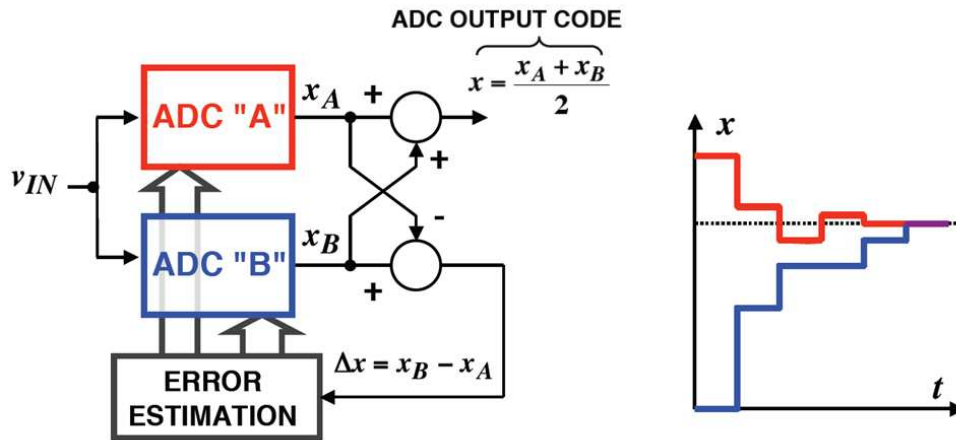


Figure 20 - Illustration of Split-ADC Concept [11]

Ideally, the concept behind the split-ADC architecture is simple to comprehend: when the difference between outputs x_A and x_B is zero, the calibration has occurred. This concept is important because it will reduce the circuit's calibration time significantly, as explained in [11]. The following graph contrasts the single ADC approach versus a split architecture.

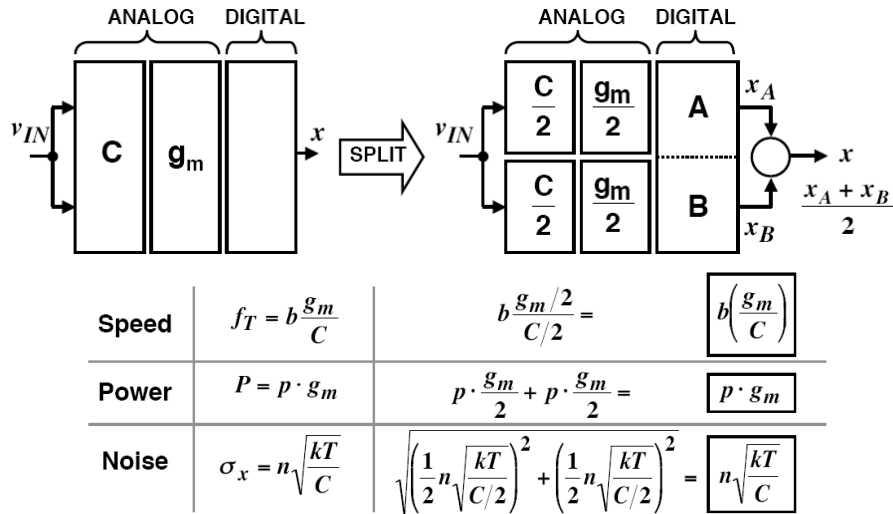


Figure 21 - Split ADC Characteristics in Contrast with Single ADC Approach

As Figure 21 shows, the trade off in complexity is small compared to the advantages in calibration. At the same time, the general speed, power and noise of circuit remains the same. This is because the same parts are used but in proportions of one half the original size.

2.8 THE CURRENT MIRROR

Biasing is very important to our project, making the necessity to build current sources imminent. One of the most common forms of creating a current source is by using a MOSFET current mirror. The current mirror relies on the assumption that transistors are closely matched, meaning that they are fabricated under the same conditions, matching closely the values of the transistors' threshold voltages, mobility, and oxide capacitance. Therefore, since this level of matching and precision can only be achieved in integrated circuits, the current is not commonly realized with discrete components. Figure 22 shows a basic configuration for a current mirror.

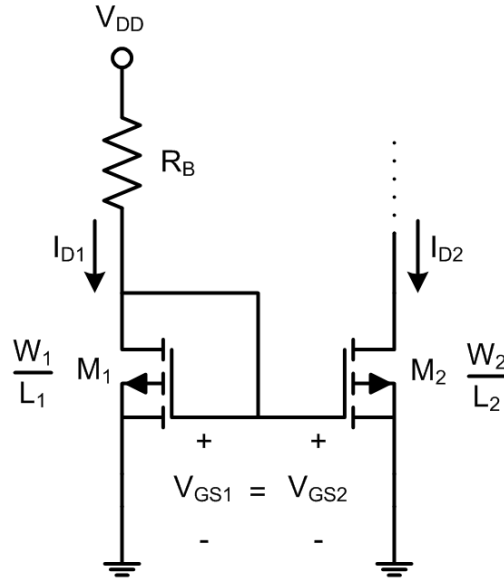


Figure 22 - Current Mirror Example

According to the MOSFET Square Law, we can define the current in the transistors as [3]:

$$I_D = \frac{\mu_n C_{ox} W}{2L} (V_{GS} - V_{th})^2 \quad \text{Eq. 11}$$

where I_D is the MOSFET drain current, C_{ox} is the capacitance of the oxide, W is the width of the transistor, L is the length, V_{GS} is the gate to source voltage and V_{th} is the threshold voltage of the transistor. Therefore for the current I_{D1} in transistor M_1 , we can solve for V_{GS1} ,

$$V_{GS1} = \sqrt{\frac{2 \cdot I_{D1} \cdot L_1}{\mu_n C_{ox} W_1}} + V_{th1} \quad \text{Eq. 12}$$

As shown in Figure 22, by tying the MOSFET gates together, we force the following relationship:

$$V_{GS1} = V_{GS2}$$

We can now input our value for V_{GS1} into the current of the second transistor:

$$I_{D2} = \frac{\mu_{n2} C_{ox2} W_2}{2L_2} \left(\sqrt{\frac{2 \cdot I_{D1} \cdot L_1}{\mu_n C_{ox} W_1}} + V_{th1} - V_{th2} \right)^2$$

Assuming the matching conditions mentioned above, we can assume that

$$\mu_{n1} = \mu_{n2}$$

$$C_{ox1} = C_{ox2}$$

$$V_{th1} = V_{th2}$$

Simplifying our results to

$$I_{D2} = I_{D1} \left[\frac{\left(\frac{W_2}{L_2}\right)}{\left(\frac{W_1}{L_1}\right)} \right] \quad \text{Eq. 13}$$

When comparing the current mirror to an ideal current source, the model falls short in a few aspects. For example, an ideal source has infinite AC impedance, while a MOS mirror has finite impedance. Also, the current mirror will have frequency limitations due to capacitive and inductive parasitics.

2.9 THE DIFFERENTIAL PAIR

The differential pair, sometimes referred to as the differential amplifier, is a vital part of our circuit. According to Sedra and Smith, “the differential pair is the most widely used building block in analog integrated-circuit design.” This is because differential amplifiers are less susceptible to noise than their single-ended counterparts and they also allow for biasing of an amplifier without the use of bypass and/or coupling capacitors, saving space on the chip being manufactured [15]. As with the current mirror, in integrated circuits, the differential pair relies largely on the ability to match components.

The differential pair can be used in various configurations. In this section we will explore two modes of operations: common-mode and differential gain modes. An example of a differential pair is shown below:

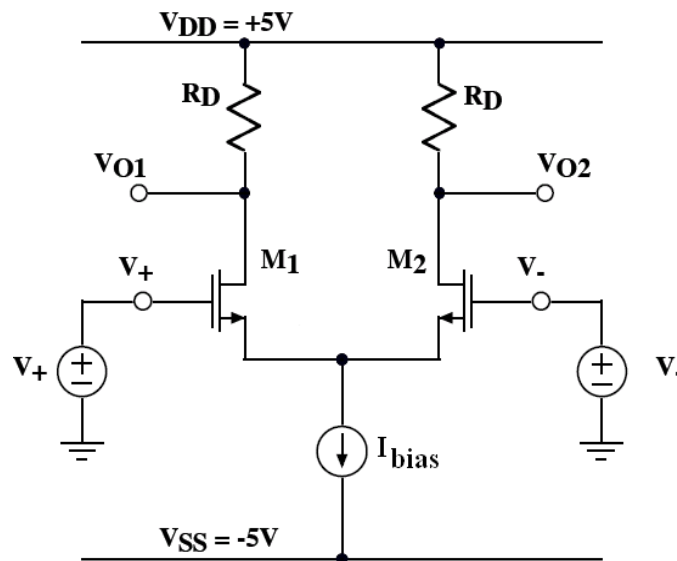


Figure 23 - Differential Amplifier Example [16]

The differential pair consists of a symmetrical system of two MOSFETS sharing the same bias current. The parameters in each transistor can be extracted using the square law equation, seen in Eq. 11:

$$I_D = \frac{\mu_n C_{ox} W}{2L} (V_{GS} - V_{th})^2$$

where the currents at each transistor are equal to $\frac{I_D}{2}$.

2.9.1 BARTLETT'S BISECTION THEOREM

The functionality of the system can be explored using Bartlett's Bisection Theorem, which is based on the symmetry of circuits and explores the fact that any two inputs can be represented in a common mode and a differential mode.

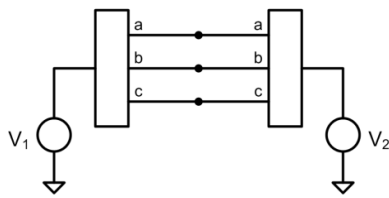


Figure 24 - Amplifier Model

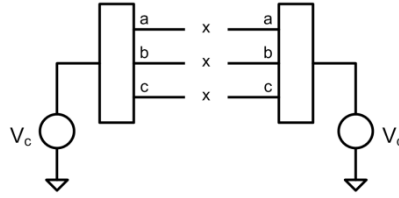


Figure 25 - Common Mode Model

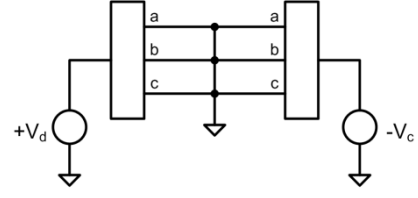


Figure 26 - Differential Mode Model

The common-mode voltage can be defined as:

$$V_c = \frac{V_1 + V_2}{2} \quad \text{Eq. 14}$$

And the differential voltage as:

$$V_d = V_2 - V_1 \quad \text{Eq. 15}$$

Using this concept, we can also verify that:

$$V_1 = V_c - \frac{V_d}{2} \quad \text{Eq. 16}$$

and

$$V_2 = V_c + \frac{V_d}{2} \quad \text{Eq. 17}$$

We can represent the half circuit of each circuit model for the example in Figure 23 using the bisection theorem, as shown below:

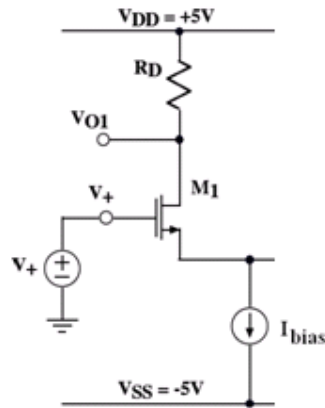


Figure 27 - Half-Circuit Model of the Common Mode

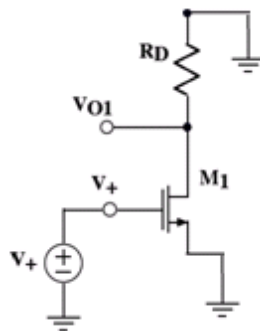


Figure 28 - Half-Circuit Model of the Differential Mode

A graph of the large signal characteristics of the differential pair is shown below:

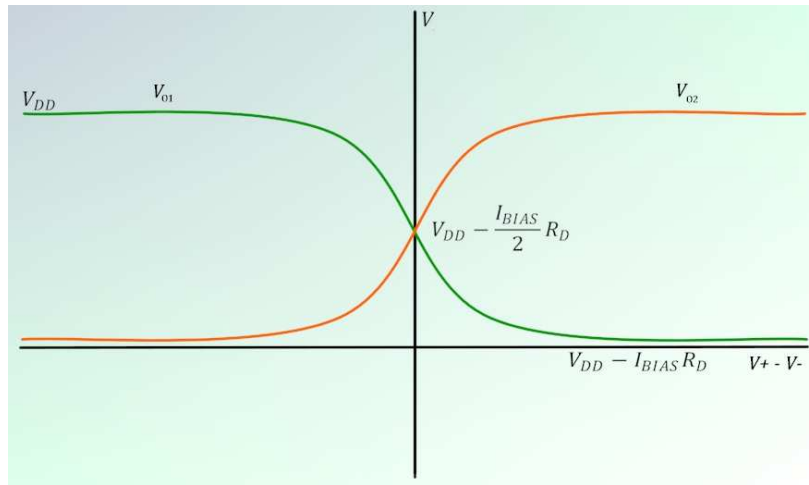


Figure 29 - Signal Input-Output Characteristics of the Differential Input to Each Output

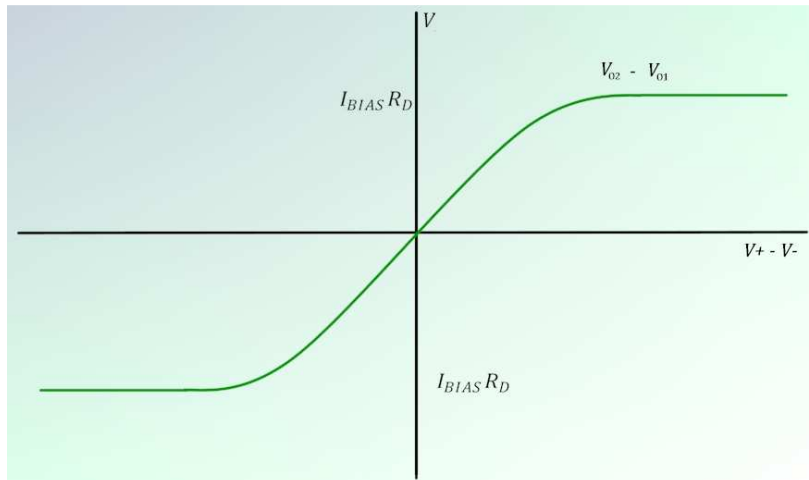


Figure 30 - Large Signal Input-Output Characteristic for the Differential Input to the Differential Output

To simplify calculations and circuitry it is common practice to attempt to operate with the linear areas of the curves shown above. As we said in the introduction, one of our project's major steps is that non-linearity is not as much of a pertinent issue to our circuit, as we will see in later sections.

3 HIGH-LEVEL DESIGN

The objective of this section is to give a brief high level overview of the integrated circuit being designed for this project.

3.1 BLOCK DIAGRAM

The figure below displays a proposed block diagram for the device. Several sub blocks are displayed in the diagram. This approach gives us a modular idea of the design.

They main blocks found in our design are:

- Switch Capacitor Array
- Open Loop Differential Amplifier
- Bias Circuitry
- Comparator Network
- Logic Sub Block
- Output Drivers

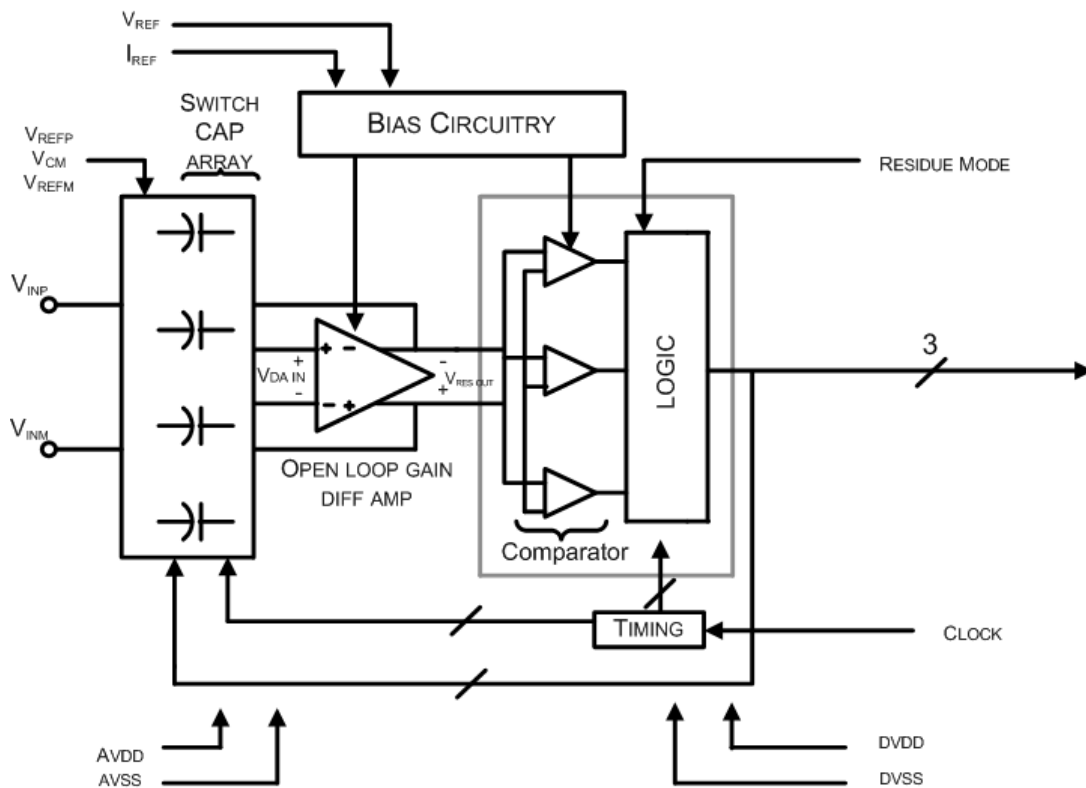


Figure 31 - Block Diagram

The next sections of the report will dissect every one of the blocks mentioned above and will outline how we implemented each portion of the circuit.

4 THE INPUT BLOCK

The input of our ADC is composed of a sample-and-hold circuit which enables us to obtain the analog input into the input capacitors. Our input block can appear quite complex at first, since we are using multiple capacitors. Therefore, for simplicity and visualization of concept, we will first start with a basic concept for the input block, shown below:

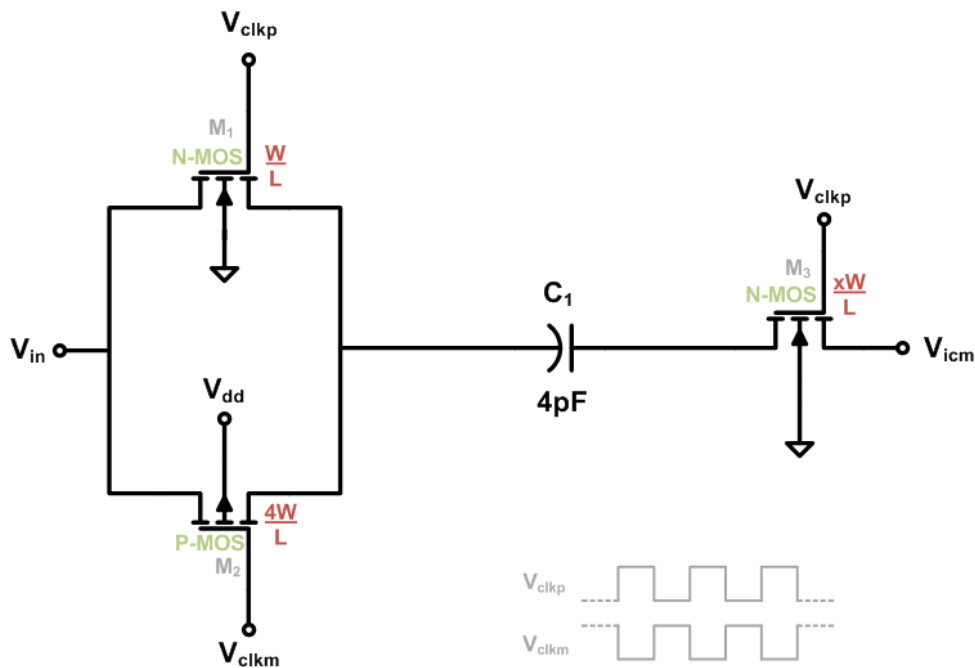


Figure 32 - Schematic of Input Block

As the figure above shows, in this simplified version of the input block, the input voltage V_{in} is sampled onto capacitor C_1 . It is done so through a CMOS transmission gate, a configuration involving a pair of opposite type MOSFETs. The use of transmission gates eliminates the undesirable threshold voltage effects which give rise to loss of logic levels [3]. The capacitor is sampled at every positive edge of the clock cycle, indicated in this case as V_{clkp} , and at every negative edge of its inverted version, V_{clkp} , to bias the p-channel transistor.²

² Note: Biasing for transistor M_3 is simplified. In actual implementation, the gate voltage on M_3 in Figure 32 is delayed slightly to reduce charge injection.

4.1 TRANSISTOR SIZE OPTIMIZATION

Transistors in this block need to be properly sized to accommodate our circuit. This task is more important than it seems. The transistor sizes will help determine and/or improve several factors of the ADC, such as spurious-free dynamic range and total harmonic distortion. Therefore, an optimization exercise was necessary to determine the correct widths of the transistors which would meet our goals for distortion and acquisition time.

4.1.1 DEALING WITH THE PRESENCE OF DISTORTION

One might wonder why distortion is such an important issue to such a simple circuit, like our input block. The key is that distortion is present due to variations on the gate voltage. We'll start by looking at the equation for the "on" resistance of the MOSFET:

$$R_{DSon} = \frac{V_{DS}}{I_D} = \frac{1}{\mu_n C_{ox} \frac{W}{L} (V_{GS} - V_{TH})} \quad \text{Eq. 18}$$

All of the values in Eq. 18 are mostly constant, with the exception of the voltage from gate to source, which changes due to the varying source voltage due to the input signal. This change in V_{GS} causes the internal resistance of the transistors to change as well. Since the transistor sizes will be different, the values in R_{DSon} will not change uniformly. All of these factors contribute to distortion of the signal.

4.1.2 PERFORMING A PARAMETRIC ANALYSIS

Our goal for this analysis was to determine the appropriate input block's transistor widths. From previous design experience, professor McNeill recommended the following assumptions:

- The p-channel (M_2) transistor will have a width that is 4 times larger than its n-channel MOSFET equivalent
- The n-channel MOSFET (M_3) on the top plate of the capacitors should have a width proportional (by a factor of x), but not necessarily equal, to the n-channel MOSFETs (M_1) on the bottom plate

We can look at this issue as a matter of how much total transistor width we can afford in the chip, in terms of chip area. Therefore, we can determine the total width, W_{Total} , as a function of M_1 's width, as shown below:

$$W_{Total} = W_{Q_1} + W_{Q_2} + W_{Q_3} = W + 4W + xW \quad \text{Eq. 19}$$

Rearranging,

$$W_{Total} = (5 + x) \cdot W$$

$$W = \frac{W_{Total}}{(5+x)} \quad \text{Eq. 20}$$

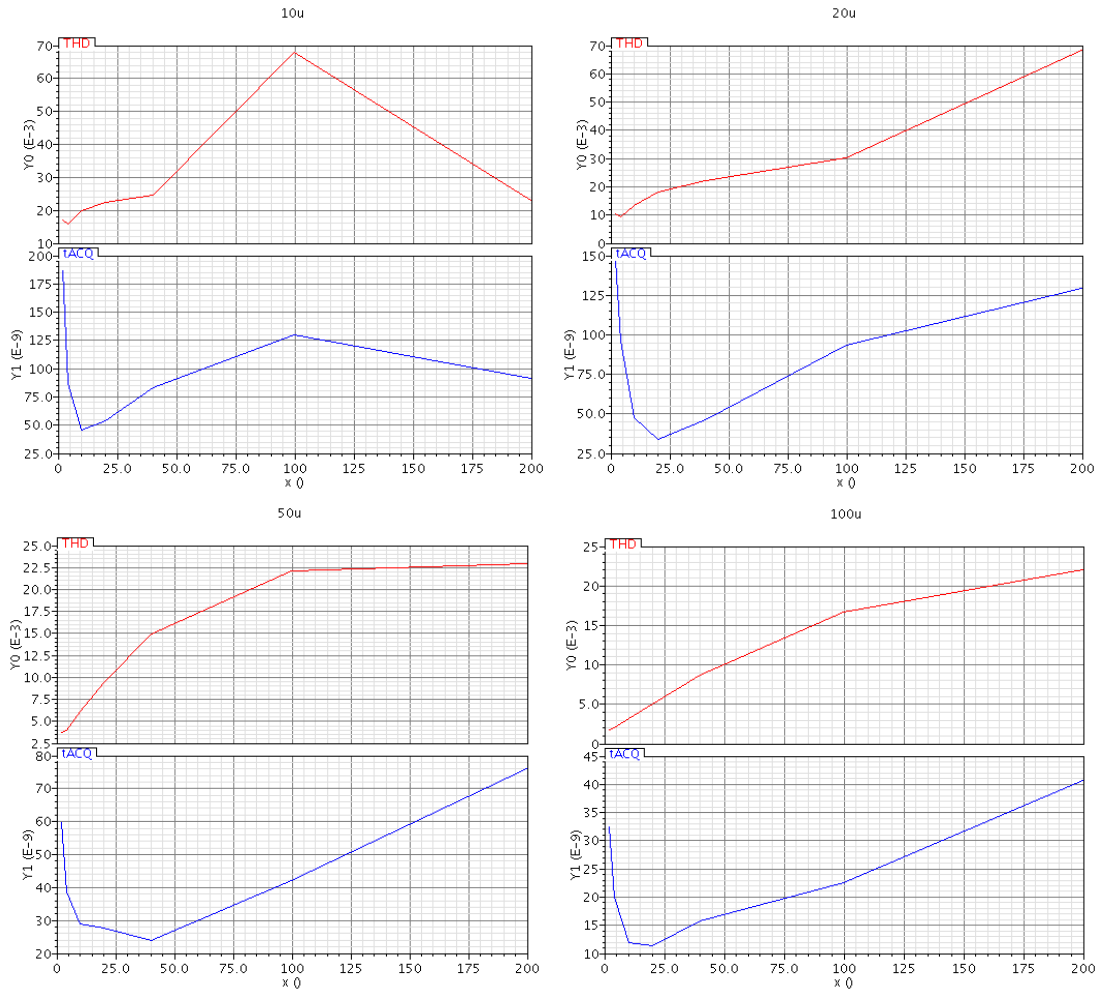
As a result, we created a series of graphs, where the values for x , W , and W_{Total} were swept, to find the smallest transistors that would fit our needs. The two main characteristics that relate to these values are acquisition time and total harmonic distortion. To deliver values for those attributes, we had to run several parametric equations on Cadence. The following table indicates the values that were simulated:

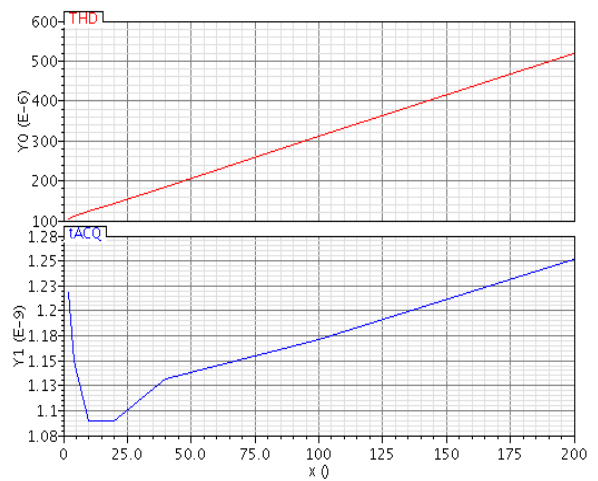
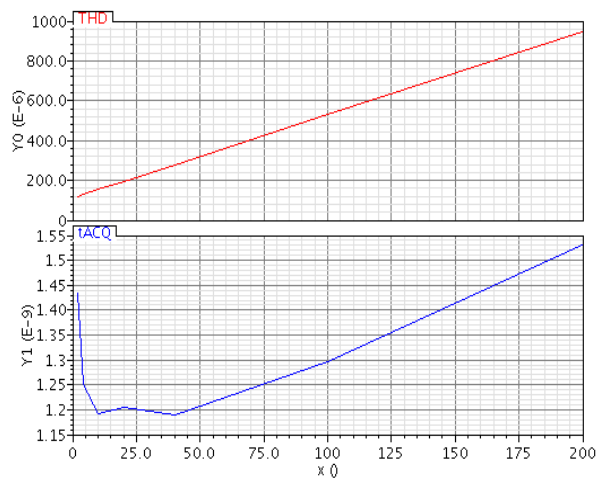
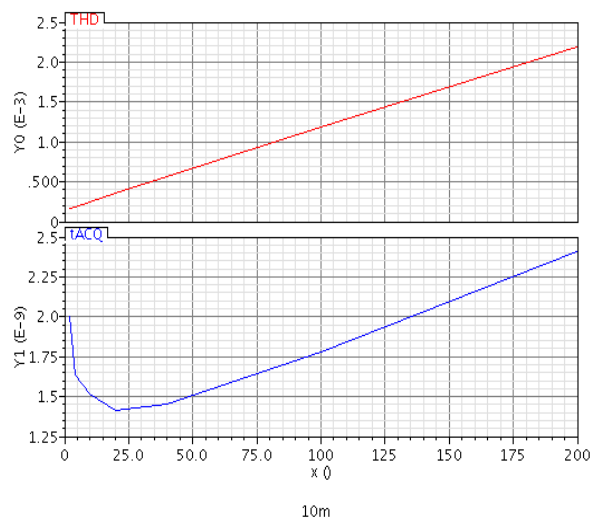
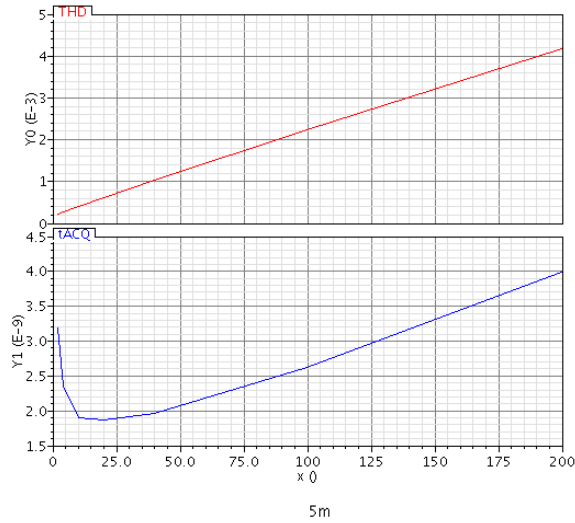
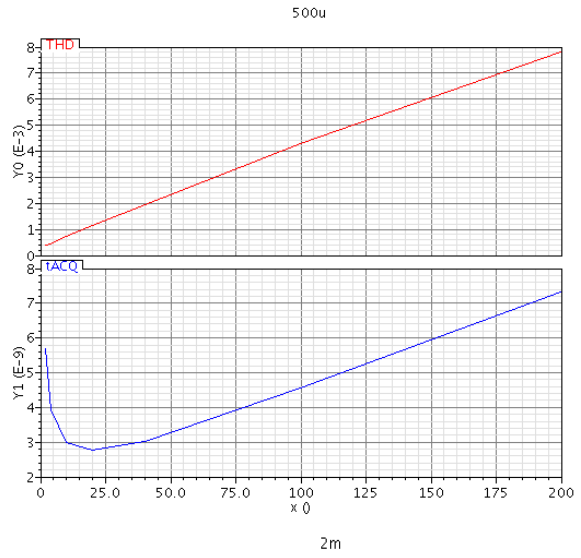
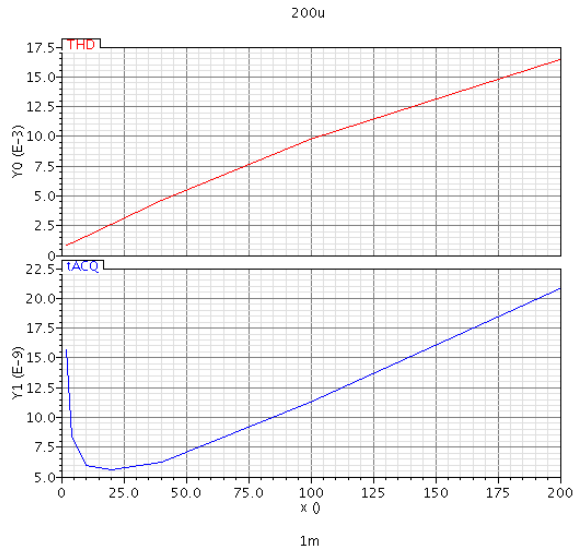
Table 7 - Swept Attributes

x	0.1	0.2	0.5	1	2	5	10			
W_{Total}	10 μm	20 μm	50 μm	100 μm	200 μm	500 μm	1mm	2mm	5mm	10mm

The title of each graph indicates the values used for W_{Total} . On the y-axis, the red lines indicate THD and the blue lines indicate acquisition time. The x-axis indicates the value of x .

Note: The values of x are scaled by a factor of 20, in order to accommodate simulation criteria in Cadence.





The results are summarized in the table below:

Table 8 - Summarized Optimization Results of t_{ACQ} and THD

W_{Total} [μm]	x	t_{ACQ} [ns]	THD [%]
10	0.25	85	1.8
20	0.5	50	1.0
50	0.5	30	0.6
100	0.5	12	0.3
200	0.5	6	0.15
500	0.5	3	0.06
1000	0.5	1.9	0.035
2000	0.5	1.5	0.025
5000	0.5	1.1	0.016
10000	0.5	1.09	0.012

The values chosen were dictated by minimum of THD, which happened at the lower side of acquisition time curve. We can observe that there is a relationship between the total width of the transistors and the parameters simulated. This relationship is shown below in Figure 33 and Figure 34.

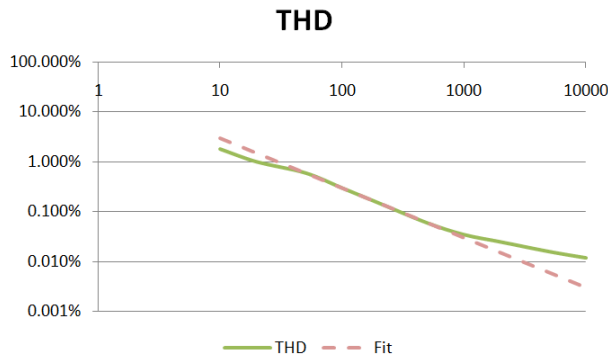


Figure 33 - THD and W_{Total} Relationship

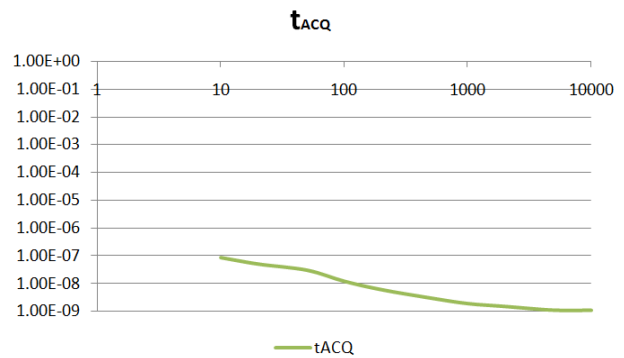


Figure 34 - Acquisition Time and W_{Total} Relationship

As the figures above indicate, the larger widths will give us better performance. However, the die area must also be sizes used for testing are rather large and must be taken into account, meaning that a compromise will be made. As a result, our next step was to set goals for distortion and acquisition time that will establish the basis for this compromise.

4.1.2.1 Goals for Parameters

To ensure that our design is competitive, Professor McNeill has indicated that from experience, the level of total harmonic distortion should be less than 0.01%. Once again, the Professor's experience in analog integrated circuit design served as a guide for an acquisition time goal. As defined in the introduction of the paper, the ADC will perform one million samples per second, translating into 1 conversion per microsecond. Therefore, we have decided to allow twenty percent of this time for sampling the input. The reason for this will be discussed later. Therefore, the goals for our ADC input parameters are as follows:

Table 9 - Parameter Goals

Parameter	Goal
Total Harmonic Distortion	< 0.01%
Acquisition Time	< 200 ns

As the graphs show, the acquisition time is not an issue for us, since all measurements met the required goal. The reason for such a loose acquisition time goal will be explained in a further subsection.

4.1.3 CHOOSING TOTAL WIDTH

When looking at our simulation results, we can see that the total harmonic distortion levels found were not below the expected mark of 0.01%. The reason for this is inferred to be the limitations of the simulator. The simulations were done under various conditions and yielded different results. However, when looking at Cadence's description of the THD formula, some parameters were not easily editable. As a result, we assumed that the total harmonic distortion levels are low enough at high values for total width that we were at a very safe margin at a W_{Total} value of 5mm.

As stated in Eq. 20, the equation derived that gives us our parameters for width is:

$$W = \frac{W_{Total}}{(5+x)}$$

Since we have established through the analysis that the total width is 5mm, we can plug in the respective values from Table 9.

$$W = \frac{5mm}{(5+0.5)}$$

$$W = 909\mu m$$

Summarizing our new transistor widths:

Table 10 - Values for Transistor Widths

	M ₁	M ₂	M ₃
Expression	W	4W	xW
Value	909 μm	3.63 mm	454.5 μm

4.2 REDUCING THE NOISE FLOOR

Until this point in the design of the input block, acquisition time has been a specification easily met. However, the reason for which we allotted 200ns for the ADC to sample is related to spectral noise reduction and SNR. In other words, the internal “on” resistance of the MOSFETs, combined with the input capacitor, create a frequency roll-off at a high frequency. The picture below shows an example of this case.

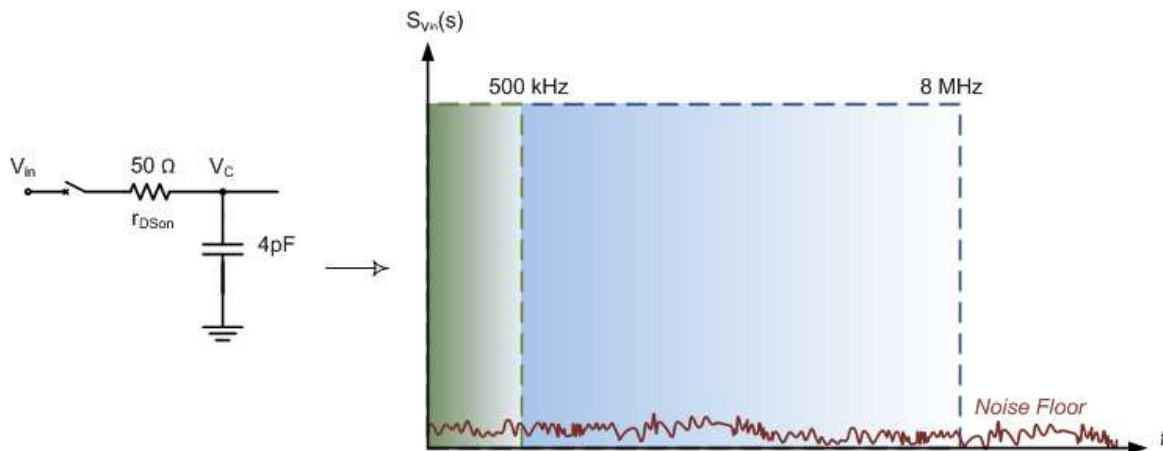


Figure 35 - Motivation for Noise Floor Reduction

If $r_{DS(on)}$ takes on a value of 50 Ω, the frequency roll off, f_h , will be found at 8 MHz, or in theory,

$$f_h = \frac{1}{2\pi \cdot RC} \quad \text{Eq. 21}$$

The blue shading indicates the location of the frequency roll-off. However, since our ADC’s bandwidth is simply 500 kHz, we can decrease the amount of noise aliased into our output by adding a series resistance to the circuit, as shown in Figure 36.

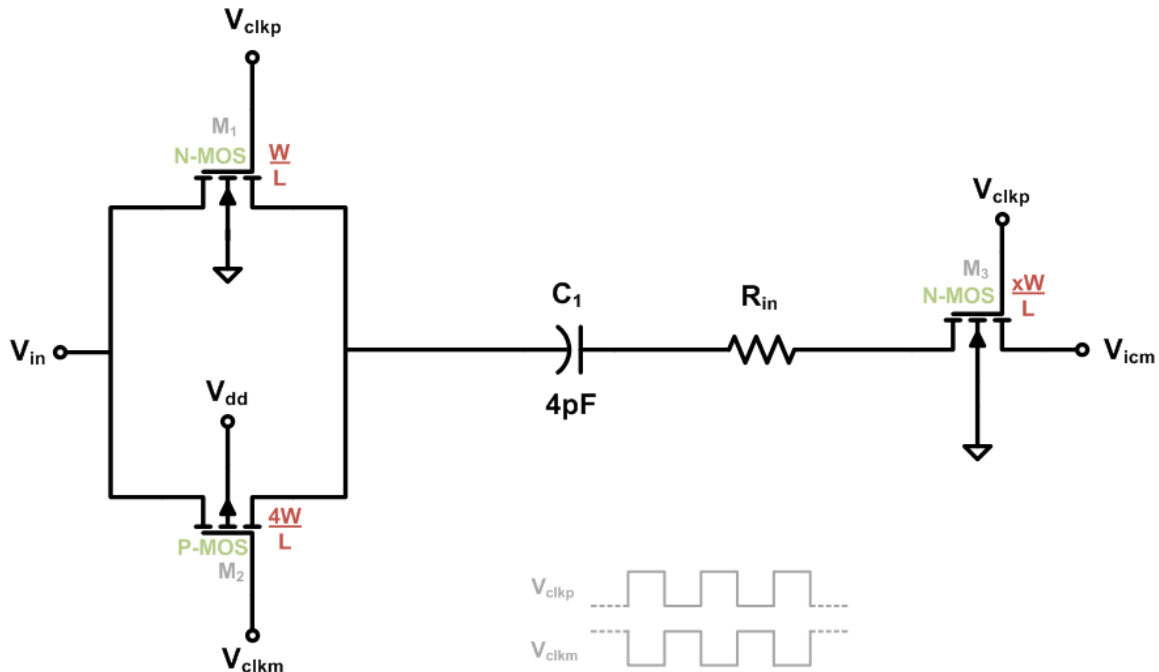


Figure 36 - New Input Circuit Model with Added Resistor

To find this resistance, we must find how many time constants are necessary to obtain the precision desired for the ADC. In this converter, since we are attempting to have a 16-bit linear converter, the accuracy level is going to be within $\frac{1}{2}$ Least Significant Bits of the ADC, as shown below:

$$t_{allow} = \ln(2^{17}) \cdot \tau \quad \text{Eq. 22}$$

where τ is the RC circuit's time constant and t_{allow} is the value pre-determined as the input sampling duration. Restructuring the equation, we'll have:

$$\tau = \frac{t_{allow}}{\ln(2^{17})} \approx \frac{200 \text{ ns}}{12} = 16 \text{ ns}$$

Knowing that our $\tau = RC$ time constant is 16ns, we can solve for the resistor size. Since we have a capacitor value of 4pF on C1,

$$R = \frac{16 \text{ nsec}}{4 \text{ pF}}$$

$$R = 4 \text{ k}\Omega$$

As expected, the input block will now have its acquisition time increased drastically. However, we had already allotted 200ns for the sampling of the circuit. To ensure the acquisition time is under 200ns, the figure below shows the acquisition time according to the different resistance values from 0 to 10k Ω :

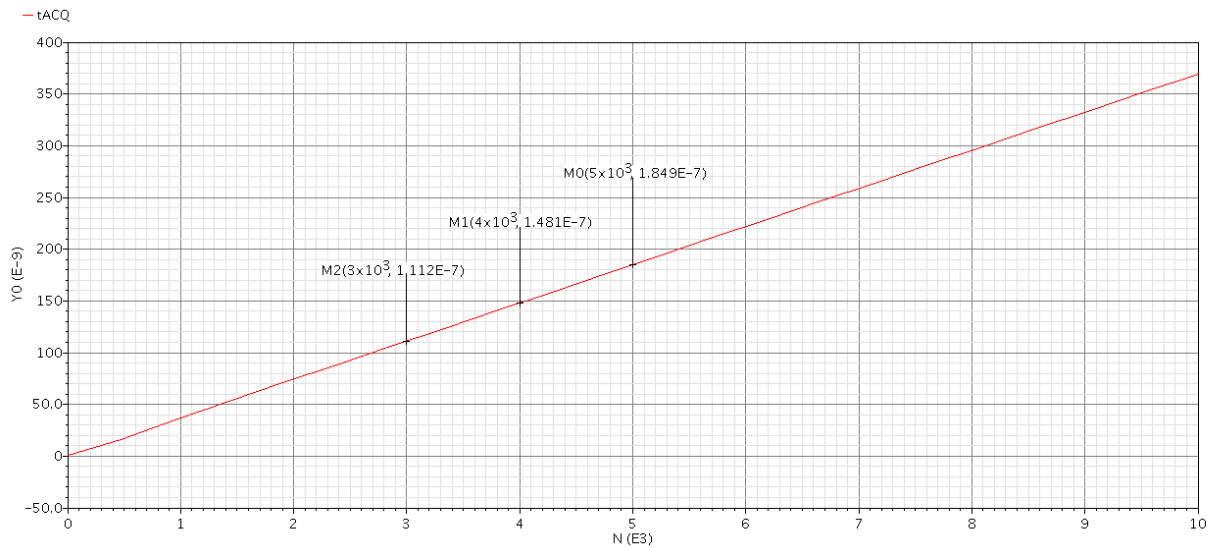


Figure 37 - Acquisition Time Dependence after Adding New Resistor

4.2.1 RESISTOR TOLERANCE

According to the JAZZ library help files, the resistor tolerances will vary approximately by 25%. That assumption is made based on the following documentation:

Salicided poly sheet resistance-Rs*	4.46	5.95	7.44	Ω/□
-------------------------------------	------	------	------	-----

Therefore, we can see that our circuit may have a higher acquisition time than expected at 5kΩ. However, that time is still below the 200ns mark.

Table 11 - Effect of Tolerances

	-25%	Expected	+25%
Value	3 kΩ	4 kΩ	5 kΩ
t_{ACQ}	111 nsec	148 nsec	185 nsec

To see the variation, the THD was also simulated. We can see that the swing in distortion does not vary much, as shown in Figure 38.

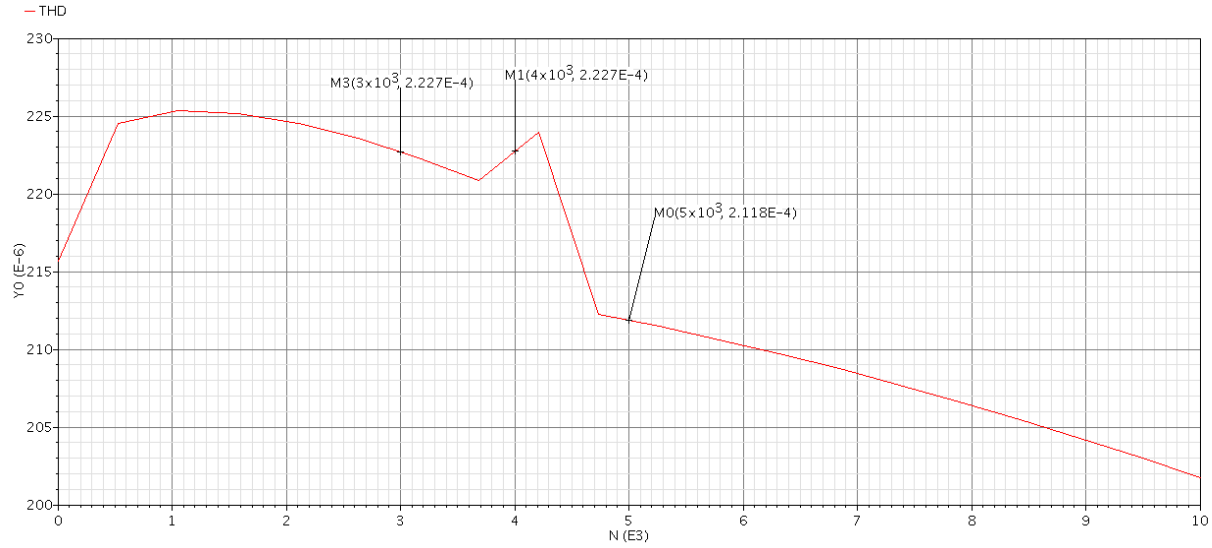


Figure 38 - THD Dependence on Resistor Variation

Using Eq. 21, our roll-off frequency will now be

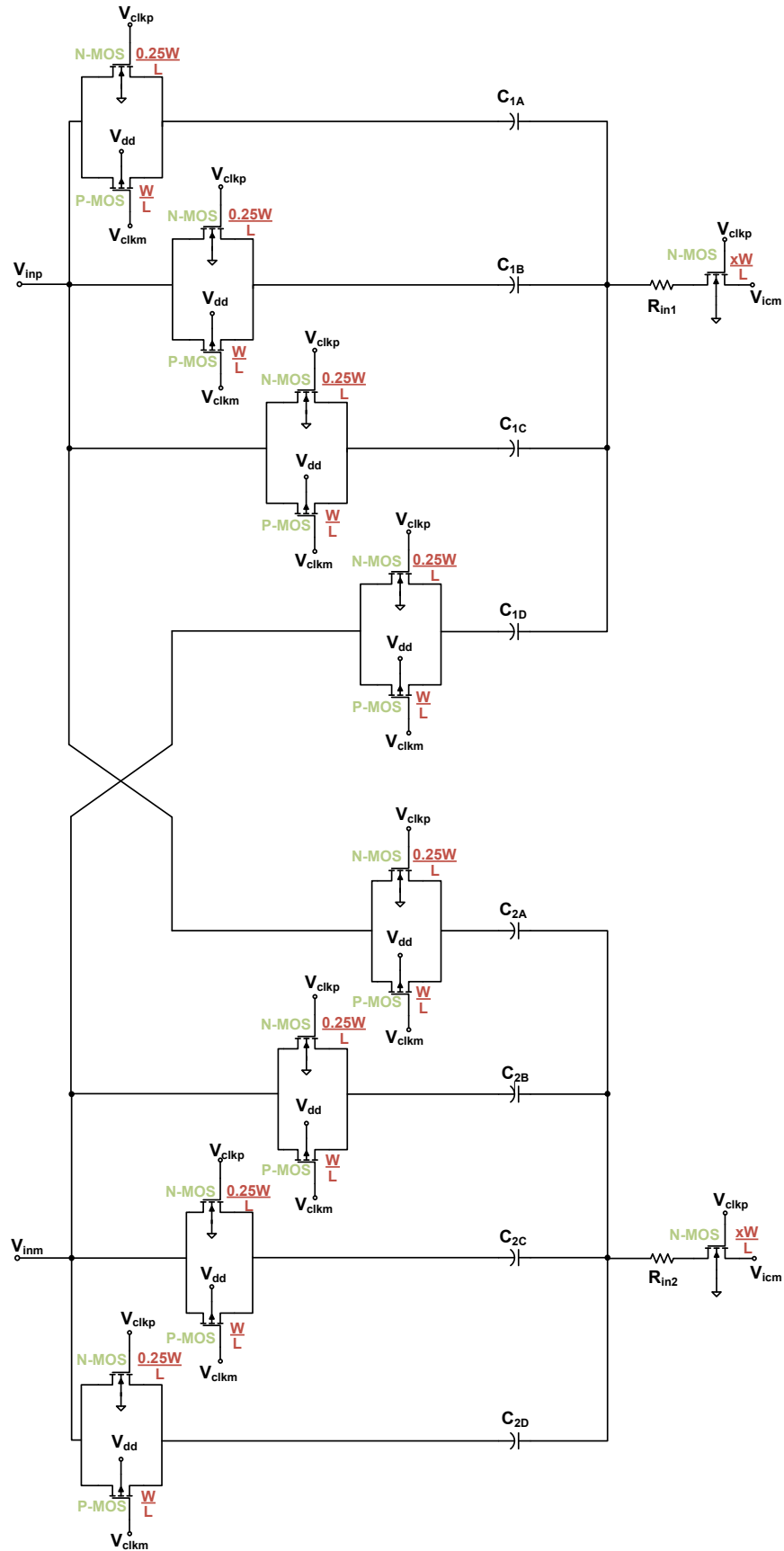
$$f_h = \frac{1}{2\pi \cdot RC} = \frac{1}{2\pi \cdot 16ns} = 9.95 \text{ MHz}$$

$$f_h \approx 10 \text{ MHz}$$

As stated in Section 2.5.1, the SNR of ADC is the integral of all the noise in a system. Therefore, by reducing the noise floor, we have reduced the signal-to-noise ratio of the ADC as well.

4.2.2 IMPLEMENTATION OF INPUT BLOCK

In the actual input block, we will use 4 capacitors in of size 1pF. Therefore we have to size all transistors accordingly. The next page shows a diagram of this concept. Also, a Split-ADC architecture will be used, meaning that the capacitor values will be half of the current values. Instead of four capacitors, eight will be used and the resistor will be sized appropriately.



5 THE SWITCHED CAPACITOR NETWORK

One of the key characteristics of the Cyclic ADC is that it is able to use sampled values after a decision has been made and apply those values to the residue amplifier. The ability to do analog math with these values and sample the input with ease comes from the switch capacitor array.

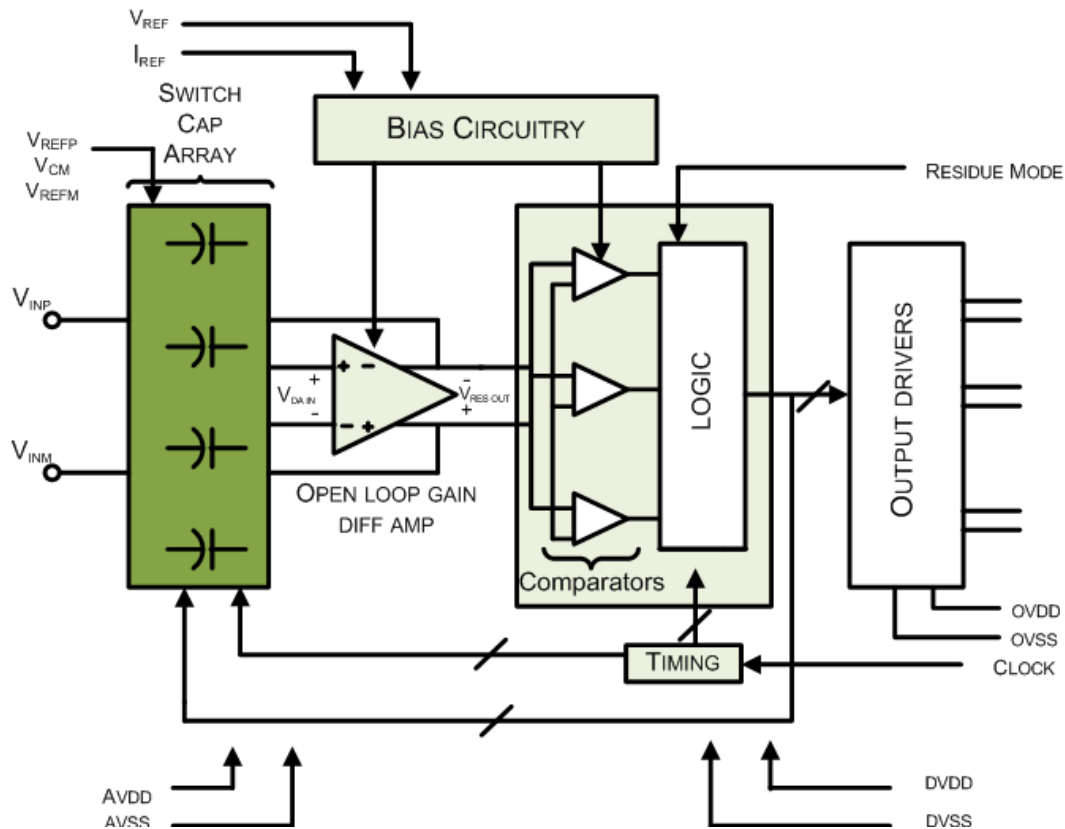


Figure 39 - Switch Capacitor Array Block and its Interaction with other Blocks

The switch capacitor network interacts with every block of our design, since the values on the capacitor dictate the input and output values of the ADC.

It is not surprising that an extensive amount of time was spent in this network. This section will serve to explain the various switch capacitor designs create and the reasons why those designs were discontinued. We will also overview the final design and its benefits.

5.1 DEFINING THE CORRECT NUMBER OF CAPACITORS FOR THE NETWORK

An important of our design, which adds to its level of complexity, is the number of capacitors used in the network. More capacitors equate to more transistors being used for switching and transmission. Therefore, our approach is to be conservative in the number of capacitors used.

5.1.1 USING ONE CAPACITOR

Before we describe our approach it is important to define what is meant by using one capacitor. As the simplified diagram below shows, there is one capacitor on the input and one capacitor on the output of the differential amplifier. The differential counterpart is not considered in this example for simplicity. One capacitor means that the amplifier's input will have one capacitor and the amplifier's output will have one capacitor as well. This number is doubled for the differential functionality.

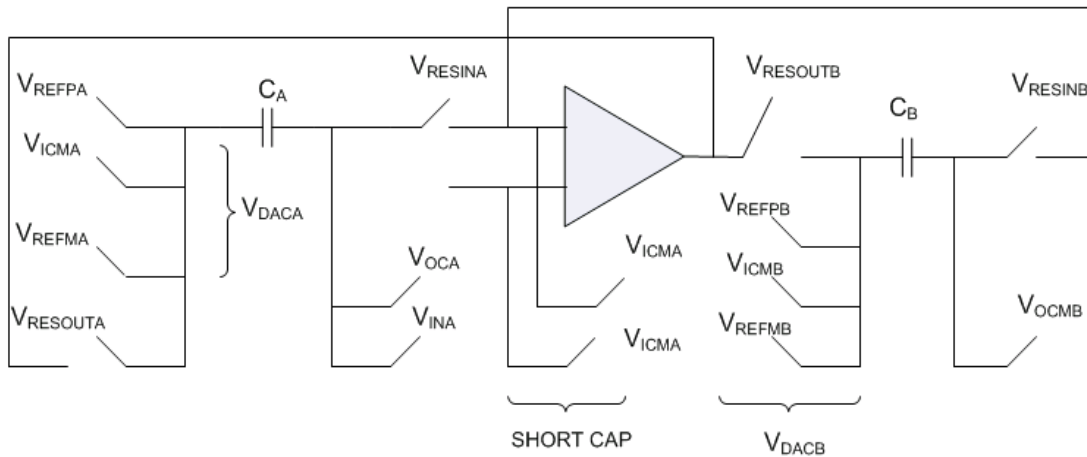


Figure 40 - Example of Using One Capacitor

Although the approach of using one capacitor makes the circuit's functionality very simple, this approach proved to be ineffective immediately. This is due to a simple factor. Symbolized in the graph as V_{DAC} is the block responsible for choosing a decision based on a previous block. The decision created by this block results in the switching to its respective voltage reference. However, since our differential amplifier does not have a perfect gain of 2, two additional decisions need to be made. With this design, two additional voltage references would need to be created. Since industry standards and common practice usually limit the amount of off-chip reference voltages, we felt it was necessary to introduce an extra capacitor to incorporate decisions -2, -1, 0, +1, and +2.

5.1.2 USING TWO CAPACITORS

To incorporate the desired decisions, the use of 2 capacitors was then implemented. Since we have a positive, negative, and common mode reference voltage available for each capacitor, the resulting decision would be represented as the diagram below indicates:

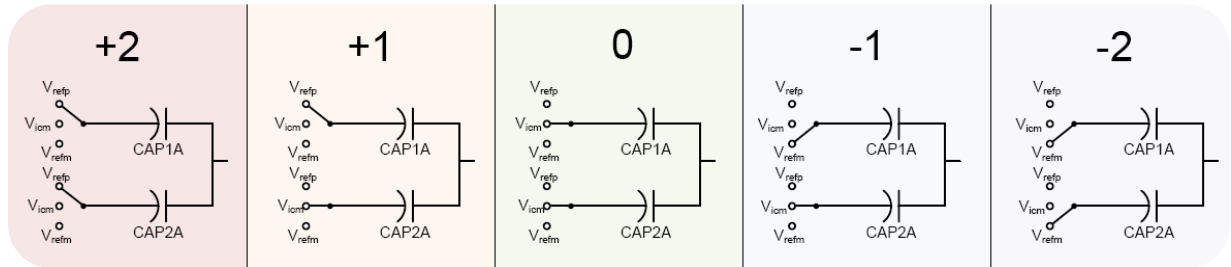


Figure 41 - Diagram of Decisions with 2 Capacitors

Figure 41 shows the position of the references in each of the 5 decisions. The voltages V_{refp} , V_{refm} and V_{icm} can be thought of “+2”, “-2” and “0” respectively due to the fact that V_{icm} is our zero reference and V_{refp} and V_{refm} are $\pm 0.34V$ away from V_{icm} it can be proven that these switching modes will produce the equivalent reference of $\pm 0.17V$ away from V_{icm} . Since each capacitor is $\frac{1}{2}$ the size as in the original one capacitor implementation the total capacitance does not change.

$$Plus\ 1 = \frac{(V_{refp} + V_{icm})}{2} \quad \text{Eq. 23}$$

$$Plus\ 1 = \frac{(1.43V + 1.09V)}{2} = 1.26V$$

$$Minus\ 1 = \frac{(V_{refm} + V_{icm})}{2} \quad \text{Eq. 24}$$

$$Minus\ 1 = \frac{(0.77V + 1.09V)}{2} = 0.93V \quad \text{Eq. 25}$$

The voltages 1.26V and 0.93V correspond to the ± 1 decision voltage levels.

5.1.3 TESTING THE TWO CAPACITOR SYSTEM

As our testing indicated, implementing the ± 1 decisions was now possible, but not as effective as expected. The circuit used for testing this decision is shown below:

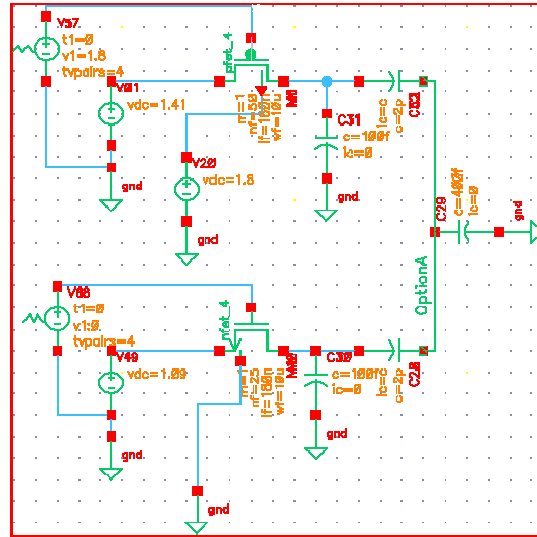


Figure 42 - Test Circuit for +/- 1 Decision

In other decisions, no charge is redistributed into the capacitors before switching. However, in this case, the issue lies with the fact that in the ± 1 decision mode, there is a 0.34V difference on the top plates of the capacitors. Since the top plates are connected to each other, charge flows from one capacitor into another implementing the averaging function. This DAC decision must be done in less than a nanosecond in order to give the differential amplifier enough time to settle itself. In order for this to be done the resistance of the switches connecting the bottom plates to V_{icm} , V_{refp} and V_{refm} must be sufficiently low. The main problem with this design was that the MOSFET switch controlling V_{icm} had a very low overdrive voltage causing the transistor to stay in the saturation region only allowing a small amount of current to flow. This caused the N_{mos} transistor connecting V_{icm} to the bottom plate of the capacitor to be sized 20 times as large as the V_{refm} transistor. This caused a substantial amount of charge from the channel of the MOSFET to be forced into the 2pF capacitor when the transistor was turned off, causing a large change in voltage in the capacitors holding voltage information of the previous cycles. Figure 43 shows this charge injection affecting our input.

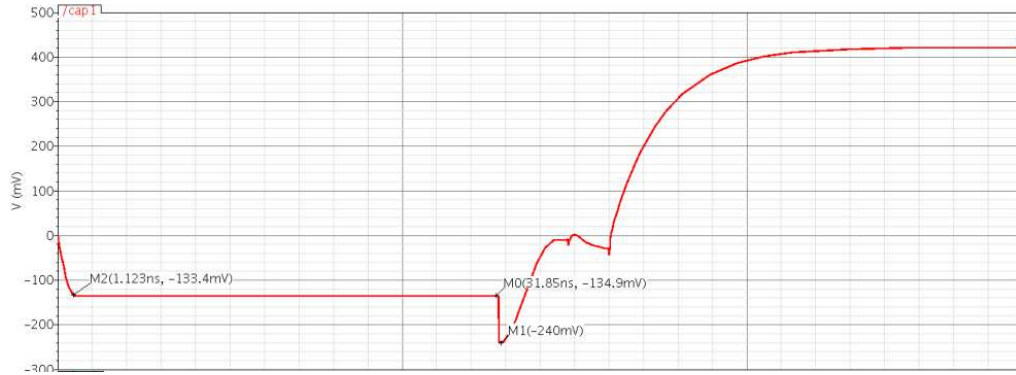


Figure 43- Example of Charge Injection: Capacitor being Switched between a 500µm PMOS and a 250µm NMOS

As the transient response above shows, the charge forced into the capacitor changes the voltage across the capacitor by over 100mV as indicated by point M1. Therefore a new alternative had to be created that did not use V_{icm} to make critical DAC decisions.

5.2 THE FINAL SWITCH CAPACITOR DESIGN: FOUR CAPACITORS

Our approach in resolving this issue was to try to minimize avoid the use of V_{icm} for decisions that needed charge redistribution. Instead four capacitors would be used to achieve the same result of the 5 DAC decisions while avoiding V_{icm} . In this model each capacitor would have $\frac{1}{4}$ of the original capacitance causing die area to not increase by a substantial amount. The four capacitor model allowed us to make the decisions as seen in Figure 44.

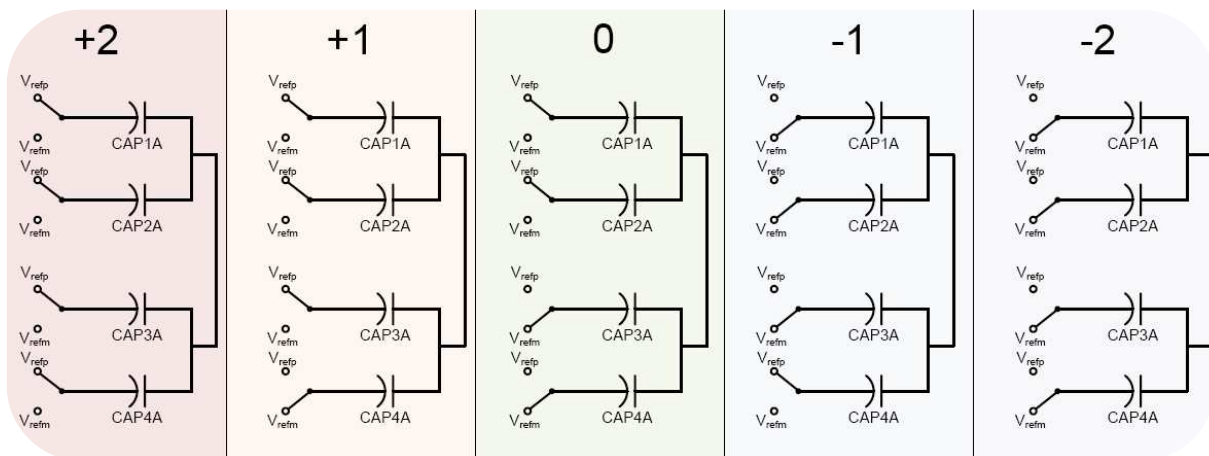


Figure 44 - Method for Using 4 Capacitors

Using this design the ± 1 decisions will be made without the use of V_{icm} as follows.

$$Plus\ 1 = \frac{(3 * V_{refp} + V_{refm})}{4} \tag{Eq. 26}$$

$$Plus\ 1 = \frac{(3 * 1.43V + 0.77V)}{4} = 1.265V$$

$$Minus\ 1 = \frac{(3 * V_{refm} + V_{refp})}{4} \tag{Eq. 27}$$

$$Minus\ 1 = \frac{(3 * 0.77V + 1.43V)}{4} = 0.935V$$

It can be seen that the 4 capacitor implementation yields a similar result as the 2 capacitor approach as seen in the table below.

Table 12 - Comparison of Decisions

Decision	2 Capacitor Implementation	4 Capacitor Implementation
+2	1.43V	1.43V
+1	1.26V	1.265V
0	1.09V	1.1V
-1	0.93V	0.935V
-2	0.77V	0.77V

Figure 45 shows a test circuit used to simulate the 4 capacitor approach:

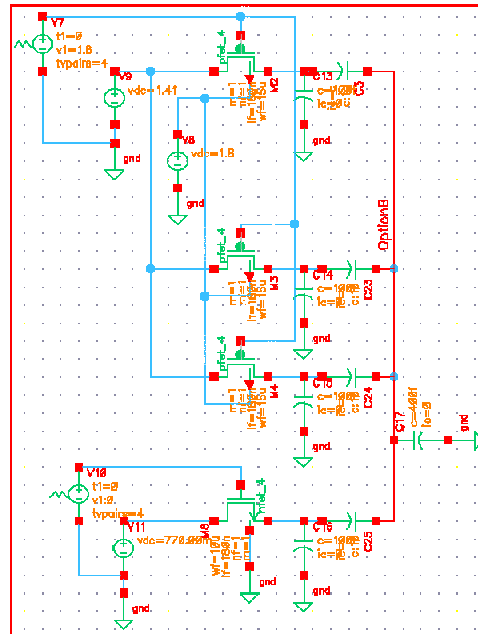


Figure 45 - Circuit Implemented with 4 Capacitors

Using the 4 capacitor implementation, the overdrive voltages for the MOSFETS are much greater, reducing the $R_{ds_{on}}$ of the MOSFETs allowing much smaller transistor widths to be used. Using this implementation, charge injection is reduced by a factor of about 21. Figure 46 and **Error! Reference source not found.** below shows a comparison of the 2 capacitor model and the 4 capacitor model for the implementation of the +1 decision.

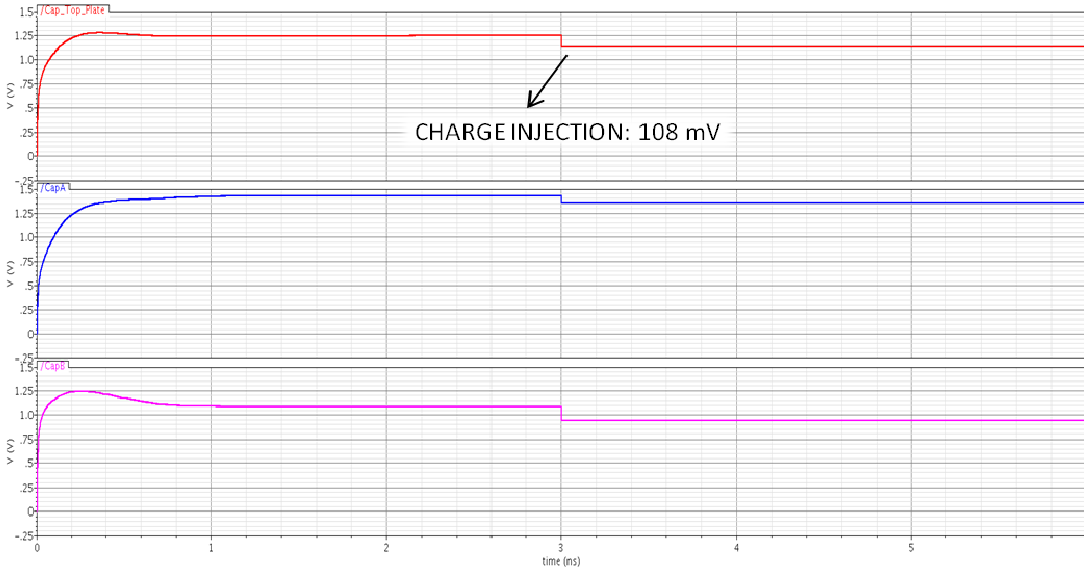


Figure 46 - 2 Capacitor Implementation of "+1" Decision

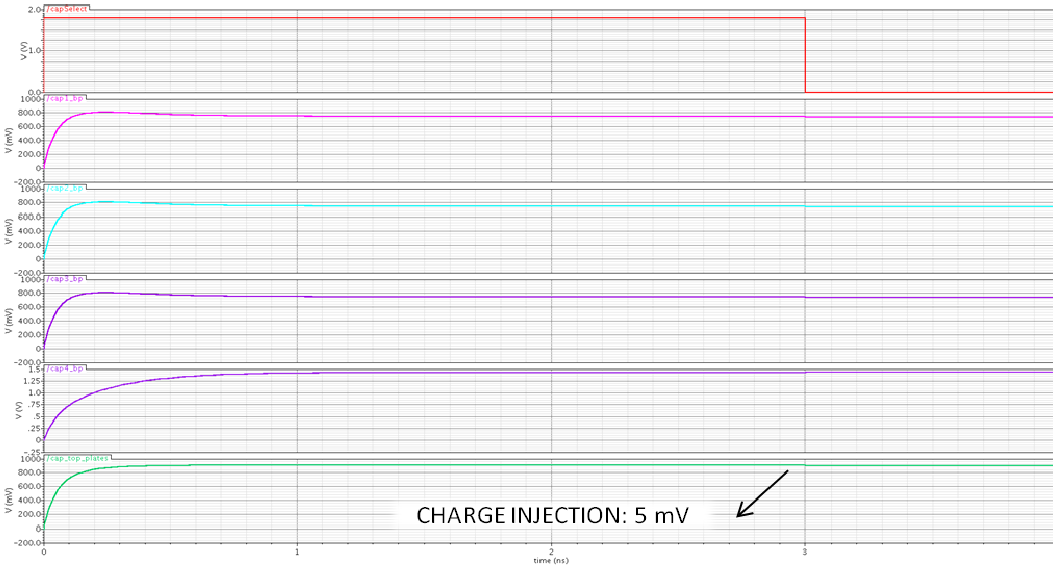


Figure 47 - 4 Capacitor Implementation of "+1" Decision

As seen in the figures above, the charge injection is reduced from 108mV to 5mV a factor of more than 21 improvements, while still complying with the 1ns charge redistribution time. Another advantage of using the 4 capacitor design is that due to the enormous decrease in MOSFET width,

the overall die area for the design is actually reduced. Figure 48 shows a schematic representation of the switched capacitor network including a model of the parasitic on the top and bottom plates of the capacitors. Each of the 1pF capacitors has 250fF of parasitic capacitance on their bottom plates and a combined 40fF capacitance on the node connecting the top plates of the capacitors.

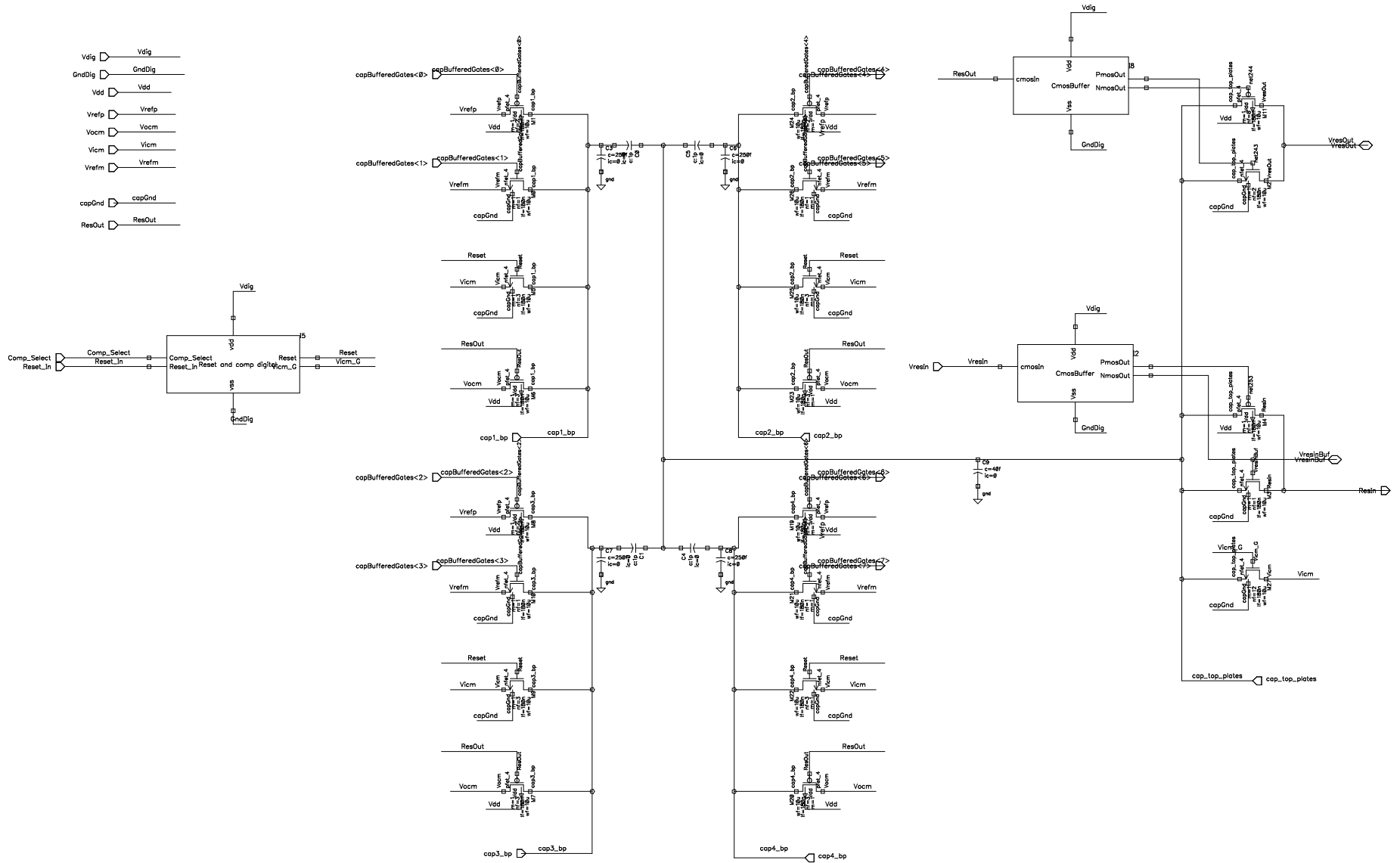


Figure 48- Switched Capacitor Circuit

5.3 DETERMINING VOLTAGE REFERENCE VALUES FOR SWITCHED CAPACITORS

The voltage references being used by the ADC were originally found when using a two capacitor approach. However, the reference voltages were kept for the four capacitor approach due to the similarities in the design. The solution is based on the principle that the positive and negative reference voltages can be found when the difference between them is the common output voltage after shorting the inputs and outputs of the differential amplifier.

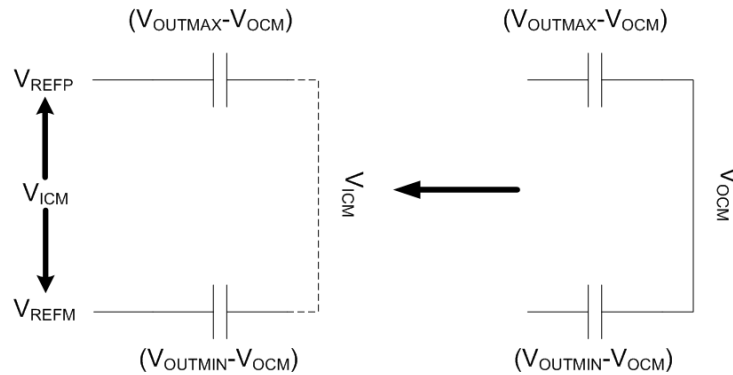


Figure 49 - Derivation for Reference Voltages

Therefore, we can derive the following two equations:

$$V_{refm} - (V_{outmin} - V_{ocm}) = V_{icm} \quad \text{Eq. 28}$$

$$V_{refp} - (V_{outmax} - V_{ocm}) = V_{icm} \quad \text{Eq. 29}$$

which, after some basic manipulation, will turn into:

$$V_{refm} = V_{icm} + V_{outmin} - V_{ocm} \quad \text{Eq. 30}$$

$$V_{refp} = V_{icm} + V_{outmax} - V_{ocm} \quad \text{Eq. 31}$$

Plugging in our values (specified in section 6.2), we get:

$$\begin{aligned} V_{refm} &= 1.09V + 0.96V - 1.3V \\ V_{refm} &= \mathbf{0.75V} \end{aligned}$$

$$\begin{aligned} V_{refp} &= 1.09V + 1.64V - 1.3V \\ V_{refp} &= \mathbf{1.43V} \end{aligned}$$

6 DIFFERENTIAL AMPLIFIER

The differential amplifier block is the heart of the residue amplifier. Figure 50 shown below is the schematic of the differential amplifier and its supportive circuitry. The behavior of the differential amplifier and equations that governed its qualitative analysis were introduced previously in section 2.9. The role of each supportive component will be described in separate sections that follow. The goal regarding the design of the differential amplifier was using an open-loop differential amplifier in order to reduce the power consumption and complexity. The nonlinearity introduced by the open-loop configuration is compensated for in the off chip calibration.

Figure 50-Schematic Representation of Differential Amplifier

6.1 FUNDAMENTAL COMPONENTS OF THE DIFFERENTIAL AMPLIFIER

There are 4 main blocks in the design of the differential amplifier as seen below

- The main part of this circuit is the differential pair
- The Replica bias sub circuit
- Resetting transistors to short inputs and outputs
- A source follower used to set the gate voltage for the bias transistors

The topology used for the load of the differential amplifier is the resistive load. The reason for using a resistive load is that the maximum gain needed for this application is a gain of two, which is a small gain that easily can be achieved by the resistive load configuration. Therefore, the use of a resistive load topology meets the constraint being faced (low gain) and minimizes the complexity of the circuit.

6.2 DIFFERENTIAL AMPLIFIER VOLTAGE LEVELS

Another aspect of the differential pair design was choosing the input, output, and common mode voltage levels for the device. In order to start the design for this part known variables were listed and several assumptions were initially considered.

- Power supply rails range from ground ($V_{SS} = 0V$) to $V_{DD} = 1.8V$.
- Threshold voltage for the transistors used in designing the differential amplifier was selected, $V_{th} = 0.45V$. The threshold voltage was found in the available Jazz libraries.

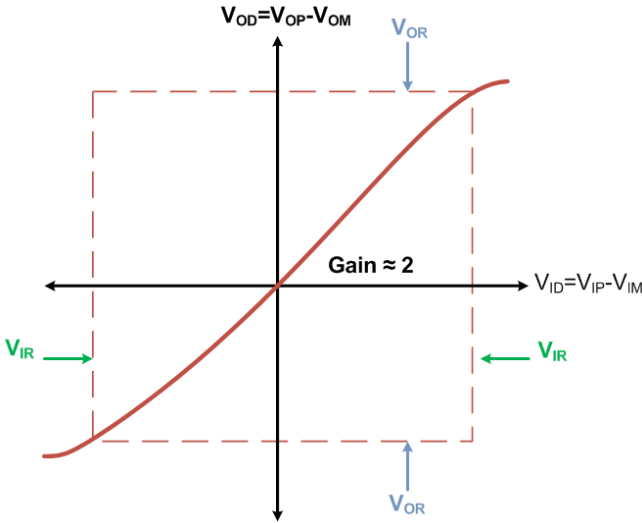


Figure 51- Differential In-Out Characteristic

The derivation of the voltage levels started based on four equations, which will be discussed in this section. The first set of equations involves determining the triode crashes within the differential amplifier. The derivation of the following equations were based on the limitations that differential amplifier faces. Below is shown the input output characteristic graph for the differential amplifier which served as a guide to derive the equations that govern the input and output ranges of the differential pair.

The low triode crash happens when inputs are equal to each other. In other words:

$$\text{Low triode crash} \rightarrow V_{IP} = V_{IM} = V_{ICM} \quad \text{Eq. 32}$$

An assumption made regarding the transistor, M9, that serves as the biasing of the differential amplifier was that the minimum drain to source voltage must be equal to, $V_{DS} = 0.3V$ for this device to be in saturation region.

Below are shown known voltages and the equation for the gate to source voltage for M1.

$$V_{th} = 0.45V$$

$$V_{DS} = 0.3V$$

$$V_{GS1} = V_{th} + V_{ov1} \quad \text{Eq. 33}$$

The four base equations used were the following;

Eq. 34 describes the low triode crash of the device:

$$V_{ICM} - (V_{th} + V_{ov1}) = 0.3V \quad \text{Eq. 34}$$

Equation Eq. 35 describes the high triode crash of the device:

$$V_{th} - 0.15 = \left(V_{ICM} + \frac{V_{IR}}{2} \right) - \left(V_{OCM} + \frac{V_{OR}}{2} \right) \quad \text{Eq. 35}$$

Equation Eq. 36 describes the output voltage range for the differential pair that is given by:

$$V_{OR} = G * V_{IR} \quad \text{Eq. 36}$$

Equation Eq. 37 relates the input range of the differential amplifier assumed to be at a value approximately equal to M1 overdrive voltage:

$$V_{IR} \approx V_{ov1} = 0.15V \quad \text{Eq. 37}$$

By using all the assumptions made above and values available, the V_{ICM} value can be found as shown. Plugging in V_{th} and solving for V_{ICM} , we obtain:

$$V_{ICM} = V_{IR} + 0.75V \quad \text{Eq. 38}$$

The next step is to solve Eq. 35. Using Eq. 36 we can substitute V_{OR} for $2V_{IR}$, and have the following:

$$V_{th} - 0.15 = \left(V_{ICM} + \frac{V_{IR}}{2} \right) - \left(V_{OCM} - \frac{2*V_{IR}}{2} \right)$$

$$0.45 - 0.15 = \left(V_{ICM} + \frac{V_{IR}}{2} \right) - (V_{OCM} - V_{IR})$$

$$0.3 = V_{ICM} + \frac{3V_{IR}}{2} - V_{OCM}$$

Eq. 39

The next step is to substitute V_{ICM} from Eq. 38:

$$0.3 = (0.75 + V_{IR}) + \frac{3V_{IR}}{2} - V_{OCM}$$

Reordering the equation to solve for V_{OCM} as a function V_{IR} we get:

$$V_{OCM} = \frac{5V_{IR} + 0.9}{2}$$

Eq. 40

Respectively, we could have solved this equation for V_{IR} :

$$V_{IR} = \frac{2V_{OCM} - 0.9}{5}$$

Eq. 41

Finally, we must find V_{ICM} . To do so, we'll plug Eq. 41 into Eq. 38, obtaining:

$$V_{ICM} = \frac{2V_{OCM} - 0.9}{5} + 0.75$$

Eq. 42

With these results, we can plot the equations on the same axes, since all equations are represented as a function of V_{IR} , as shown below:

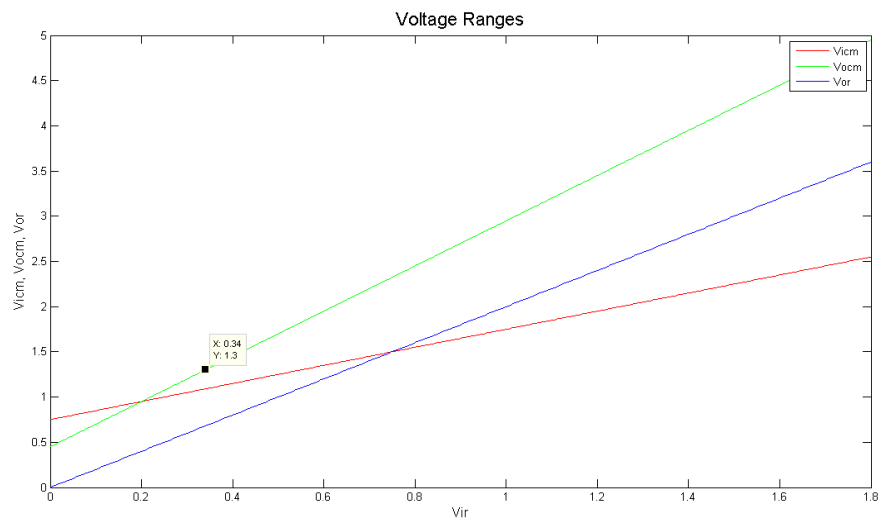


Figure 52 - Voltage Ranges Plot

We can use the voltages shown on Figure 52 to observe the impact of changing the voltage ranges of the circuit. As the figure above shows, we can use the point of intersection between V_{ICM} and V_{IR} as our choice for voltage ranges:

$$\begin{aligned}V_{ir} &= 0.34V \\V_{ICM} &= 1.09V \\V_{or} &= 0.64V \\V_{OCM} &= 1.3V\end{aligned}$$

Once the above voltage levels were found, they were used in the derivations of the resistive load values and the differential pair bias current.

6.2.1 *KT/C CAPACITOR SIZING*

The sampling capacitor size for the sample and hold circuit is determined by the KT/C noise floor the input voltage range and the desired SNR. Eq. 48 below shows the relationship of capacitance and temperature to the RMS noise of a system. In order to achieve a 12 bit noise floor for our ADC we would need an SNR of 74 db

$$SNR = 6.02\text{db} * N + 1.76 \text{ db} \tag{Eq. 43}$$

$$SNR = 6.02\text{db} * 12\text{bits} + 1.76 \text{ db} = 74\text{db}$$

In order to achieve an SNR of 74 db a minimum capacitance value of 3.63pF would be needed achieve a 74db resolution. The capacitors chosen in our circuit is 4pF as seen in Eq. 49 in order to take into account differences from the ideal ADC quantization error.

$$C = \frac{2KT}{\left(\frac{\left(V_{in} \frac{\sqrt{2}}{2}\right)}{\left(\frac{(SNR)}{10^{\frac{20}{20}}}\right)}\right)^2} \tag{Eq. 44}$$

$$C = \frac{(2 * 1.3806 * 10^{-23} * 303.15K)}{\left(\frac{\left(V_{in} \frac{\sqrt{2}}{2}\right)}{\left(\frac{(74\text{db})}{10^{\frac{20}{20}}}\right)}\right)^2} = 3.63\text{pF}$$

6.2.2 DERIVATIONS OF RESISTIVE LOAD VALUES AND BIAS CURRENT

Proper biasing of the differential amplifier is an essential part in this design. In the differential pair circuit the bias current determines factors such as the slew rate of the amplifier, speed and acquisition time of the amplifier while keeping all of the internal MOSFETs in their active region. For the differential pair bias current there is a tradeoff of power consumption and speed. The faster the settling time needed to achieve a small error margin, the more current is needed to bias the differential pair. In this circuit the voltage on the load capacitor needs to be resolved to 14 bits accuracy in less than 20ns.

In order to acquire a signal and resolve to 14 bits resolution on the load capacitor we must have at least 9.7τ (RC time constants) as shown in the equation below:

$$\ln(2^{-(\# \text{ of bits to resolve})}) = \# \text{ of } \tau \text{ needed to achieve resolution} \quad \text{Eq. 45}$$

$$\ln(2^{-14}) = 9.7\tau \quad \text{Eq. 46}$$

To find the resistance needed to achieve at least 9.7τ in the 20ns allotted we must find what τ is in the circuit, which is seen in the equations below:

$$\tau = \frac{20ns}{10} = 2ns \quad \text{Eq. 47}$$

With the RC time constant known and the capacitance value assumed to a certain value as shown below, the resistance necessary for the resistor load for the differential pair can be calculated by making a use of the equation below:

$$R = \frac{\tau}{C} \quad \text{Eq. 48}$$

The capacitor value used in the above equation was chosen to be, $C = 4pF$. The C value was decided while keeping in mind the SNR requirement in this project. For SNR description refer to section 2.2. After putting all values in the resistor equation the resistor value needed for differential amplifier load was found to be:

$$R = \frac{2.061ns}{4pF} = 515.3\Omega \approx 500\Omega \quad \text{Eq. 49}$$

Knowing the values of the resistors in the resistive load portion of the ADC and the V_{ocm} one can calculate the bias current needed to operate the differential pair. The equation below is used to determine the current through each branch of the differential amplifier:

$$\frac{I_{Bias}}{2} = \frac{V_{dd} - V_{ocm}}{R_{resistor\ load}} \quad \text{Eq. 50}$$

Plugging the values from above the current through one branch of the differential pair results to be:

$$\frac{I_{Bias}}{2} = \frac{1.8V - 1.3V}{500\Omega} = 1mA \quad \text{Eq. 51}$$

Therefore, the differential pair bias current would be the sum of the currents from both branches that results to be:

$$I_{Bias} = \frac{I_{Bias}}{2} + \frac{I_{Bias}}{2} = 2mA \quad \text{Eq. 52}$$

6.3 REPLICA BIAS ANALYSIS

A replica bias circuit is designed to mimic the behavior of the differential pair. That way, variations from the input are accounted for by helping to stabilize V_{DS} . One of the advantages of such circuitry is that it applies a reference voltage to a targeted transistor in order to keep the current mirror as consistent as possible with input voltage.

6.3.1 ADVANTAGES AND PURPOSE OF USING REPLICA BIAS

The use of replica bias minimizes the channel length modulation on the current bias source. Replica bias creates the same V_{DS} as the original circuit being replicated, thus minimizing channel length modulation. Designing a replica bias circuit requires a special care in terms of transistor matching. As the name of this circuit suggests, it replicates the behavior and functions of the circuit that it supports, in this case the differential amplifier. The transistors in the replica bias is a factor of 10 smaller compared to the transistors in the differential pair in order to minimize the current usage, die area, and power consumption of the replica bias by a factor of 10.

6.3.2 DESIGNING REPLICA BIAS

The role of the source follower in the circuit is that it sets the bias gate voltage by subtracting a constant voltage, 309.5mV, from the common drain node of the replica bias transistors (the constant voltage drop was measured in the actual node of the replica bias).

First, when V_{IP} and V_{IM} are the equal, the common source voltage is in its lowest level, which lowers the current through the bias transistor due to the channel length modulation. Since the current through bias transistor decreases, there is an excessive current supplied by I_{in} which in turn charges the gate of the source follower. When the voltage on the source follower is increased, the V_{DS} of the source follower is decreased causing the gate voltage of the bias transistor to be

increased. This increase of gate voltage leads to an increase of the current through the current source, therefore reestablishing the current in the whole circuit. Since the gate of the bias transistor in the replica bias is connected to the bias of the differential amplifier, the current in the differential amplifier is held constant.

6.3.3 SIMULATION OF THE REPLICA BIAS CIRCUIT

Shown below is the result of a simulation performed to verify the proper functionality of the replica bias circuit. Notice, for $V_{IM} = V_{IP}$ the gate voltage of M9 is at its highest level. Indeed, notice the behavior of the differential pair bias current; there is only a $6\mu A$ ripple in the $2mA$ bias current.

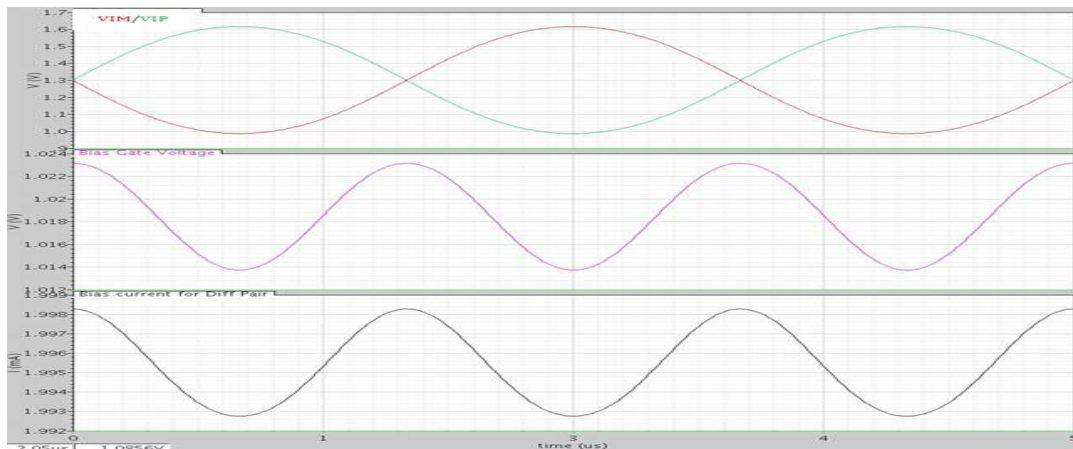


Figure 53-Replica Bias Simulation

All the above derivations contribute to the design of the differential amplifier.

6.3.4 DIFFERENTIAL PAIR SYMBOL REPRESENTATION

The figure that follows is a symbol representation of the differential amplifier schematic shown above. Once the differential amplifier was designed a symbol representation was created. Notice all the input and output pins attached to the differential amplifier.

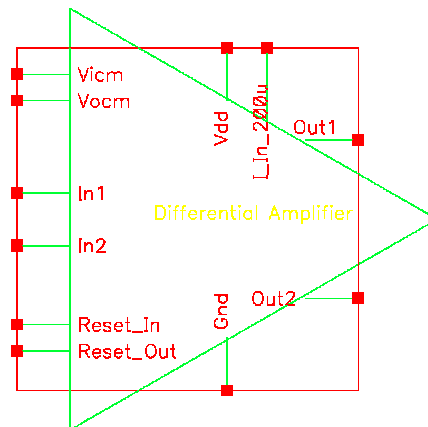


Figure 54-Symbol Representation of Differential Amplifier

7 THE LOGIC BLOCK

Our circuitry is highly dependent on logic to operate. Many functions like, the control and timing of switching, the digital decision making, and others are performed by this block. In this section we will outline the various components created to perform the necessary logic functions for the cyclic ADC.

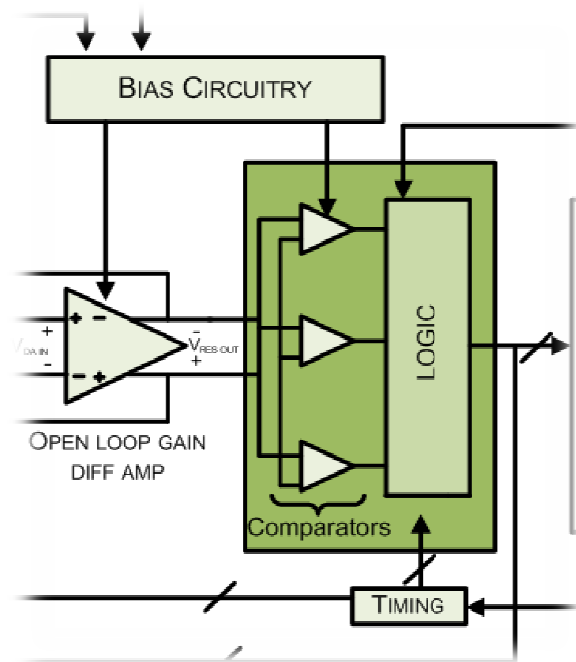


Figure 55 - Logic Block and its Interaction with other Blocks

7.1 DRIVING TRANSISTOR GATES THROUGH OPTIMIZATION

Digital blocks in our ADC don't have the current handling capability necessary to switch the large transistors used in our analog circuitry. Due to the ability of a given gate to turn on and off within a short required time is critical in certain parts of our circuit for instance, in the sample-and-hold circuit, a buffer circuit is needed to provide the current handling capability necessary to drive the large gate capacitances of our analog circuitry.

7.1.1 TAPERED BUFFER

The specific topology of a tapered buffer refers to a series of buffers connected together with transistor widths increasing by a factor of 4 compared to the previous stage. The advantage of using the following configuration is that the current handling capability of the digital block is increased incrementally until the necessary driving current is attained

7.1.2 ADVANTAGES OF USING TAPERED BUFFERS

The advantages of using tapered buffers is that it greatly reduces the rise time of an analog transistor driven by an on chip digital block but it introduces a propagation delay into the circuit. In order to maximize the usefulness of the tapered buffers the buffer size needs to be tailored to the transistor gate being driven.

7.1.2.1 Buffer Schematics and Symbol

Below are displayed the minimum buffer size used in designing all necessary buffers for driving the sample and hold circuit gates and a tapered buffer schematic in transistor level.



Figure 56 - Discrete Buffer Component

Notice that the minimum buffer size used has a length of factor 16 of the processes being used for designing these buffers available in Jazz library.

The following figure represents the tapered buffer schematic in transistor level. Notice the width of the second stage increases by an “n” factor compared to the first stage.

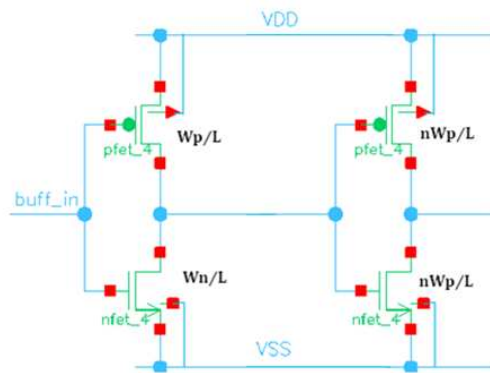


Figure 57-Schematic of a Buffer in Transistor Level

The figure below shows a two stage tapered buffer of size 32. As it can be seen the second stage is a factor of two bigger compared to the first stage.

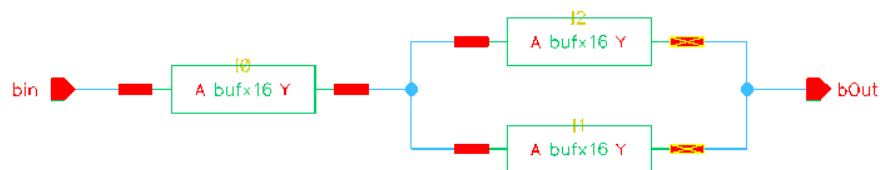


Figure 58 - Tapered Buffer of Size 32

The representation of the buffer above is in schematic form. After the schematics were designed symbol representations were created and stored.

Figure below is a representation of a tapered buffer (size 32) symbol that can be imported into a given schematic in order to optimize a specific signal.



Figure 59 - Tapered Buffer Symbol (size 32)

A number of buffers that ranged from 16 to 1024 were designed and stored in working libraries for later use. Indeed, for greater flexibility the designed buffers increased by a factor two. In other words, the designed buffers ranged from 16, 32, 64... 512, 1024. A graphical representation of the buffer series is shown below.

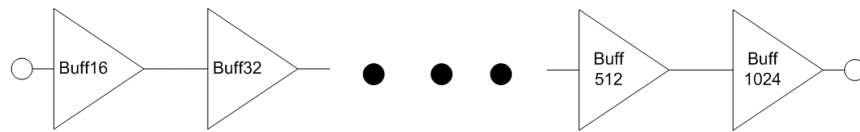


Figure 60-Representaion of the Tapered Buffer Topology

An example where the buffers were used to optimize the output signal of a digital block in order to drive the transistor gates was the sample-and-hold circuit.

7.2 SAMPLE AND HOLD CIRCUIT SIMULATIONS

Initially all the tapered buffers describe above were designed to drive the gates involved in the sample and hold circuit at the front end of the design. In the figure below V_{in} represents the analog input signal to be sampled; M_1 and M_2 represent the signals coming from a digital block in order to drive the gates of the CMOS switch constructed by *nfet_4* and *pfet_4* in ICFB. At the output side M_3 is another signal that drives the output gate which in turn loads the value stored in capacitor C_1 into the residue amplifier (not shown here).

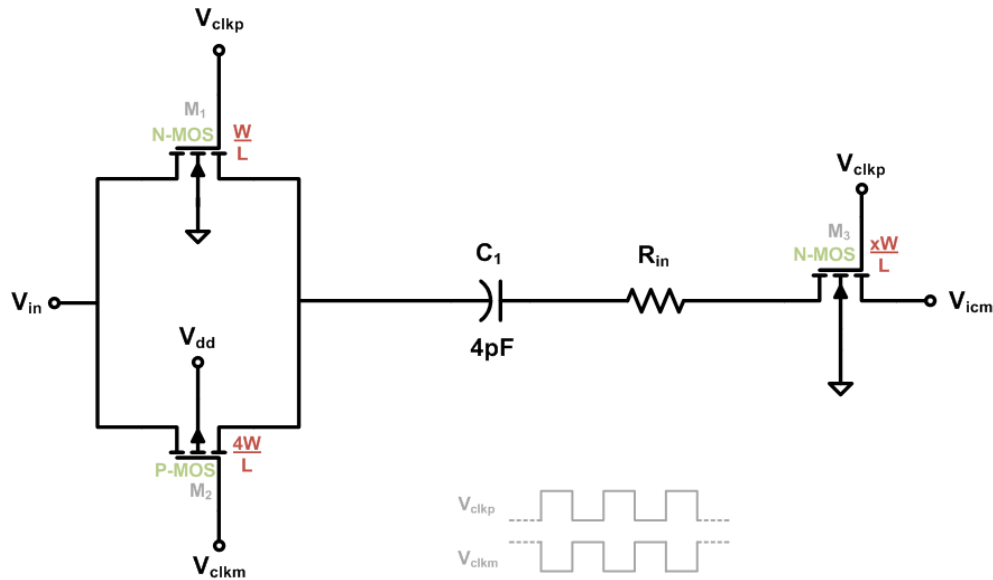


Figure 61-Schematic Representation of the Sample and Hold Circuit

After designing a number of tapered buffers a series of simulations were conducted in order to analyze the signal response based on the applied buffer size and determine the appropriate buffer size needed to be used to drive a given gate.

7.2.1.1 Rise Time and Fall Time Measurements

The table below shows the combinations of components used for a series of simulations where the rise time, fall time, and the delay time with respect to the original signals were studied. For measuring the rise time a voltage level of 0V to 1.0V was used, whereas for measuring the fall time the range from 1.8V to 1.0V was substituted instead. Also, notice that in order to get more data points the buffer size was incremented by a factor of two.

Table 13 - Rise Time and Fall Time Measurements for Sample and Hold Circuit Simulations

NMOS Switch (910 μ m)S2	Rise Time (psec)	Fall Time (psec)	PMOS Switch (3705 μ m)S3	Rise Time (psec)	Fall Time (psec)	NMOS (460 μ m)S1	Rise Time (psec)	Fall Time (psec)
-----			-----			-----		
Buffer Sizes			Buffer Sizes			Buffer Size		
16	270	145	16	1750	1021	16	162	90
32	140	86	32	940	528	32	90	59
64	84	53	64	450	460	64	60	40
128	53	41	128	230	120	128	40	32
256	46	41	256	100	69	256	31	30
512	33	27	512	81	47	512	28	24
1024	30	25	1024	53	35	1024	28	22

7.2.1.2 Rise Time and Rise-Time Delay Response Analysis Though Simulations

The following figure shows all signals grouped together for the NMOS gate at the output stage of the sample-and-hold circuit; the original signal is represented by S1. The following simulations are used for measuring rise time, and time delay for each output signal. Signal S1 refers to the original signal coming from the digital block and the rest of the signals are the outputs for each applied buffer. Starting from left to right it can be seen that buff16 does not optimize the original signal due to the fact that the rise time is similar to S1 and time delay is longer compare to buff64 output signal. Buff64 has a shorter rise time compare to buff16 and buff32 and relatively the same rise time compare to buff128, buff256, buff512, and buff1024. Also, buff 64 has a shorter time delay compare to the rest of the signals leading to the conclusion that for driving this gate this buffer size is the one that gives the best gate behavior.

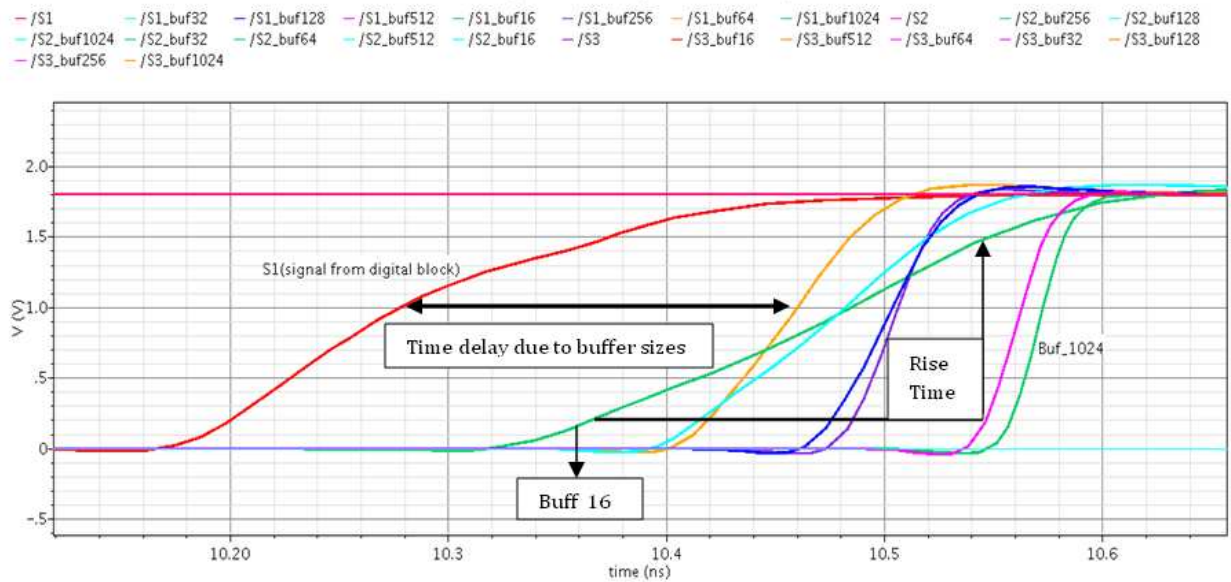


Figure 62-Rising Edge of Signal for Different Buffer Sizes

7.2.1.3 Fall Time and Fall-Time Delay Response Analysis Though Simulations

Another simulation was performed for analyzing the falling time and falling-time delay response. In this case the NMOS transistor gate at the CMOS switch was observed. Signal S2 refers to the original signal coming from the digital block and the rest of the signals are the outputs of the applied buffers. For analyzing the following simulation the same procedure used for analyzing the rise time case was applied leading to the conclusion that for driving this transistor gate in the given dimensions buff64 is the best fit.

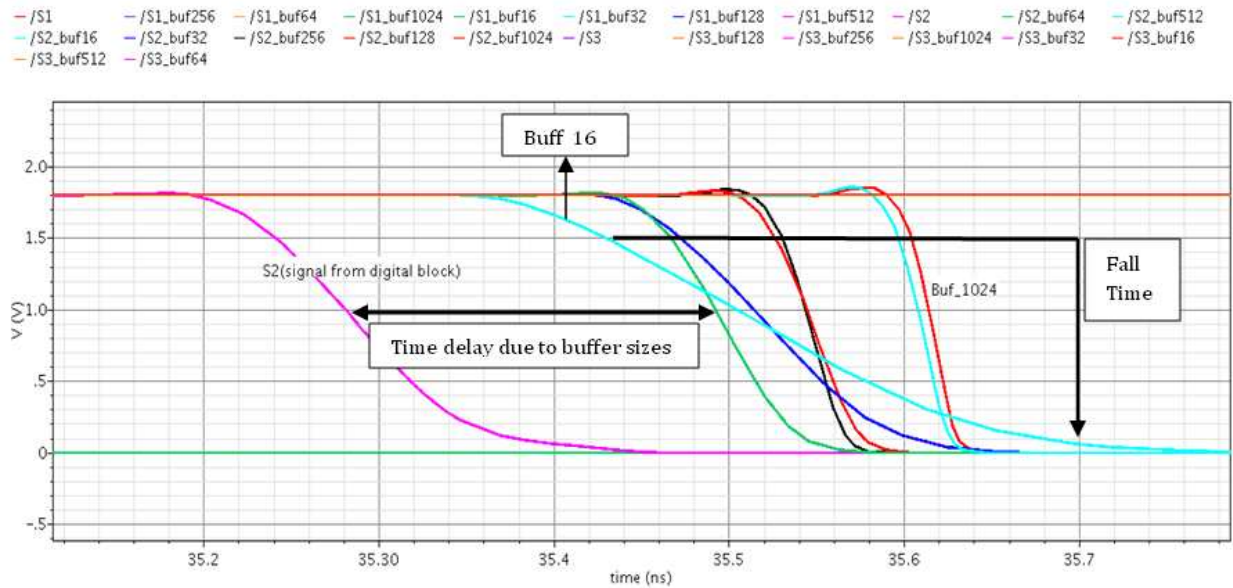


Figure 63-Falling Edge of a Signal for Different Buffer Sizes

7.2.1.4 Rise-Time Delay and Fall-Time Delay Measurements

Shown below is a table with the recorded data for time delay analysis for all gates. In order to have a better understanding of the results the time delay was plotted versus the buffer sizes used.

Table 1-Rise-Time Delay and Fall-Time Delay for the Optimized Signal

Buffer_Sizes	S1 Time in (pSec)		S2 Time in (pSec)		S3 Time in (pSec)	
	Rise_Delay	Fall_Delay	Rise_Delay	Fall_Delay	Rise_Delay	Fall_Delay
16	210	264	316	225	1817	1370
32	200	210	262	230	1040	750
64	180	193	212	211	590	450
128	223	253	242	263	430	342
256	227	256	238	262	329	300
512	283	322	290	326	336	345
1024	293	330	298	332	320	342

7.2.1.5 Choosing Buffer Sizes through Graphical Approach

Figure 64 Figure 69 show the graphs of time delays versus buffer sizes. It can be seen time delay decreases as the buffer size increases up to a certain buffer size thereafter the time delay increases rapidly. Thus, we can see the tradeoff between increasing the buffer size and decreasing the time delay for a given gate and decide which buffer to use.

RiseT_D	log(RisT_D)	BufSize	log(BufSize)
2.10E-10	-9.68	16	1.20
2.00E-10	-9.70	32	1.51
1.80E-10	-9.74	64	1.81
2.23E-10	-9.65	128	2.11
2.27E-10	-9.64	256	2.41
2.83E-10	-9.55	512	2.71
2.93E-10	-9.53	1024	3.01

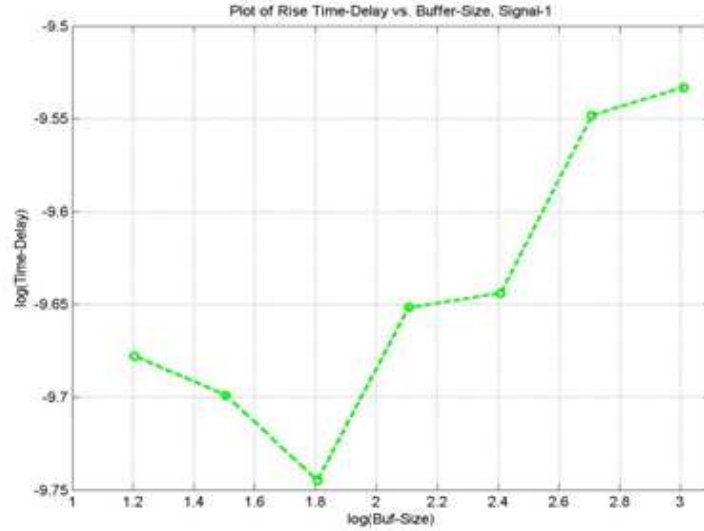


Figure 64-Plot of Rise Time Delays vs. Buffer Sizes for the Gate at the Sampling Capacitor

The graph above shows that the rise-time delay for NMOS gate at the output decreases to its minimum for buff64 ($\log_{10} = 181$) and rise-time delay ($\log_{10} = -9.74$), which is the same result observed in the simulations approach.

FallT_D	log(RisT_D)	BufSize	log(BufSize)
2.64E-10	-9.58	16	1.20
2.10E-10	-9.68	32	1.51
1.93E-10	-9.71	64	1.81
2.53E-10	-9.60	128	2.11
2.56E-10	-9.59	256	2.41
3.22E-10	-9.49	512	2.71
3.30E-10	-9.48	1024	3.01

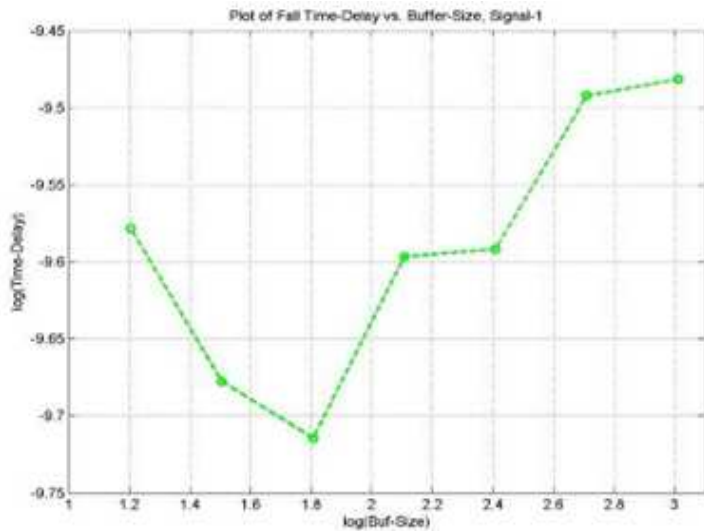


Figure 65-Plot of Fall Time Delays vs. Buffer Sizes for the Gate at the Sampling Capacitor

The fall-time delay for the same gate decreases to a lower value for buff 64 and fall-time delay ($\log_{10} = -9.71$), again it is the same result observed in the simulation presented above.

RiseT_D	log(RisT_D)	BufSize	Log(BufSize)
3.16E-10	-9.50	16	1.20
2.62E-10	-9.58	32	1.51
2.10E-10	-9.68	64	1.81
2.42E-10	-9.62	128	2.11
2.38E-10	-9.62	256	2.41
2.90E-10	-9.54	512	2.71
2.98E-10	-9.53	1024	3.01

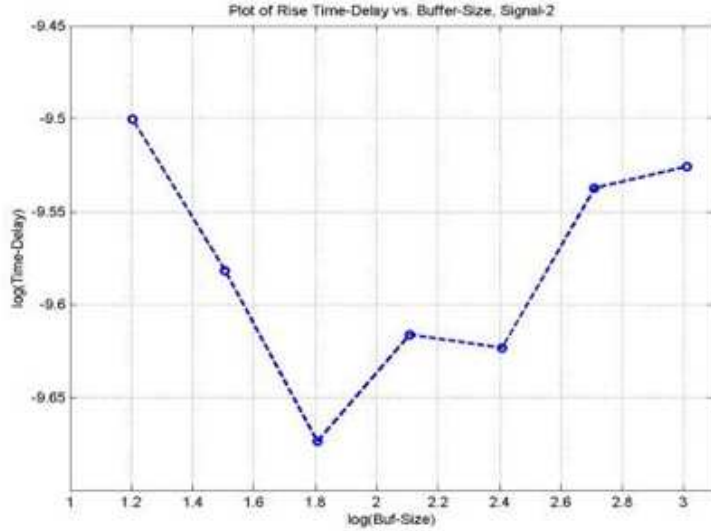


Figure 66-Plot of Rise Time Delays vs. Buffer Sizes for the NMOS Gate at the Sampling Switch

The figure above displays the plot of rise-time delay vs. buffer size for NMOS gate at the CMOS switch. In this case time delay reaches its minimum value for buff64 and rise-time delay ($\log_{10} = -9.68$).

FallT_D	log(RisT_D)	BufSize	Log(BufSize)
2.25E-10	-9.65	16	1.20
2.30E-10	-9.64	32	1.51
2.11E-10	-9.68	64	1.81
2.63E-10	-9.58	128	2.11
2.62E-10	-9.58	256	2.41
3.26E-10	-9.49	512	2.71
3.32E-10	-9.48	1024	3.01

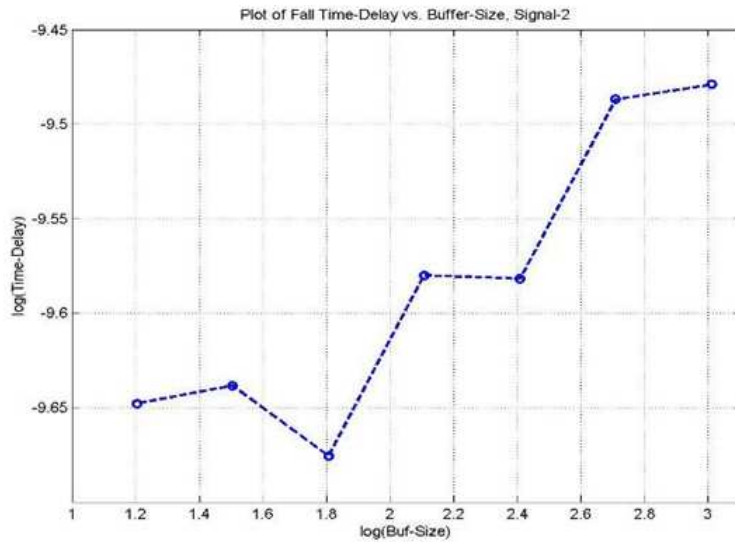


Figure 67-Plot of Fall Time Delays vs. Buffer Sizes for the NMOS Gate at the Sampling Switch

The fall-time delay for the NMOS gate at the CMOS switch decreases to a lower value for buff 64 and fall-time delay ($\log_{10} = -9.68$), leading to a conclusion similar to the one presented above for the particular gate.

RiseT_D	Log(RisT_D)	BufSize	Log(BufSize)
1.87E-09	-8.73	16	1.20
1.04E-09	-8.98	32	1.51
5.90E-10	-9.23	64	1.81
4.30E-10	-9.37	128	2.11
3.29E-10	-9.48	256	2.41
3.36E-10	-9.47	512	2.71
3.20E-10	-9.49	1024	3.01

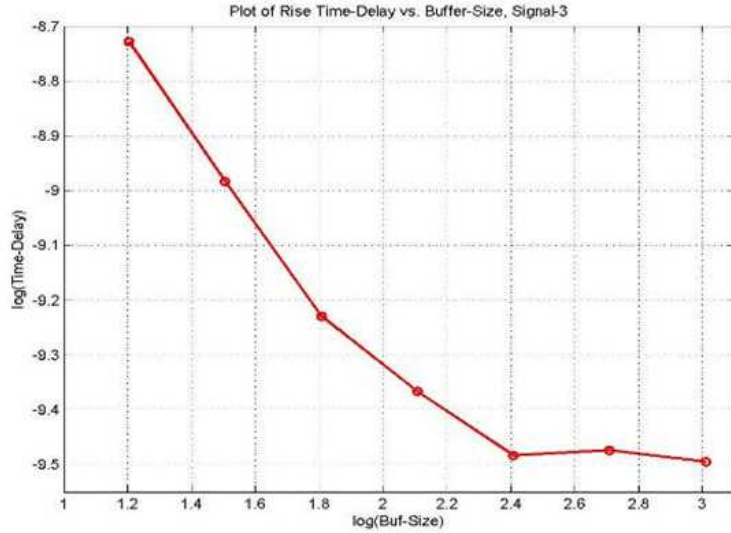


Figure 68-Plot of Rise Time Delays vs. Buffer Sizes for the PMOS Gate at the Sampling Switch

The graph above displays the plot of rise-time delay vs. buffer size for PMOS gate at the CMOS switch. This case results to a minimum time delay for buff256 ($\log_{10} = 2.41$) and rise-time delay ($\log_{10} = -9.48$). It is an expected result since the gate size for a PMOS transistor is larger compare to an NMOS transistor gate.

FallT_D	Log(RisT_D)	BufSize	Log(BufSize)
1.37E-09	-8.86	16	1.20
7.50E-10	-9.12	32	1.51
4.50E-10	-9.35	64	1.81
3.42E-10	-9.47	128	2.11
3.00E-10	-9.52	256	2.41
3.45E-10	-9.46	512	2.71
3.42E-10	-9.47	1024	3.01

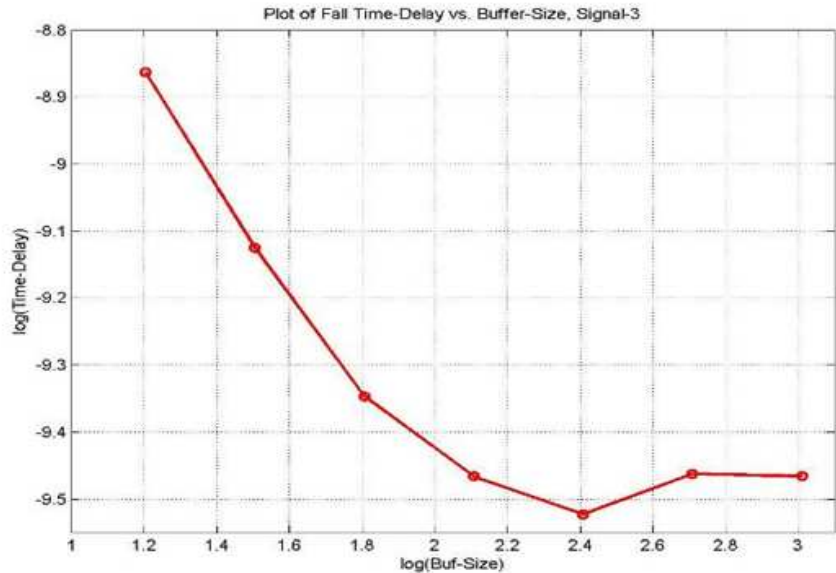


Figure 69-Plot of Fall Time Delays vs. Buffer Sizes for the PMOS Gate at the Sampling Switch

Figure 69 displays the plot of fall-time delay vs. buffer size for the same gate at the CMOS switch. For this case the time delay for buff256 ($\log_{10} = 2.41$) and rise-time delay ($\log_{10} = -9.52$) is the shortest time delay. Yet, considering that the decrease in time delay from buff128 to buff256 is only

0.42E-10 (from the table), it seems that buff128 is a better tradeoff since its physical size of buff128 is twice smaller.

7.3 DRIVING TRANSISTOR GATES AT CAPACITOR ARRAY

Another crucial block of the digital design involved creating logic circuitry to drive the transistor gates in the switched capacitor array based on the comparators' outcome, a capacitor select signal, and a residue mode signal. Signals that represent the comparators' outcome and the capacitor select are on-chip signals, whereas residue mode signal is an off-chip signal coming from an external source such as an FPGA device. As shown below at Figure 70 each comparator's outcome is assigned a grey code value that represents one of the four outcomes to be considered, whereas the rest of the combinations are ignored. Also, four possible logic combinations for the capacitor select signal and residue mode signal are shown in the truth table,

Table 14 that follows below. In other words, based on the combination of the input signals, comparators' outcome and capacitor-select/residue-mode, output signals are generated that drive eight assigned transistor gates at the capacitor array for forming one of the five output decisions of the residue amplifier.

7.3.1 IMPLEMENTING RESIDUE AMPLIFIER DECISIONS

Shown below is the matching of the comparators' outcome to the residue amplifier decisions based on the input signals described above. Notice that the solid arrow represents the residue -mode signal that selects decisions -2, 0, and +2, whereas the dashed arrow represents the residue-mode signal that selects decisions -1 and +1.

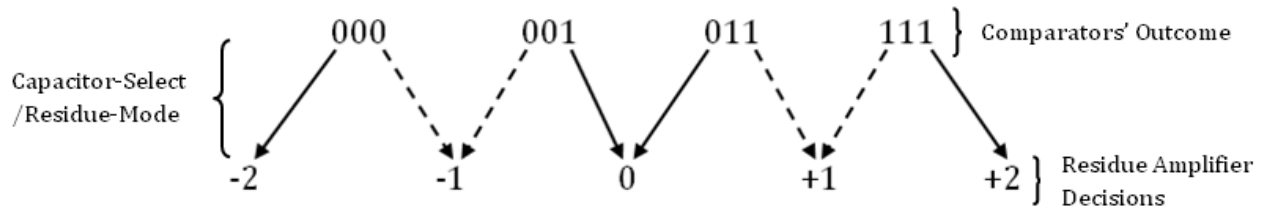


Figure 70- Matching of Comparators' Outcome to Residue Amplifier Decisions

The truth table shown below is used to implement the functionalities described above. The truth table was derived by considering all possible combinations of the variables described above.

Table 14-Truth Table for Gate Driver Digital Block

CAPACITOR-SELECT/RESIDUE-MODE COMBIANTIONS				
Comparators' Outcome	00	01	10	11
000	10101010	10101010	11111111	11111100
001	10101010	10101010	11110000	11111100
011	10101010	10101010	11110000	11000000
111	10101010	10101010	00000000	11000000
ELSE	10101010			
Outputs, Transistor Gates				

7.3.2 EXAMPLE OF A DECISION IMPLEMENTATION

In order to further understand the complex operation of the gate digital driver it may be helpful to consider an example of a decision implementation. For instance, let's derive the implementation of a "+2" decision. Shown below is the capacitor array whose gates are to be driven by the digital driver.

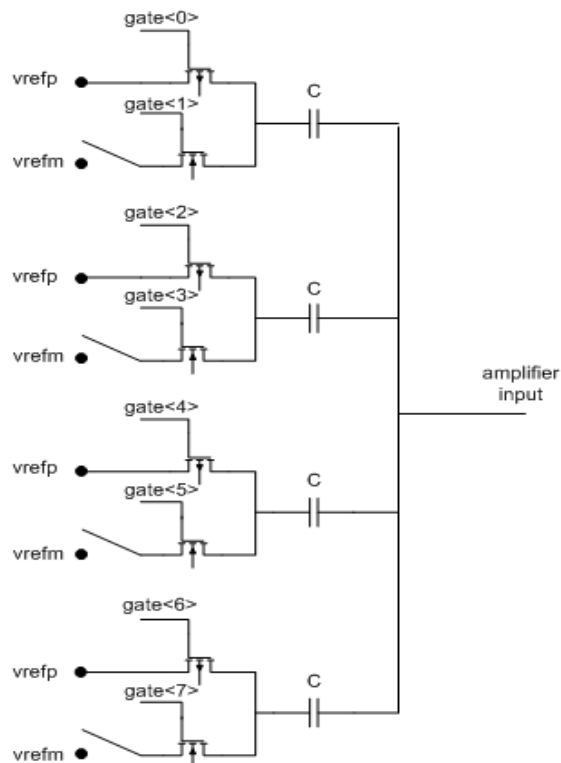


Figure 71-Capacitor Array Block

In order to realize a “+2” decision the comparators output should be “111” and the capacitor-select/residue-mode combination must be “10”, which means that capacitor-select signal allows the capacitor array to perform its functions and residue-mode selects the “+2” decision. From the truth table it can be seen that for the given comparators’ output, “111” and capacitor-select/residue-mode combination “10” the signals to be sent to eight transistor gates are “00000000” with the far left being the signal sent to the first gate, gate<0>. Going back to the capacitor array circuit and assigning to each gate from gate<0> to gate<7> the corresponding bit, it can be seen that all PMOS transistors will be “on” and all NMOS transistors will be “off”. This configuration connects all the capacitors to the positive reference values, *vrefp*, thus giving rise to the “+2” decision. In addition, by applying all combinations in the truth table to the capacitor array block one can realize all five residue amplifier decisions.

7.3.3 FINAL STEP IN DESIGNING THE GATE DIGITAL DRIVER

Once the truth table was created a hard ware description language (HDL) script was written in VHDL using a digital designing graphical user interface (GUI), Xilinx 10.1i. Moreover, once the code was written a test bench wave form (tbwf) was performed to verify the functions above. In this project, as mentioned above, Cadence is used as an IC designing tool. Yet, Cadence’s digital environment does not support VHDL code; it supports Verilog instead. In order to use the written VHDL code an intermediate path is followed. Cadence has the capability of converting a VHDL code to Verilog code, which in turn is then synthesized using the available digital compiler. For all the steps from writing a VHDL code in Xilinx to completing the digital design in Cadence a tutorial was written. After the designing process was completed the necessary power supply pins (VDD, VSS) were attached to the digital component and a symbol was created for a simpler representation. The newly digital driver was stored in a library for later use in circuit; its symbol representation is shown below.

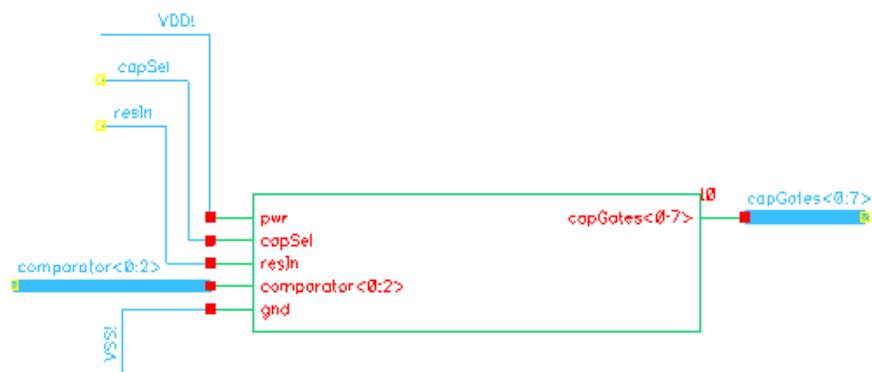


Figure 72-Digital Transistor Gate Driver

7.4 DRIVING TRANSISTOR GATES OF INPUT-OUTPUT CAPACITORS OF RESIDUE AMPLIFIER

This section concerns a digital block that drives the gates of switches that allow connecting capacitors to the residue amplifier. The graphical behavior of the block is represented below through the timing diagram. In this block the only external input controlling signal is the *capSelect* signal, whereas the *vresoutBuf* signal is an output delayed signal that is feed back as an input to the digital block. Delays between signals *vresout* and *vresoutBuf*, and *vresin* and *vresinBuf* are realized through buffers as shown in circuit schematic representation below the timing diagram. The functionalities of the digital block in discussion are as follows. When *capSelect* signal goes high *vresout* switches to low in order to turn on the gate of the PMOS transistor leading to the connection of C_{out} to the residue amplifier. Then, *vresin* goes high which in turn turns on the NMOS transistor leading to the connection of C_{in} to the amplifier. On the other side, when *capSelect* goes low the reverse operations take place. First, the capacitor C_{out} is disconnected followed by the disconnection of C_{in} .

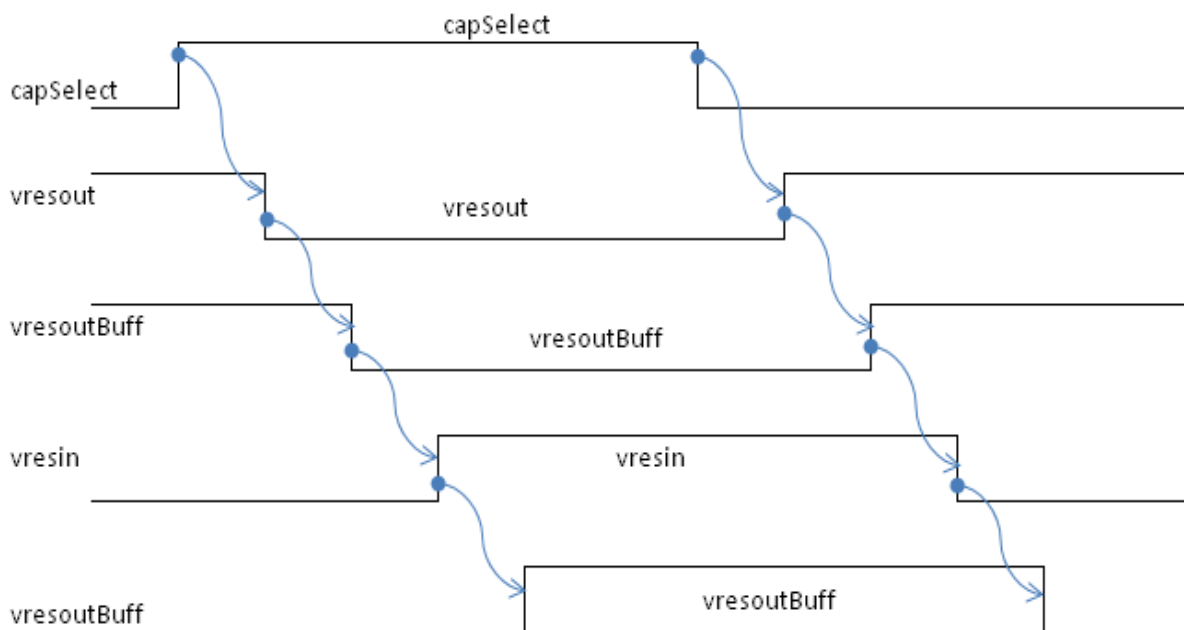


Figure 73-Behavior of “vresin-vresout switch” Digital Block

Below is shown an artistic circuit schematic representation together with the pins that connect to the digital block described above.

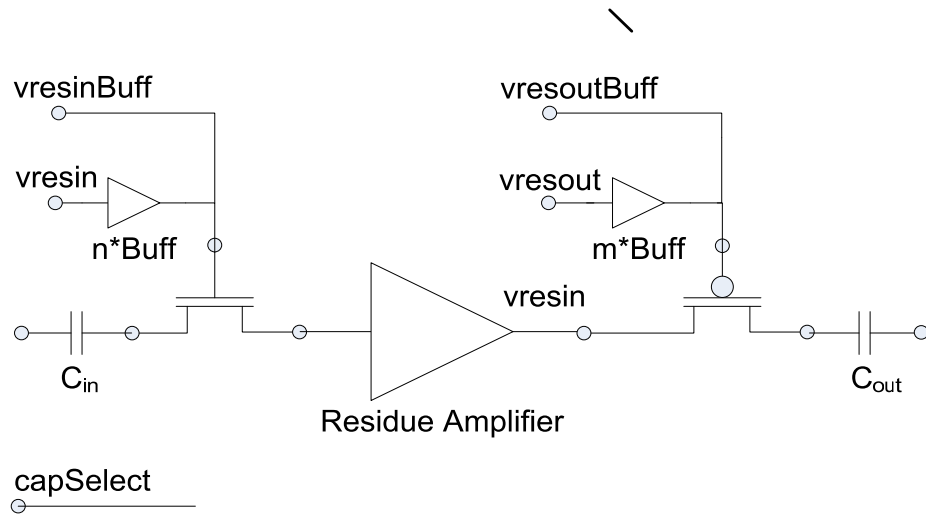


Figure 74-Representation of Gates to Drive With “vresin-vresout switch” Digital Block

7.4.1 REALIZING THE DIGITAL BLOCK

For designing “vresin-vresout switch” digital block the same procedure was followed. First, a VHDL code was written in Xilinx and its functionality was verified through a tbwf before imported to Cadence. Once imported to Cadence the code was synthesized using cadence digital designing tools, completed by attaching power supply pins and the newly designed digital block was ready for use. Below is displayed a symbol representation of “vresin-vresout switch” digital block.

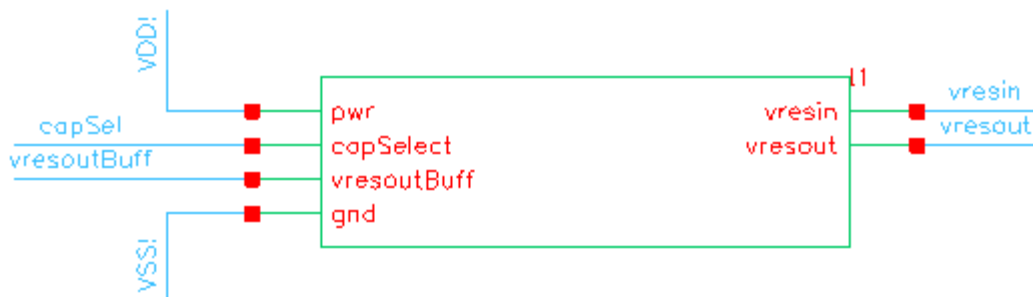


Figure 75-“vresin-vresout switch” Digital Block

7.5 DESIGNING “GENERICDEMUX”

A demultiplexer (in this design called genericDemux) was another digital sub circuit designed with the purpose of driving specific transistor gates based on certain input signal combinations. The inputs of this digital block driver are the input to be send to a selected output pin, and the output pin select signal. For each case two variables are considered, which give rise to four possible input combinations. Yet, for this application only two combinations are needed for each case; the rest are used to set the output values to zero “low” values. In the tables below the left columns represent the input signal combinations and the right columns show the output results. On the left column the bit on the far left corresponds to the input signal, whereas the bit on the right represents the select output pin signal.

Table below shows the relationship between the input-select signal and output1 pin.

Table 15- input/output1 Relationship for “genericDemux”

input-select	output1
00	0
10	1
ELSE	0

The following table represents the relationship between the input-select signal and output2 pin.

Table 16- input/output2 Relationship for “genericDemux”

input-select	Output2
01	0
11	1
ELSE	0

7.5.1 “GENERICDEMUX” SYMBOL REPRESENTATION

After the logic behavior of the demux was established a VHDL script was written in Xilinx and synthesized in Cadence’s digital designing tools. A symbol representation of the demultiplexer circuit was created and the newly designed digital driver was tested to verify its proper functionalities. Below is shown the symbol representation of this digital block.

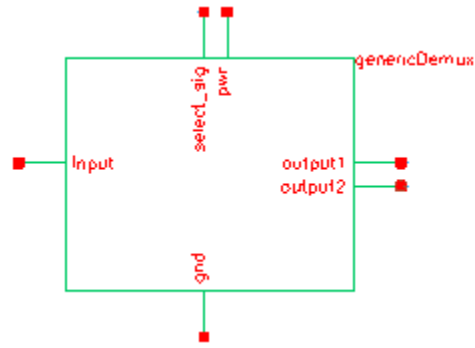


Figure 76- “genericDemux” Symbol Representation

In order to verify the demultiplexer’s proper functionality a simulation test was performed. For instance, let’s consider an input combination from the truth table that represents the relationship between input/output2, and observe the output. Shown in the graph is a dotted arrow that shows the input combination of input-select as “11”. For this input combination the expected outputs (from the truth table) are output1 “0” and output2 “1”. Moreover, by following the same procedure one can verify that the designed demux implements all logic combinations described in the truth tables above.

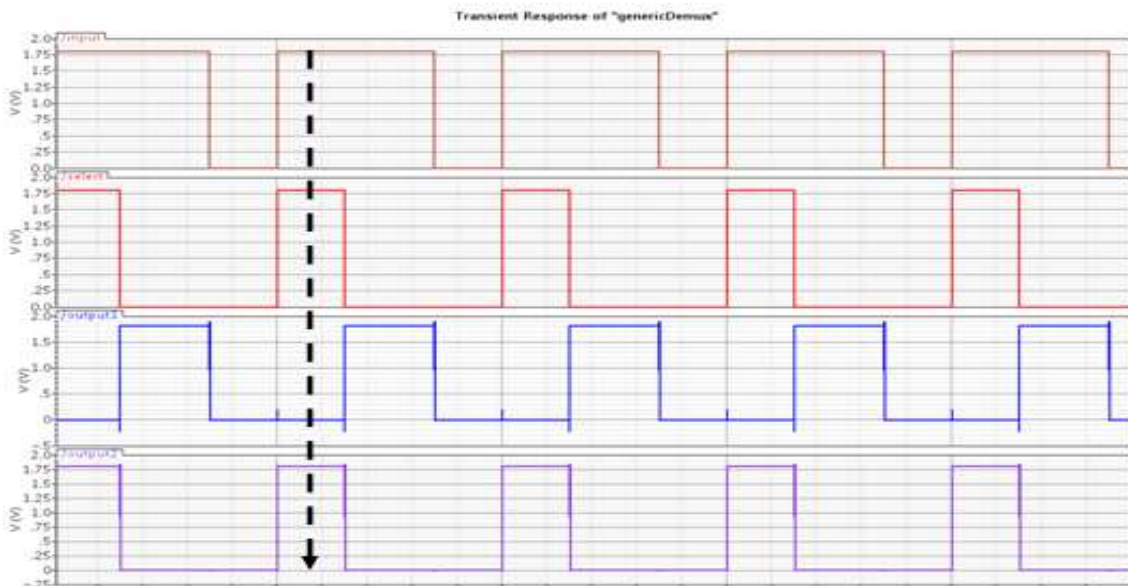


Figure 77-Results “genericDemux” Simulation

8 THE COMPARATORS

The Cyclic ADC that we are designing uses 3 comparators to create the digital decisions. The comparators are connected to the output of the residue amplifier and are arranged in a thermometer code. The comparators consist of the preamps, which are used to set the decision levels, amplify the difference between the inputs and set the proper input voltage for the analog latch. The analog latch uses two inverters that are connected to each other in positive feedback to keep them at their metastable point until nudged by the output of the preamplifier to trigger the latch. The final component in the comparators is the digital latch. The digital latch holds the value of the decision throughout the next cycle and buffers the output to drive the external FPGA.

8.1 THE PRE-AMPLIFIERS

There are two designs for the preamps. One design compares V_{outp} directly to V_{outm} and amplifies their difference this is used in the “0” comparator. The other preamplifier design is used in the “+1” and “-1” comparators to evaluate V_{outp} to $V_{outm}+0.34V$. This comparator is used to see if the difference of V_{outp} to V_{outm} is greater than $\frac{1}{2} V_{ref}$.

8.1.1 THE ± 1 PREAMP

The ± 1 preamp is used to compare 1.47V to 1.13V and amplify the difference between the inputs. Figure 78 shows a schematic representation of preamp. Some issues that arose in the making of this preamp was the fact that the voltage difference of the output is less than the V_{th} of our MOSFET's, the input voltage is centered at 1.3V and, the output voltage needs to be centered at around 0.9V.

In order to create an imbalance in the preamplifier decision levels an intentional mismatch was created in the differential pair and also a mismatch in the source followers. With an input of 1.47V for V_{inp} and 1.13V V_{inm} , the source followers reduce this voltage mismatch and lower the common mode voltages to 770mV and 600mV. This leaves 170mV of mismatch to be compensated for by the differential pair. Like the source followers, the Diff pair is mismatched. The differential pair uses a self biased active load to have high output impedance and was biased with a replica bias that was set to the comparator threshold voltage on the input. In order to keep the voltage threshold of the comparators stable, the bias current of the replica was set by comparing the output of the 1 leg of the replica bias circuit to 0.9V using a differential pair current amplifier. One issue that was found with using a feedback loop was that there were two stable states in which 0.9V could be achieved. One state is when there is 50 μ A going through the circuit and the other state is when

there is pico amps of current flowing through it. To mitigate the two stable states a $35\mu\text{A}$ bias current is used in addition to the replica bias transistor which makes it so that the only stable state is the state with $50\mu\text{A}$

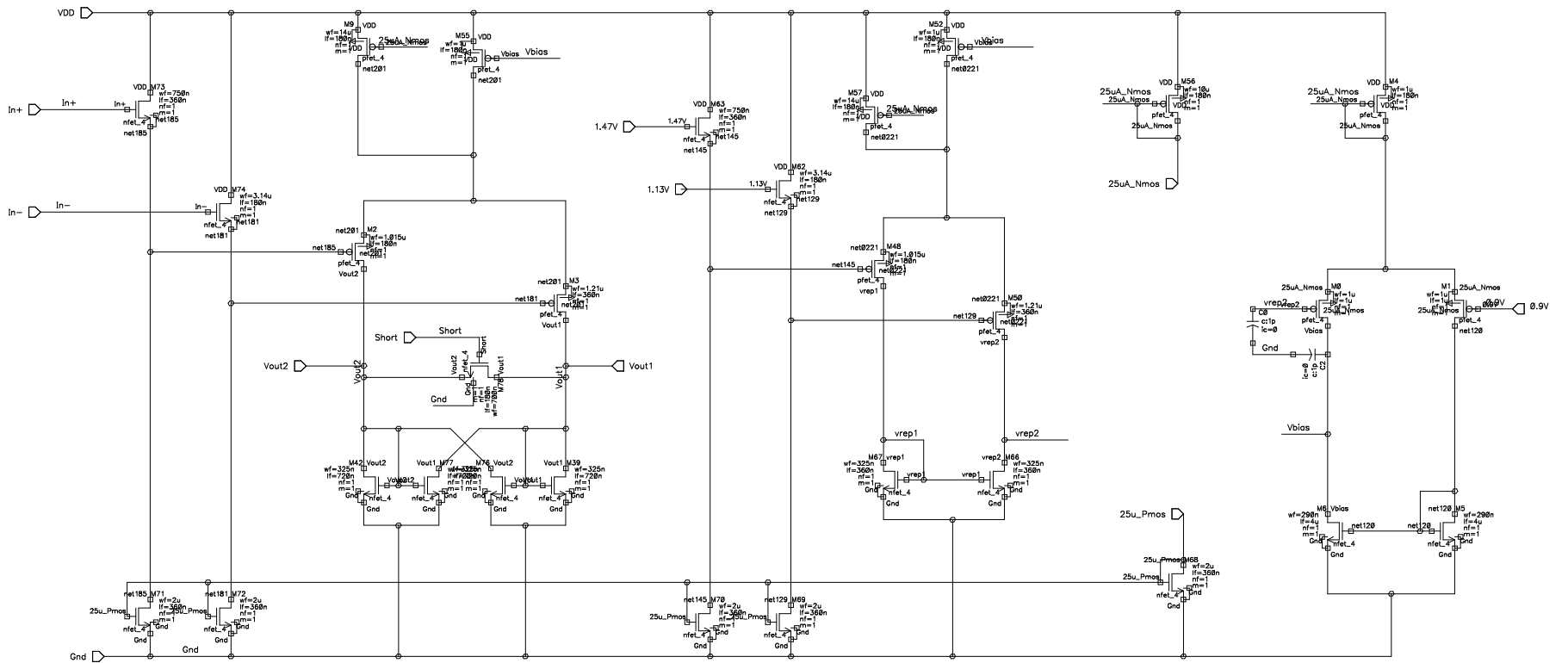


Figure 78 - ± 1 Preamplifier

Figure 79-Figure 81 below shows the startup transient of the replica bias circuitry. The first plot in each figure shows the gate voltage of V_{bias} . This voltage is set by the negative feedback amplifier. The second plot in each figure shows the convergence of V_{rep1} and V_{rep2} as the startup transients of the preamplifier dies out. The third plot in each figure shows the current through the differential amplifier.

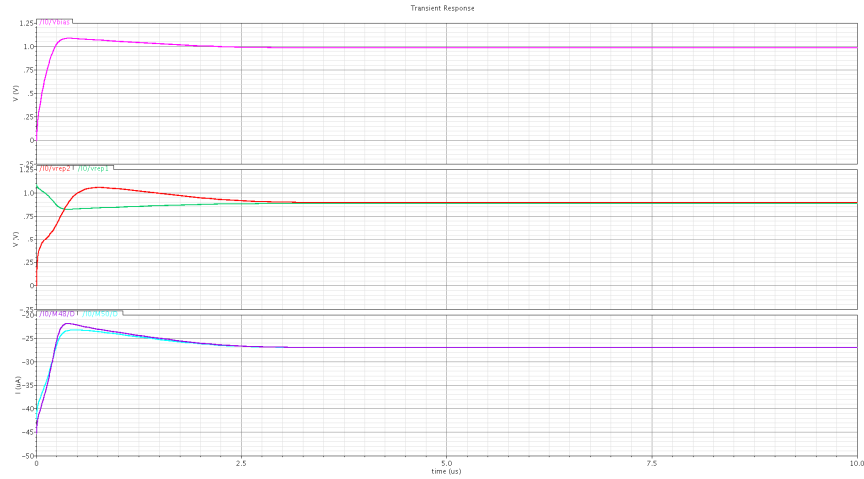


Figure 79- Startup transient 27° C of ±1 Preamp

Figure 79 shows that the startup transient of the preamp at 27° C takes about 2.75µs to converge and differential amplifier uses about 54uA.

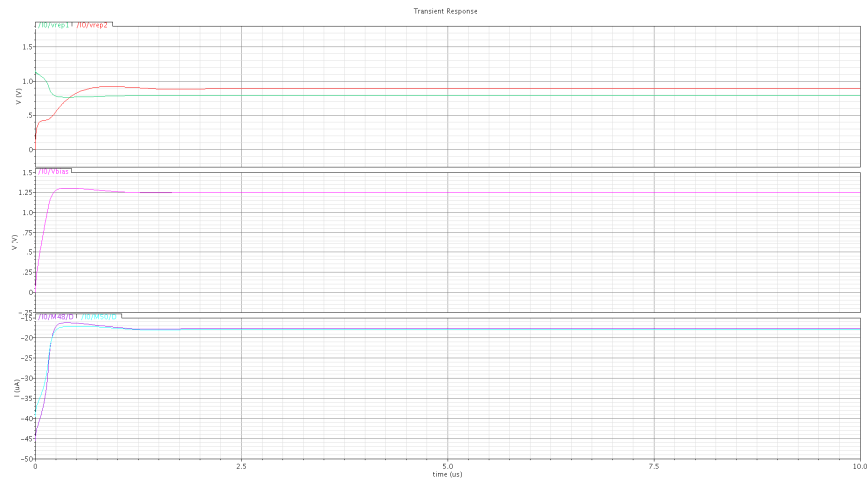


Figure 80- Startup Transient at 70° C of ±1 Preamp

Figure 81Figure 80 shows that the startup transient of the preamp at 70° C takes about 2μs to converge and differential amplifier uses about 34uA. Also due to the high temperature there is a small output offset not seen in the 27°C simulation.

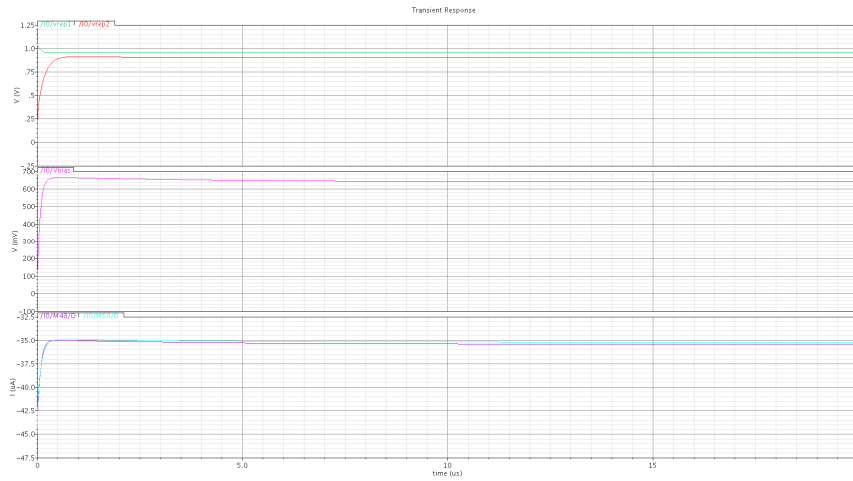


Figure 81- Startup Transient at 0°C of ±1 Preamp

Figure 81Figure 81 shows that the startup transient of the preamp at 0° C takes about 12μs to converge and differential amplifier uses about 70uA. Also due to the low temperature there is a small output offset not seen in the 27°C simulation.

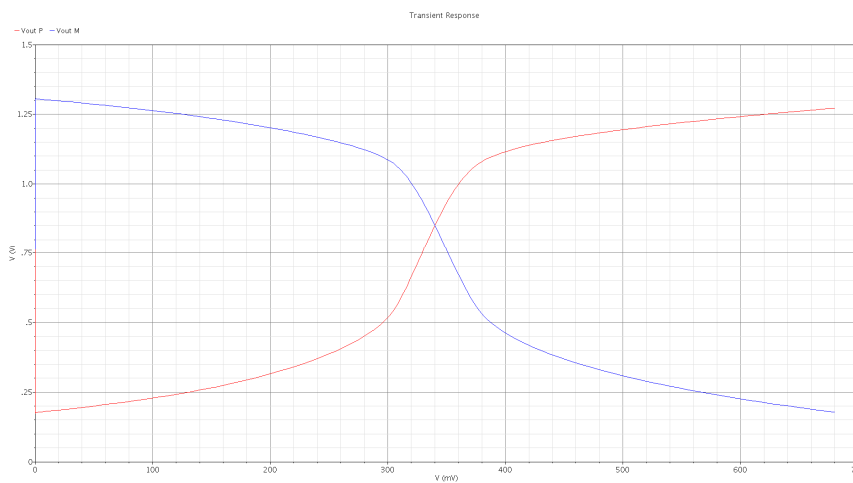


Figure 82 - Dc sweep of ±1 Preamp

Figure 82 shows a DC sweep of the ± 1 preamplifier. There is a 340mV differential offset on the preamplifier which is used to set the decision level of the comparators. The gain of this preamplifier at 170mV single ended (zero crossing of output) is $35.1 \frac{V}{V}$ as seen in Figure 83. Unlike in the successive approximation analog to digital converter where the preamplifiers need to have a high gain and low noise, the cyclic ADC can recover from decision errors in the next residue cycle.

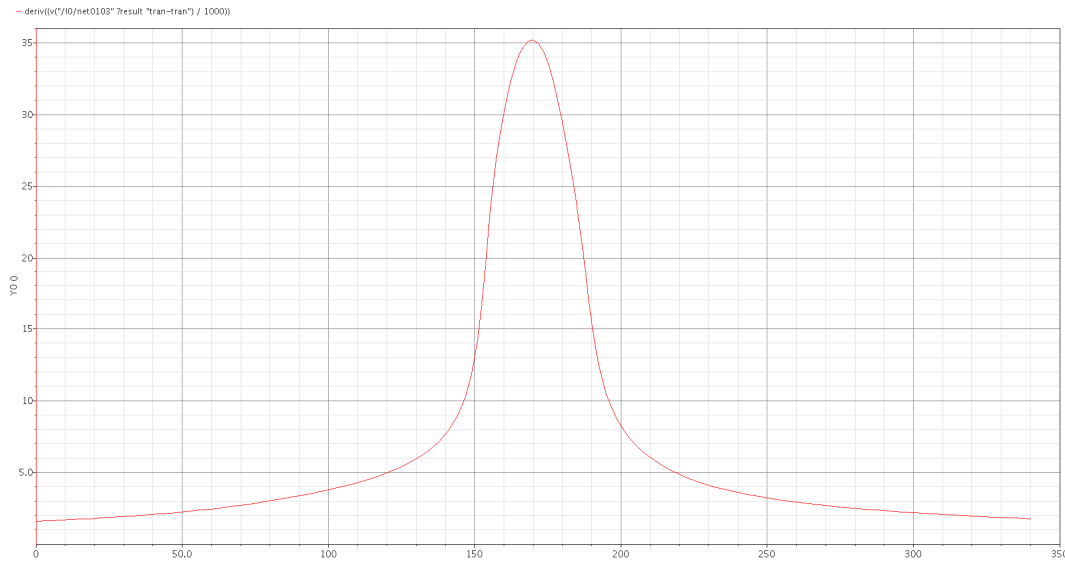


Figure 83- Preamplifier DC Gain Plot

8.1.2 THE 0 PREAMP

The zero preamp is used as the middle comparator in the thermometer code. The comparator schematic is shown in Figure 84 and is much simpler than the ± 1 comparator due to the fact that there does not need to be any intentional mismatch between the inputs of the differential pair or the source followers. This differential pair is also actively loaded with a self biased load to assure simple and effective biasing. The length and width of the transistors was determined by finding the proper ratio to allow for a 0.9V output common mode voltage. To keep a stable bias over input range, a replica bias was used that mimics the entire circuit which keeps the drain to source voltages on the biasing transistors equal which creates a much better current mirror.

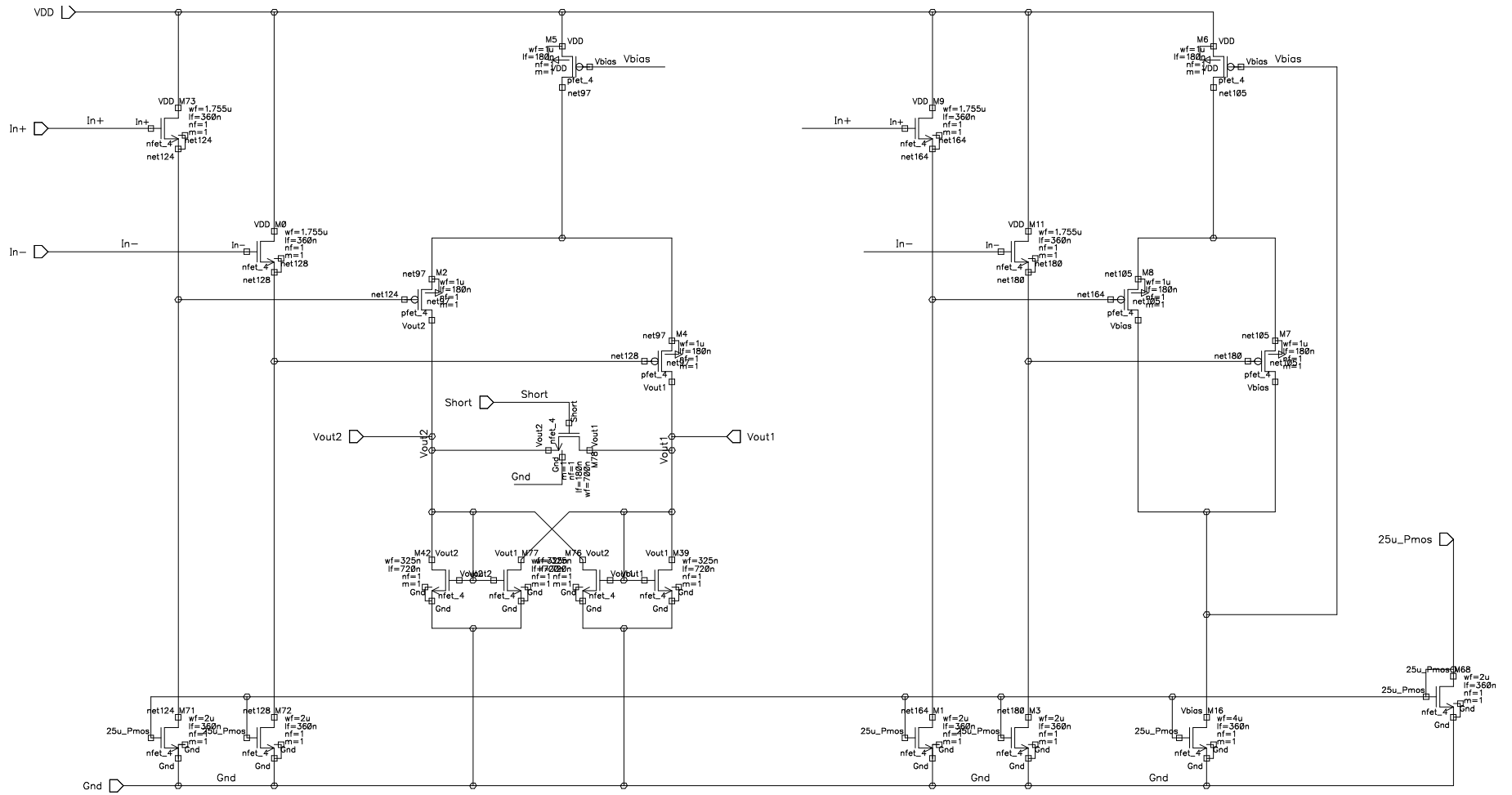


Figure 84 -Preamplifier for the Zero Comparator

Figure 85 below shows a DC sweep of the preamplifier for the zero comparator. The maximum gain of this circuit is $32.1 \frac{V}{V}$, this occurs at 0V differential input as seen below.

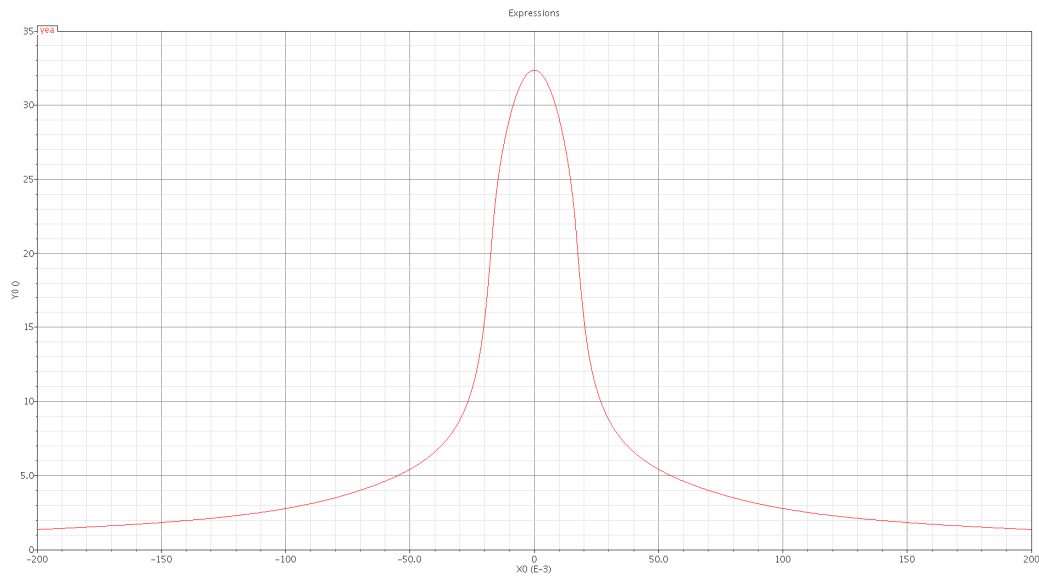


Figure 85- DC plot of the Zero preamp

8.2 ANALOG LATCH

The analog latch employs positive feedback to take the differential output from the preamplifiers and to amplify it until the differential output hits the rails. The circuit is built by using two inverters connected in a positive feedback configuration that is clamped with 2 pmos transistors. This inverter configuration is then nudged by a differential pair with inputs connected to their corresponding preamplifier. Figure 86 shows the actual schematic of the analog latch that was borrowed from Cody Brenneman for use in a self calibrating successive approximation ADC.

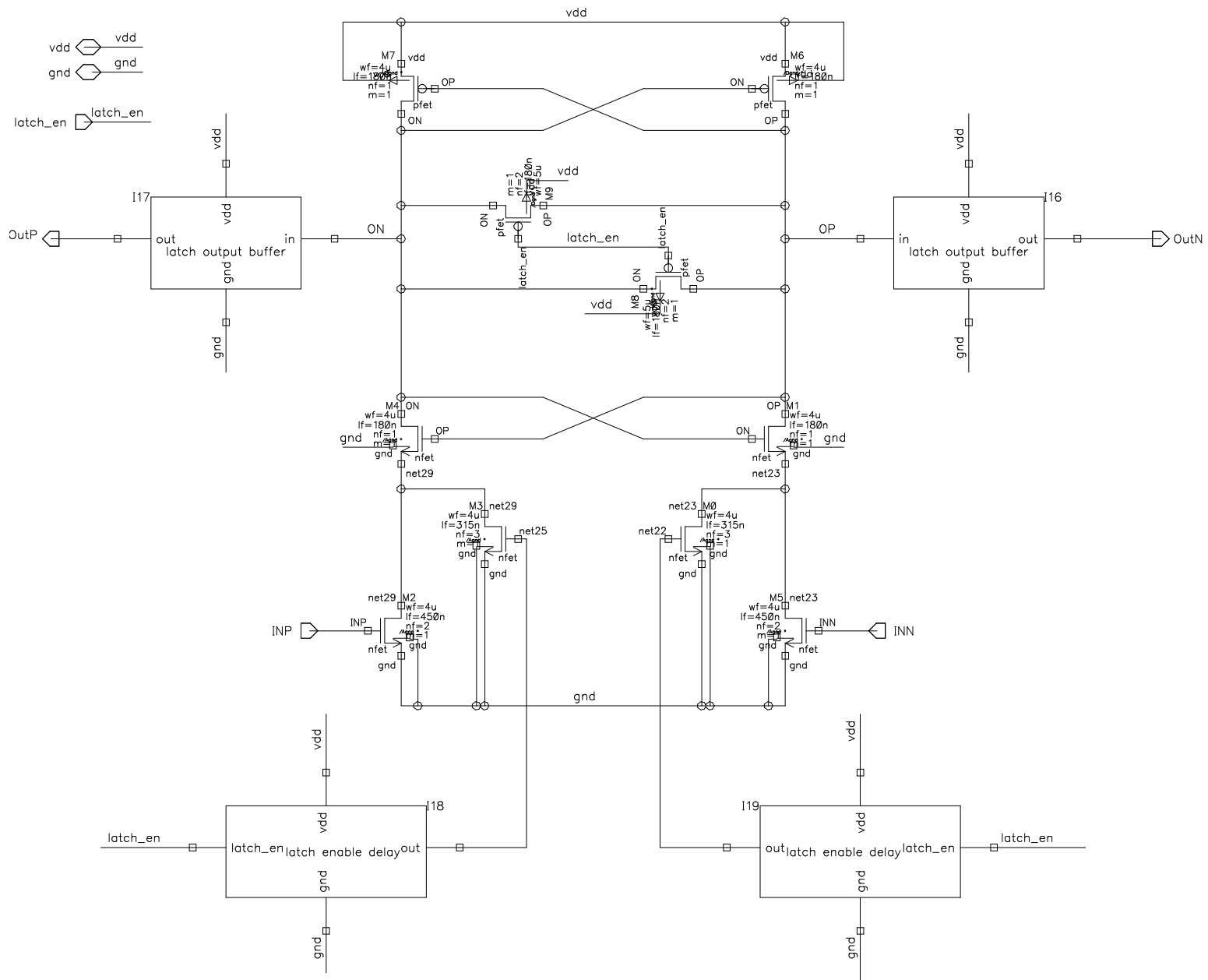


Figure 86- Analog Latch

8.3 DIGITAL LATCH

This project makes use of 2 different types of digital latches a latch that when reset holds a “0” state and a latch that resets to a “1” state. This is used to set the logic levels during the first conversion when a zero decision needs to be made. The thermometer code for the comparators needs to be “001” to create a zero decision. The digital latch was created using the basic D-flip flop topology and adding logic to create a “1” state when the reset input is high. To create a “0” resetting latch, the outputs Q and Q_{bar} were switched and an input inverter was used to invert the signal to negate the Q_{bar} output. In order to sample only on the rising edge of the clock, 2 delay blocks and an inverter were placed in the circuit to create a race condition to the and-gate as seen in Figure 87. The schematics of the “1” and “0” reset latches are shown in figures Figure 88 and Figure 89

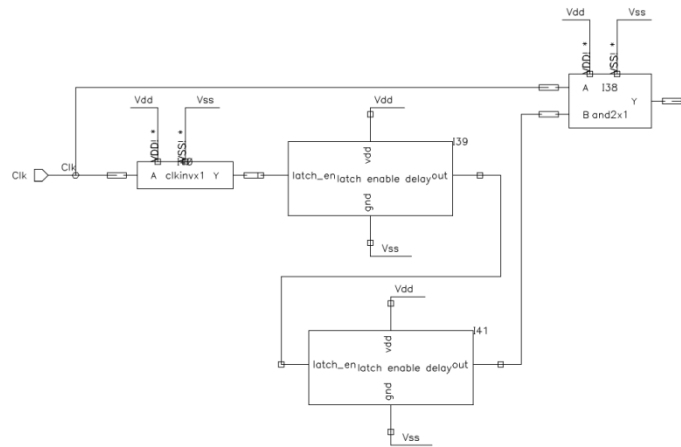


Figure 87- Rising edge detector

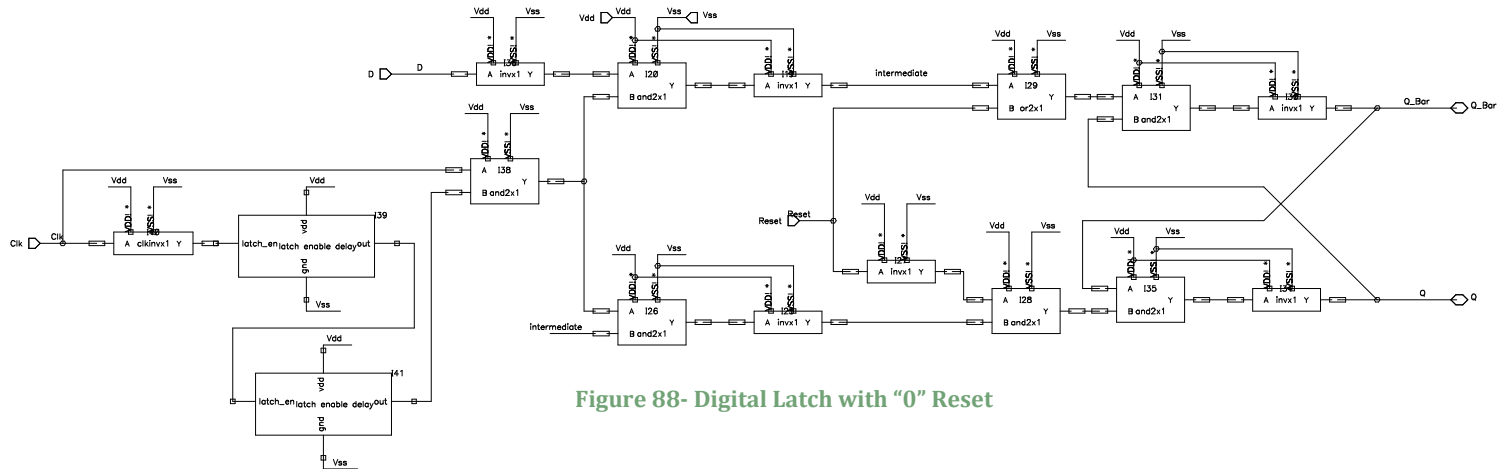


Figure 88- Digital Latch with "0" Reset

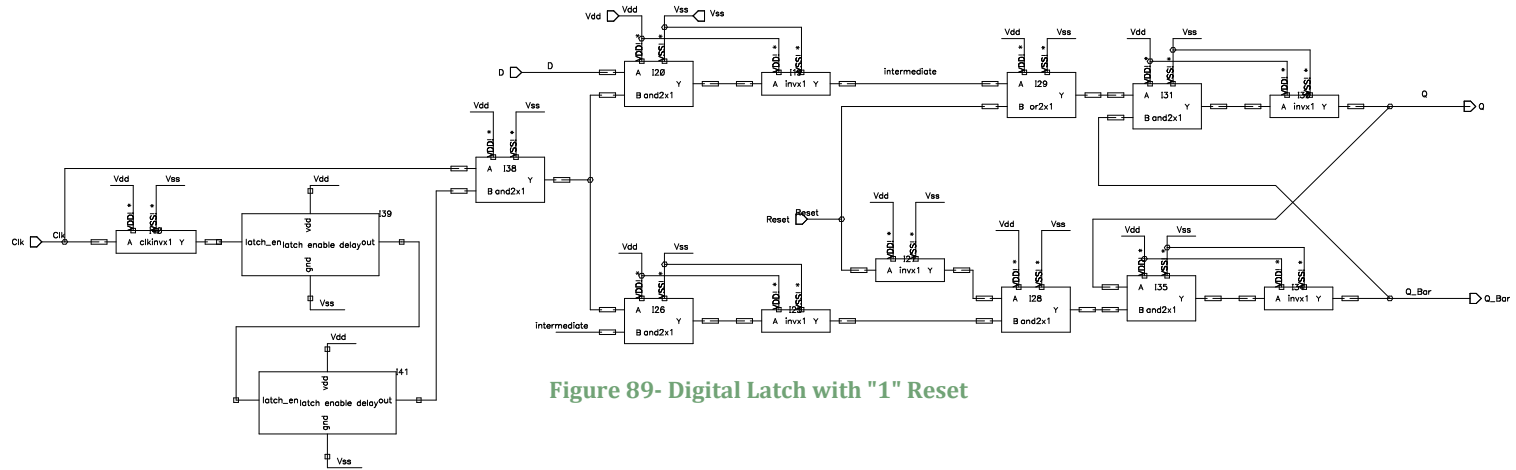


Figure 89- Digital Latch with "1" Reset

8.4 PUTTING IT ALL TOGETHER

Once all the separate sub-systems were built, a new schematic was made that incorporated all the blocks and the appropriate connecting circuitry. A symbol was then made to be used in the top level schematic as seen in Figure 90.

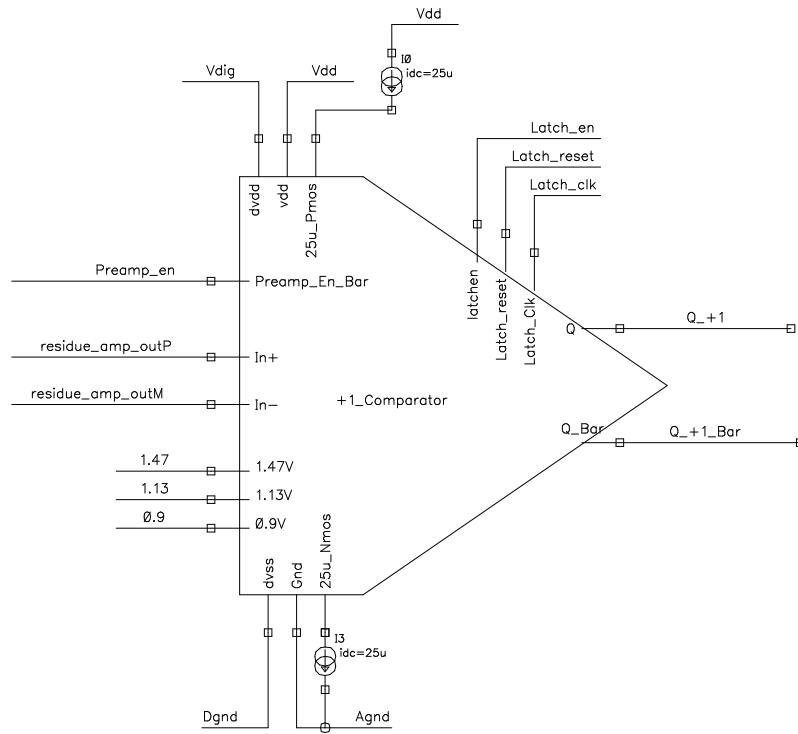


Figure 90 - "+1" Comparator Symbol

Whole block simulations were done to assess the operation of test the accuracy of the comparator threshold voltages and the timing of the input signals. a transient simulation was completed in Figure 92 using the "+1" comparator and a 240mV input signal. This caused a low decision by the comparator due to its 340mV threshold for a high logic level.

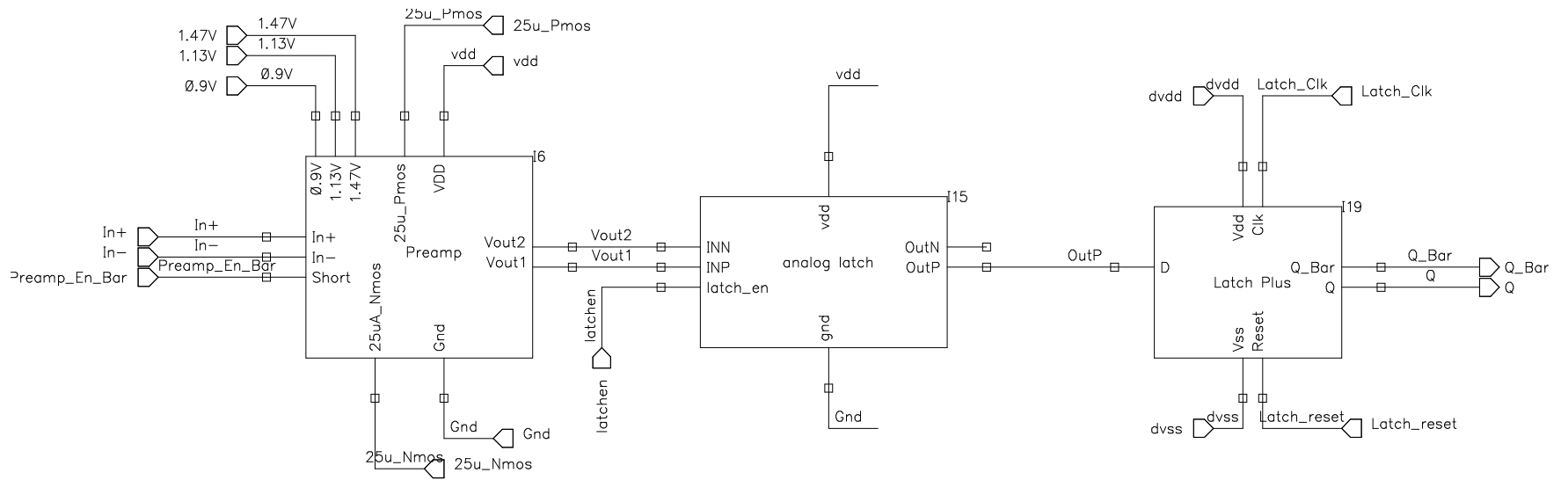


Figure 91 – Schematic Block Diagram of Comparators

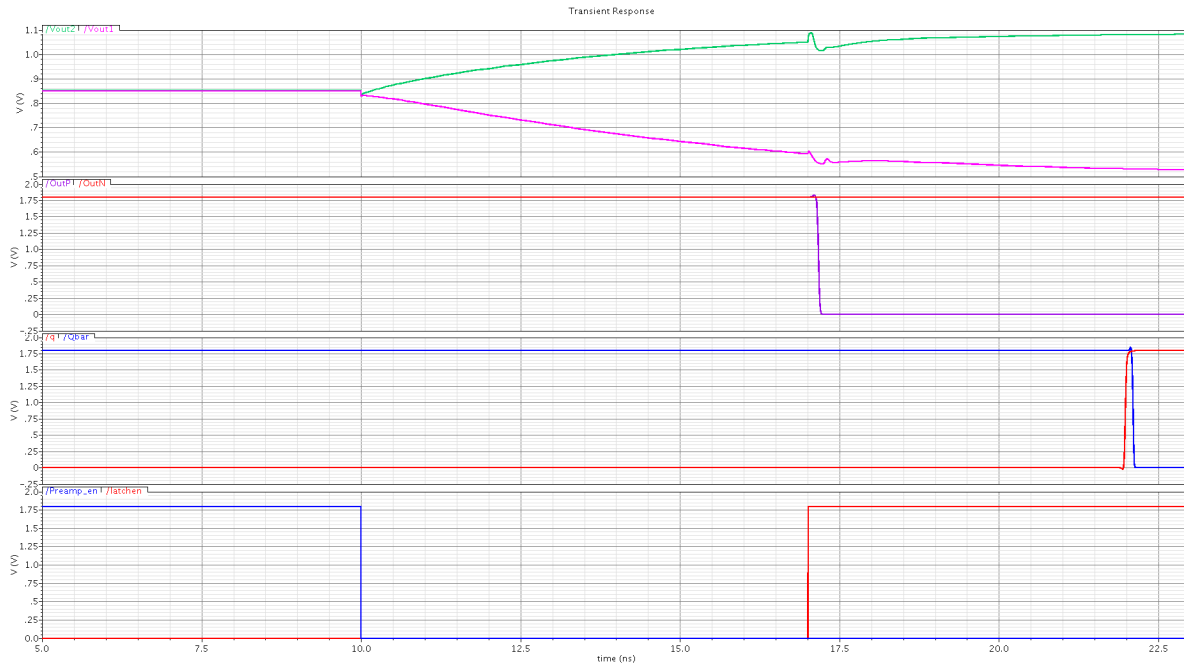


Figure 92- Transient Simulation of +1 Comparator using a 280mV differential input

The first simulation in Figure 92 shows the transient response of the preamplifiers firing at 10ns. At 17ns the analog latch is released as seen in the second simulation causing the preamp settling to have a ripple in it due to the parasitic capacitance to the drain and source of the gates of the MOSFET's in the analog latch injecting charge into the output node of the preamps. The third simulation shows the output of the block, the digital latch transitioning at 21ns. The fourth simulation shows the control signals used to trigger the comparators.

9 THE OUTPUT BLOCK

One of the issues we had originally discussed extensively in the project's preliminary design was the concept of driving the outputs, instead of simply outputting low voltage CMOS signal levels. To do this, as we represented in the background section, we researched a common method known as Low Voltage Differential Signaling (LVDS). This block would follow our Logic block, as the diagram below indicates.

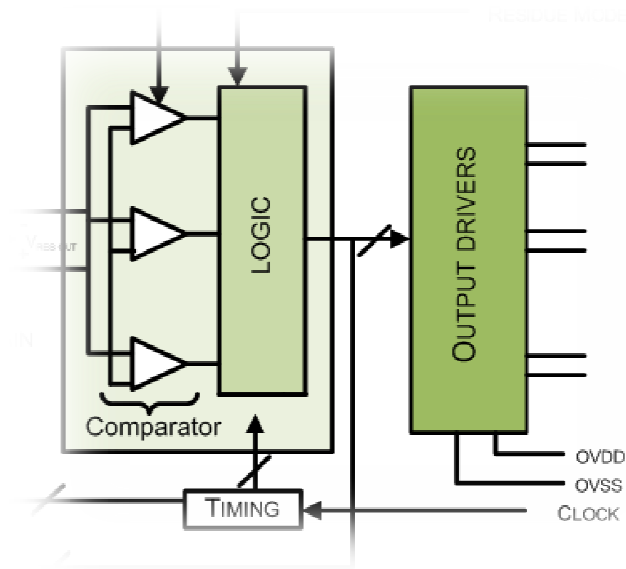


Figure 93- Block Interaction between Logic and Output Drivers

9.1 CREATING LVDS DRIVERS

After performing research, we have seen that there is a common industry standard for LVDS design. The specifications of the standard are shown below:

Table 17 - LVDS Standards

	Standard	Min	Max
Voltage Across Resistor	350mV	247mV	454mV
Common Mode Voltage	1.2V	1.125V	1.375V
Current	3.5mA		
Output Resistor	100Ω		

Shown below is a copy of Figure 18. In our case, the receiver would be an FPGA that is capable of taking LVDS outputs, which usually requires some signal translation.

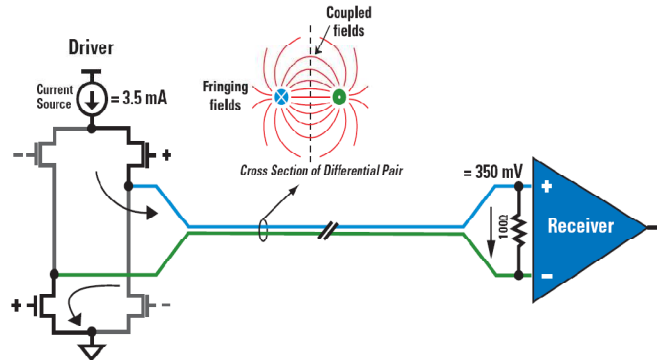


Figure 94 - LVDS Revisited: Theoretical Schematic

We had to make our design comply with the requirements dictated by the standards mentioned above. To bias the LVDS, we used an N-MOS current mirror, with values designed to match our desired 3.5mA. Also, the values on the transistors are set to allow for the 1.2V common mode. Our schematic is shown below:

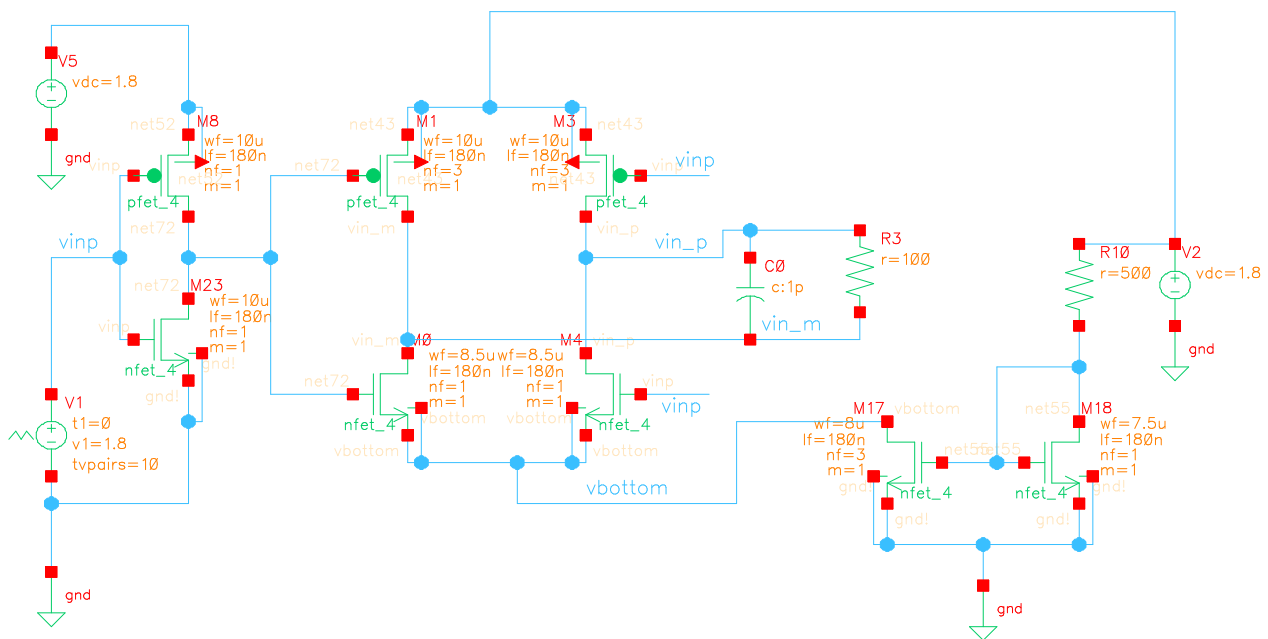


Figure 95 - LVDS Schematic: Actual Circuit Implementation

As we can see above, there is a transmission gate (M8, M23) at the input, which is fed by an input voltage. This value is then obtained by the 4 transistors (M0, M1, M3, M4) forming the LVDS driver. The biasing for the transistors is done by a simple current mirror (M17, M18). R3 is the output resistor, with a parasitic capacitor next to it. To confirm that our circuit was running we performed a transient analysis in Cadence. The results of that analysis are shown below:

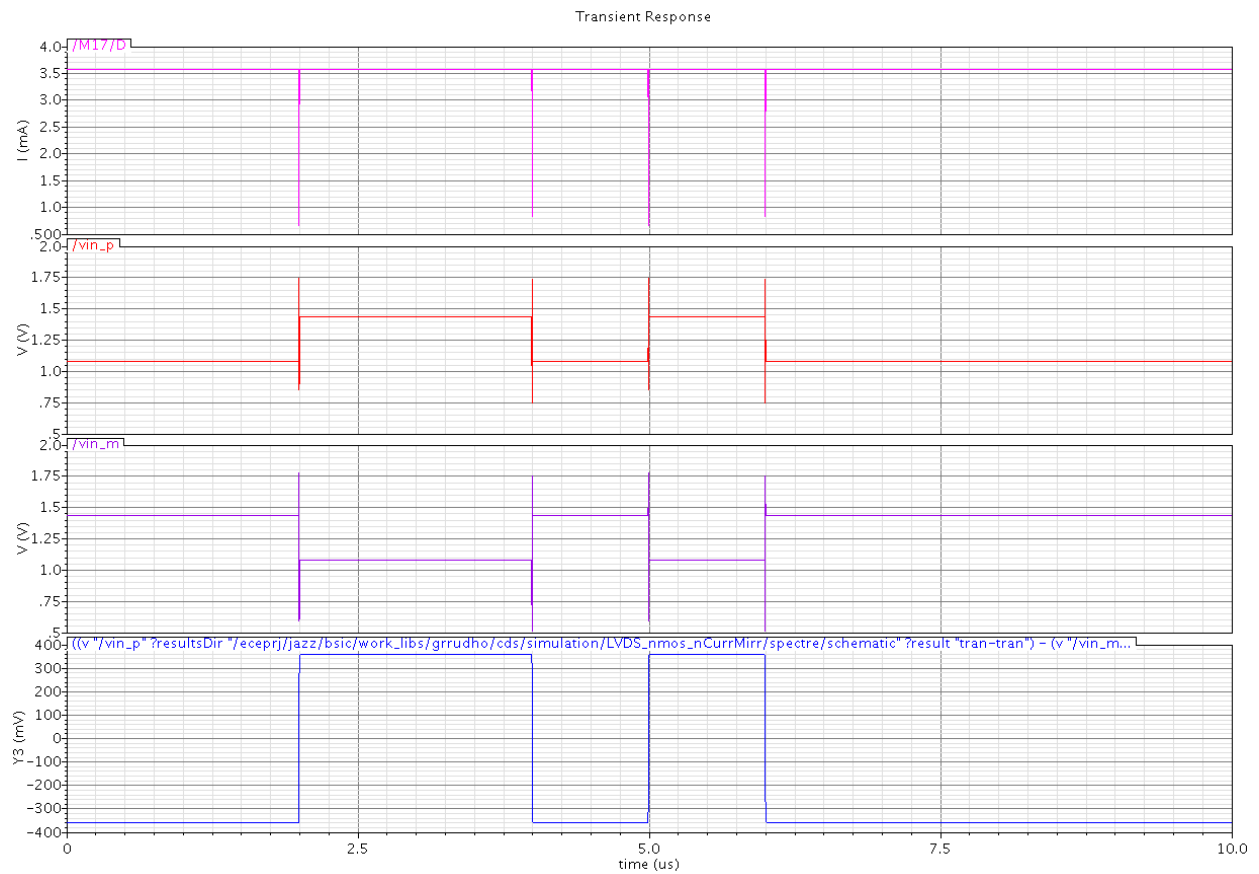


Figure 96 – Simulated LVDS Outputs

From the top: (1) As we can see the current stays constant at 3.5mA. (2) The input voltage is shown as a piecewise linear function. (3) Differential counterpart to input. (4) Differential voltage seen by the receiver.

By looking at Figure 96, we can observe that standards outlined in Table 17 have all been met. Therefore the LVDS is ready for use.

9.2 MAKING THE CHOICE BETWEEN LVDS AND LVCMOS

Although we created a working version of an LVDS driver, it was necessary to analyze if creating these drivers would be a worthwhile effort for this project. Therefore, the chart below was created:

Table 18 - LVDS and LVCMOS Comparison

Specification	LVDS	LVCMOS	Preference
Number of Wires	12	6	LVCMOS
Complexity	The design of a driver that can adhere to LVDS standards is necessary, which adds high complexity, comparatively.	Simple MOSFET drivers with common voltage references within the circuit	LVCMOS
Noise	Reduces noise in long wire distances by being differential, especially in higher frequencies.	More prone to noise in longer distances, due to jitter and interference in system	LVDS
Power	Lower Power, in general	Low Power	LVDS
Transmission	Serial or Parallel	Parallel	LVCMOS
Speed	Accommodates very high frequencies.	Less used for high frequencies	LVDS
Signal Processing	Serialization	Translation	LVCMOS

The table above shows a contrast between our two most feasible options: LVDS, being a great technology in high-speed applications that require low noise levels, and LVCOMS, being the simpler, more trivial option.

Due to the complexity of this project, we feel it may be more convenient and efficient to use the LVCMOS standard, because it will encompass all of our needs without intense extra circuitry on the analog and digital sides. For example, to make LVDS a more convincing choice, we would have to add circuitry to serialize the data and transmit our 3 simultaneous bits. Also, since it is differential, LVDS will require twice the amount of pins as LVCMOS would demand for output. Therefore, our final choice was to discontinue the LVDS approach and maintain a simple LVCMOS output.

9.3 OUTPUT PROCESS

Since we have decided on simply using the output of our logic block to be sent to the FPGA, some the following characteristics apply to this block:

- Output will be a thermometer code
- Output code will be given per cycle, not per conversion.

10 CONCLUSION

This project fulfills the expectations that were originally instituted as requirements for a successful major qualifying experience at Worcester Polytechnic Institute. It encompasses a strong theoretical background and a real-world application, mimicking a professional integrated circuit design process. Most importantly, it enables learning through a close relationship with the advisor and the group members.

10.1 FUTURE WORK

As the reader may have noticed, the scope of this project consists of a broad spectrum of concepts – some of which are not typically seen by the typical electrical engineering undergraduate student. Therefore, since the project's conception, it was expected that the project would have enough content to require some continuation after this capstone was completed. Since the expected outcomes of the project have been met (fully functional blocks have been made), the expectation is that the project will be finished under Shant Orchanian's Master's Degree Thesis. This new level in the project involves the following tasks:

- Linking all functional blocks and simulation of a full conversion
- Application of Split-ADC architecture
- Layout of Integrated Circuit
- Tape-out and fabrication of Chip with Jazz Semiconductor
- Testing of circuit's functionality and interaction with FPGA and digital correction algorithm

The expected timeline for the tape-out of the chip is in the fall of 2009.

10.2 RECOMMENDATIONS FOR FUTURE PROJECTS

As the project reached its end, our group was able to create suggestions and recommendations for future undergraduate students. These recommendations exist as a consequence of approaches that functioned well for our project's dynamics. Also, some of the suggestions include advice we hoped to have received at the start from fellow undergraduates:

- At the start of the project, it can be helpful to designate one project partner for practicing and researching integrated circuit layout, so that if the time comes, you may be able to tape-out the chip before the academic year is over.

- Ensure that the writing done from the first weeks is consistent and well-written for every weekly report until the last term. This will shorten the MQP Final Report writing time extensively.
- Document everything and create a shared files folder whenever possible for redundancy.
- It is beneficial to take time early to conquer the simulation software, such as performing parametric analyses, changing component parameters, and using the presets in the calculator block of the simulator.
- Experiment with the simulator and the different ways in which logic can be implemented within the chip, such as using VHDL, Verilog, discrete components, and other existing methods to generate logic blocks.
- Do not complicate your design if a specification has been met. For example, although using a cascode to boost gain may sound like an appealing concept to our circuit, we would recommend keeping the current simplicity of the differential amplifier. Blocks like a cascode may improve linearity, but will create a trade-off with output voltage range and will add complexity to the circuit when it's not strictly necessary. Since linearity is not a major concern to this cyclic ADC format, a cascode might be overkill.

Obviously, every experience will be different. However, we believe that these methods will jump start a project of similar scope.

10.3 RECAPITULATION

This project emerged with the need to adapt sub-micron processes to the idea of the Self-Calibrating Cyclic ADC. Using the Cyclic ADC architecture, we were able to divide our chip into several major blocks: the switched capacitor network, responsible for the sampling of the capacitors; the residue amplifier, consisting of an amplifier of an open-loop gain of 2; a comparator block, responsible for outputting the ADC thermometer code; a voltage reference block, which is used to in conjunction with the switched capacitor network; and a logic block, which enables the switching to the voltage references. Finally, the timing and calibration is done completely off-chip.

Once again, is important to reiterate that the digital calibration algorithm (done off chip) was simultaneously created by Hattie Spetla. The ability to have this algorithm enhances our design in various levels. For example, it reduces analog-side chip space. It also reduces complexity in the analog domain.

10.4 IMPORTANCE AND IMPACT

As a learning experience, this project was extremely valuable to our group as MQP students. It was a tough assignment that required much engagement and time. It was a unique experience. Since this project is in a niche that is not as common as other analog design fields, such as microelectronics or power systems, we were able to learn various techniques that were unknown to us, such as the replica bias, the switched capacitor network, among others. Also, one of the most important aspects of the project is that the usual assumptions based on the square law, learned in the semiconductor design classes do not hold true in sub-micron processes.

Assuming that once fabrication is completed, the chip functions as desired, it can be used for various applications. For example, an application in industry would be a medical device that needs various converters. This application would benefit from small chip size – and since the calibration is done externally, only one FPGA would be necessary to process multiple chips, using the algorithm created for it.

Finally, although many Cyclic ADC configurations have been developed, our research has not been able to find a chip that is self-calibrating and meets our specifications in the 0.18 μ m process. Therefore, it is especially gratifying to know that we are driving innovation by participating in this project.

TABLE OF FIGURES

Figure 1 - Spurious-Free Dynamic Range Illustration[7].....	9
Figure 2 - Ideal (left) and Non-Ideal (right) Examples of ADC Transfer Function [4]	10
Figure 3 - Integral Non-Linearity Example [4]	10
Figure 4 – (a) Quantization Process [8] and (b) Quantization Error Illustrations (right) [4]	11
Figure 5 - Block Diagrams for Nyquist and Oversampled ADCs	12
Figure 6 - Block Diagram of a 16-bit Pipelined ADC [8]	13
Figure 7 - Flow Chart of Successive-Approximation Approach	15
Figure 8 - DAC-based Successive-Approximation Converter [9].....	15
Figure 9 – 5-bit Charge-Redistribution ADC [9].....	17
Figure 10 – High Level Block Diagram of a Cyclic Converter [11]	18
Figure 11 - Residue Plot at $G=2$ [11]	19
Figure 12 - Residue Plot with $G < 2$ [11].....	19
Figure 13- Diagram of Hold capacitor with Thermal Noise	20
Figure 14 - Point-to-Point Configuration	22
Figure 15 - Data Distribution Using Point-to-Point Configuration	22
Figure 16 - Multidrop Configuration.....	23
Figure 17 - Example of a Three-Node Multipoint Configuration.....	23
Figure 18 - LVDS Driver and Receiver [13]	24
Figure 19 - Digital Signaling Model.....	24
Figure 20 - Illustration of Split-ADC Concept [11].....	26
Figure 21 - Split ADC Characteristics in Contrast with Single ADC Approach.....	27
Figure 22 - Current Mirror Example	28
Figure 23 - Differential Amplifier Example [16].....	29
Figure 24 –Amplifier Model.....	30
Figure 25 - Common Mode Model	30
Figure 26 - Differential Mode Model	30
Figure 27 - Half-Circuit Model of the Common Mode.....	31
Figure 28 - Half-Circuit Model of the Differential Mode.....	31
Figure 29 - Signal Input-Output Characteristics of the Differential Input to Each Output.....	32
Figure 30 - Large Signal Input-Output Characteristic for the Differential Input to the Differential Output.....	32
Figure 31 - Block Diagram	33
Figure 33 - Schematic of Input Block.....	34
Figure 34 - THD and W_{Total} Relationship	38
Figure 35 - Acquisition Time and W_{Total} Relationship	38
Figure 36 – Motivation for Noise Floor Reduction	40
Figure 37 - New Input Circuit Model with Added Resistor	41
Figure 38 - Acquisition Time Dependence after Adding New Resistor	42
Figure 39 - THD Dependence on Resistor Variation	43
Figure 40 - Switch Capacitor Array Block and its Interaction with other Blocks.....	45
Figure 41 - Example of Using One Capacitor	46
Figure 42 - Diagram of Decisions with 2 Capacitors.....	47
Figure 43 - Test Circuit for +/- 1 Decision.....	48
Figure 44- Example of Charge Injection: Capacitor being Switched between a 500 μ m PMOS and a 250 μ m NMOS.....	49
Figure 45 - Method for Using 4 Capacitors.....	49
Figure 46 - Circuit Implemented with 4 Capacitors	50
Figure 47 - 2 Capacitor Implementation of “+1” Decision.....	51

Figure 48 – 4 Capacitor Implementation of “+1” Decision	51
Figure 50- Switched Capacitor Circuit	53
Figure 51 - Derivation for Reference Voltages	54
Figure 52-Schematic Representation of Differential Amplifier.....	55
Figure 53- Differential In-Out Characteristic	56
Figure 54 - Voltage Ranges Plot	58
Figure 57-Replica Bias Simulation.....	62
Figure 58-Symbol Representation of Differential Amplifier	62
Figure 59 - Logic Block and its Interaction with other Blocks.....	63
Figure 60 - Discrete Buffer Component.....	64
Figure 61-Schematic of a Buffer in Transistor Level	64
Figure 62 - Tapered Buffer of Size 32.....	64
Figure 63 - Tapered Buffer Symbol (size 32).....	65
Figure 64-Representaion of the Tapered Buffer Topology.....	65
Figure 65-Schematic Representation of the Sample and Hold Circuit.....	66
Figure 66-Rising Edge of Signal for Different Buffer Sizes.....	67
Figure 67-Falling Edge of a Signal for Different Buffer Sizes	68
Figure 68-Plot of Rise Time Delays vs. Buffer Sizes for the Gate at the Sampling Capacitor	69
Figure 69-Plot of Fall Time Delays vs. Buffer Sizes for the Gate at the Sampling Capacitor.....	69
Figure 70-Plot of Rise Time Delays vs. Buffer Sizes for the NMOS Gate at the Sampling Switch	70
Figure 71-Plot of Fall Time Delays vs. Buffer Sizes for the NMOS Gate at the Sampling Switch	70
Figure 72-Plot of Rise Time Delays vs. Buffer Sizes for the PMOS Gate at the Sampling Switch.....	71
Figure 73-Plot of Fall Time Delays vs. Buffer Sizes for the PMOS Gate at the Sampling Switch	71
Figure 74- Matching of Comparators’ Outcome to Residue Amplifier Decisions.....	73
Figure 75-Capacitor Array Block.....	74
Figure 76-Digital Transistor Gate Driver	75
Figure 77-Behavior of “vresin-vresout switch” Digital Block.....	76
Figure 78-Representation of Gates to Drive With “vresin-vresout switch” Digital Block.....	77
Figure 79-“vresin-vresout switch” Digital Block.....	77
Figure 80- “genericDemux” Symbol Representation	79
Figure 81-Results “genericDemux” Simulation.....	79
Figure 82 - ± 1 Preamplifier.....	82
Figure 83- Startup transient 27° C of ± 1 Preamp	83
Figure 84- Startup Transient at 70°C of ± 1 Preamp	83
Figure 85- Startup Transient at 0°C of ± 1 Preamp.....	84
Figure 86 - Dc sweep of ± 1 Preamp.....	84
Figure 87- Preamplifier DC Gain Plot	85
Figure 88 –Preamplifier for the Zero Comparator.....	86
Figure 89- DC plot of the Zero preamp	87
Figure 90- Analog Latch.....	88
Figure 91- Rising edge detector.....	89
Figure 92- Digital Latch with “0” Reset.....	90
Figure 93- Digital Latch with “1” Reset.....	90
Figure 94 - “+1” Comparator Symbol.....	91
Figure 95 – Schematic Block Diagram of Comparators	92
Figure 96- Transient Simulation of +1 Comparator using a 280mV differential input	93
Figure 97- Block Interaction between Logic and Output Drivers	94
Figure 98 - LVDS Revisited: Theoretical Schematic	95
Figure 99 - LVDS Schematic: Actual Circuit Implementation.....	95
Figure 100 – Simulated LVDS Outputs.....	96

INDEX OF TABLES

Table 1 - Specifications	5
Table 2 - Speed and Accuracy Correlation with ADCs.....	13
Table 3 - Charge-Redistribution (Figure 9) ADC Explanation	16
Table 4 - Comparison Table of Differential Standards	21
Table 5 - Industry Standards for Various LVDS Technologies [13].....	22
Table 6 - Bus Configurations vs. Standards.....	23
Table 7 - Swept Attributes.....	36
Table 8 - Summarized Optimization Results of t_{ACQ} and THD	38
Table 9 - Parameter Goals.....	39
Table 10 - Values for Transistor Widths	40
Table 11 - Effect of Tolerances.....	42
Table 12 - Comparison of Decisions.....	50
Table 13 - Rise Time and Fall Time Measurements for Sample and Hold Circuit Simulations	66
Table 14- Truth Table for Gate Driver Digital Block	74
Table 15- input/output1 Relationship for “genericDemux”	78
Table 16- input/output2 Relationship for “genericDemux”	78
Table 17 - LVDS Standards	94
Table 18 - LVDS and LVCMOS Comparison	97

REFERENCES

- [1] B. Murmann and B. E. Boser, "A 12-bit 75-MS/s Pipelined ADC Using Open-Loop Residue Amplification," *IEEE JOURNAL OF SOLID-STATE CIRCUITS*, vol. 38, no. 12, pp. 2040-2050, Dec. 2003.
- [2] Analog Devices. (2009, Feb.) Key Data Converter Terms and Specifications. [Online]. http://www.analog.com/analog_root/static/solutionsBulletins/dac03-05/dac_terms.html
- [3] R. J. Baker, *CMOS Circuit Design, Layout, and Simulation*, 2nd ed. Piscataway, New Jersey: John Wiley & Sons, 2008.
- [4] D. Auclair, C. Gammal, and F. Huang, "12b 100MSps Pipeline ADC with Open-Loop Residue Amplifier," Worcester Polytechnic Institute, Worcester, MA, Major Qualifying Report, 2008.
- [5] Data Translation, Inc., "Overall Accuracy = ENOB (Effective Number of Bits)," White Paper, 2008. [Online]. <http://www.datatranslation.com/docs/whitepapers/Overall-Accuracy-ENOB.pdf>
- [6] B. Razavi, *Principles of Data Conversion System Design*, 1st ed. New York, United States: Wiley, 1995.
- [7] J. Garcia, S. G. LaJeunesse, and D. Bartow. (1995, Jan.) Intersil - Measuring Spurious Free Dynamic Range in a D/A Converter. [Online]. <http://www.intersil.com/data/tb/tb326.pdf>
- [8] A. Nair and S. Goluguri, "Design of a 16-bit 10-MHz Pipeline ADC Using the Split-ADC Architecture in 0.25 μ CMOS," Worcester Polytechnic Institute, Worcester, MA, Major Qualifying Project Report, 2007.
- [9] D. A. Johns and K. Martin, *Analog Integrated Circuit Design*, 1st ed. Toronto, Canada: John Wiley and Sons, Inc., 1996.
- [10] C. R. Nave. (2006) HyperPhysics - Georgia State University, Department of Physics and Astronomy. [Online]. <http://hyperphysics.phy-astr.gsu.edu/hbase/hframe.html>
- [11] J. A. McNeill. (2006, May) Worcester Polytechnic Institute - Electrical Engineering Department. [Online]. http://ece.wpi.edu/~mcneill/papers/DSM_Creativity.pdf
- [12] J. Goldie. (2008, Sep.) National Semiconductor - Analog Edge. [Online]. <http://www.national.com/nationaledge/feb02/flavors.html>
- [13] National Semiconductor, *LVDS Owner's Manual*, 4th ed. United States, 2008, Fourth Edition.
- [14] J. A. McNeill, S. Goluguri, and A. Nair, "'Split-ADC' Digital Background Correction of Open-Loop Residue Amplifier Nonlinearity Errors in a 14b Pipeline ADC," in *International Symposium on Circuits and Systems*, New Orleans, 2007, pp. 1237-1240.
- [15] A. S. Sedra and K. C. Smith, *Microelectronic Circuits*, 5th ed. New York, New York: Oxford

University Press, 2004.

[16] J. McNeill. (2008, Feb.) Analog IC Design. [Online].

http://ece.wpi.edu/~mcneill/4902/labs/lab1/4902_C2008_Lab7.pdf

[17] D. G. Morrison, "Basics of Design: Analog to Digital Converters," *Electronic Design*, Oct. 2003.